INVESTIGATIONS ON WASTE REINFORCED RECYCLED PLA BASED COMPOSITE PREPARED THROUGH FUSED FILAMENT FABRICATION

Thesis Submitted For the Award of the Degree of

DOCTOR OF PHILOSOPHY

in

Mechanical Engineering

By

Ravi Kumar

Registration Number: 41700109

Supervised by
Dr. Kapil Chawla
(Associate Professor)
School of Mechanical Engineering

Co-Supervisor by
Dr. Jaspreet Singh
(Professor)
School of Mechanical Engineering

LOVELY PROFESSIONAL UNIVERSITY, PUNJAB

2026

DECLARATION

I Ravi Kumar, bearing Registration No. 41700109, hereby declared that the presented work in the thesis entitled "**Investigations on Waste Reinforced Recycled PLA Based Composite Prepared Through Fused Filament Fabrication**" in fulfilment of degree of **Doctor of Philosophy (Ph. D.)** is outcome of research work carried out by me under the supervision of Dr. Kapil Chawla working as Associate Professor and Co-Supervision of Dr. Jaspreet Singh, working as Professor, in the School of Mechanical Engineering of Lovely Professional University, Punjab, India. In keeping with general practice of reporting scientific observations, due acknowledgements have been made whenever work described here has been based on findings of other investigator. This work has not been submitted in part or full to any other University or Institute for the award of any degree.

Ravi Kumar

(Signature of Scholar)

Ravi Kumar

Registration No.: 41700109

School of Mechanical Engineering

Lovely Professional University, Punjab, India

CERTIFICATE

This is to certify that the work reported in the Ph. D. thesis entitled "**Investigations on Waste Reinforced Recycled PLA Based Composite Prepared Through Fused Filament Fabrication**" submitted in fulfillment of the requirement for the award of degree of **Doctor of Philosophy (Ph.D.)** in the School of Mechanical Engineering, is a research work carried out by Ravi Kumar, Registration No. 41700109, is bonafide record of his original work carried out under my supervision and that no part of thesis has been submitted for any other degree, diploma or equivalent course.

(Signature of Supervisor)
Dr. Kapil Chawla
Associate Professor
School of Mechanical Engineering
Lovely Professional University, Punjab, India

(Signature of Co-Supervisor)
Dr. Jaspreet Singh
Professor
School of Mechanical Engineering
Lovely Professional University, Punjab, India

ABSTRACT

Polymers are widely utilized in many applications due to their light weight, ease of processing and multi-dimensional properties, finding their utilization in automobile sector and packaging. However, the fast growth in consumption leads to dangerous environmental issues such as landfill accumulation and soil pollution. The uncontrolled use of polymers especially single use plastics has intensifies the need of sustainable solutions.

Recycling of polymers has risen as an effective method to decrease environment impact and dependency on virgin polymers. Recycling of thermoplastics such as Polylactic Acid (PLA) supports circular economy but recycled polymer materials normally exhibits degraded thermal and mechanical properties. To overcome these problems, the re-use of waste based reinforcement materials for composites introduces a potential solution. Introducing waste reinforcements such as almond skin and wood powder into recycled polymers not only increases performance of composites. The combined use of recycled polymer matrix materials and waste-based reinforcement materials enables the production of sustainable materials suitable for 3D printing, contributing to both environment protection and optimum utilization of resources.

The current study examines the rheological, mechanical, thermal, morphological properties of sustainable fused filaments produced using Secondary (2°) Polylactic Acid (PLA) reinforced with waste almond skin and wood powder. Rheological properties shows a reduction in Melt Flow index (MFI) with increasing reinforcement content, where nozzle clogging was observed when reinforcement content increases beyond 9 wt.% which indicates practical upper bar for extrusion. Among all the fused filaments, 2° PLA reinforced with 6 wt.% almond skin exhibited superior tensile performance, showing a 27.46% higher Peak Strength than the corresponding wood powder reinforced filament. The maximum % Break Elongation (%BE) was found as 8.86% for 2° PLA + 6 wt.% wood powder and 5.12% for 2° PLA + 6 wt.% almond skin.

Optimization of process result shows that 2° PLA + 6 wt.% almond skin fused filaments exhibits increases thermal stability and consistent mechanical properties, with optimal extrusion conditions of 0.3Nm torque, 7.5kg load and 175°C temperature. In comparison, 2° PLA + 6 wt.% wood powder demonstrate inferior high-temperature tolerance due to their low specific heat capacity, requiring careful control of processing conditions to maintain acceptable

mechanical properties. ANOVA analysis indicated that temperature was the dominant factor influencing Peak Strength (69.2%) and %Break Elongation (48.82%) of almond skin based reinforcement filaments, whereas load was the governing factor for wood powder based reinforcement fused filaments, contributing 92.9% to Peak Strength and 88.39% to % Break Elongation. FESEM and porosity analysis confirmed a strong correlation between mechanical properties and porosity where lower porosity leading to enhanced strength.

Further, almond skin reinforced filaments processed at lower parameters (0.1 Nm torque, 7.5 kg load and 175 °C) exhibited superior thermal stability, higher heat capacity and improved crystallinity. Tensile and flexural testing of 3D printed specimens showed that almond skin reinforced samples out-performed wood powder based reinforced counterparts, achieving up to 15.71% higher tensile Peak Strength and 12.57% higher flexural Peak Strength. For 3D printed samples, raster angle was found as the most significant factor which affects Peak Strength, while infill density predominantly influenced % Break Elongation. Optimized printing parameters led to higher flexural strength compared to tensile strength, highlighting the suitability of these composites for high-strength automotive components. The primary objective of the present study is to print tensile and flexural specimens with maximum strength for automotive industry.

ACKNOWLEDGEMENT

I would like to express my sincere gratitude to my research supervisors, Associate Professor (Dr.) Kapil Chawla and Professor (Dr.) Jaspreet Singh, for providing me with the opportunity to carry out research in the area of 3D printing. Their invaluable guidance, continuous encouragement, insightful suggestions and patient mentoring throughout the course of this research were instrumental in the successful completion of this work. Their academic expertise and constructive feedback greatly enhanced the quality of this research and contributed significantly to my professional development.

I am deeply thankful to the technical staff of Guru Nanak Dev Engineering College (GNDEC), Ludhiana and the Central Instrumentation Facility Laboratory, Lovely Professional University, for their consistent technical support, cooperation and assistance during the experimental investigations. Their expertise and prompt help ensured the smooth execution of the experimental work.

I would also like to acknowledge Lovely Professional University for providing the necessary facilities, infrastructure and a conducive research environment required to carry out this research work effectively.

Finally, I extend my heartfelt thanks to my family members, friends and colleagues for their constant encouragement, patience, moral support and motivation throughout this journey. Their support played a vital role in helping me overcome challenges and successfully complete this research work.

LIST OF ABBREVATIONS AND SYMBOLS USED

2º PLA	Secondary Recycled Polylactic Acid
AM	Additive Manufacturing
ABS	Acrylonitrile Butadiene Styrene
Adj. SS	Adjusted Sum of Square
Adj. MS	Adjusted Mean Square
ANOVA	Analysis of Variance
BS	Break Strength
%BE	Percentage Break Elongation
CAD	Computer Aided Design
DSC	Differential Scanning Calorimetry
E	Modulus of Elasticity
EDS	Electron Dispersive Spectroscopy
FESEM	Field Emission Scanning Electron Microscopy
FFF	Fused Filament Fabrication
f-value	Fisher's value
HDPE	High Density Polyethylene
LDPE	Low Density Polyethylene
LIBS	Laser-induced breakdown Spectroscopy
LOM	Laminated Object Manufacturing
MFI	Melt Flow Index
OA	Orthogonal Array
PLA	Polylactic Acid
p-Value	Probability Value

PS	Peak Strength
PP	Polypropylene
PC	Poly Carbonate
PVC	Polyvinyl Chloride
PPSF	Polyphenylsulfone
PE	Polyethylene
PA	Polyamide
PEEK	Polyether Ether Ketone
STL	Standard Triangulation Language
T_g	Glass Transition Temperature
T	Modulus of Toughness
TSE	Twin Screw Extruder
UTM	Universal Testing Machine

TABLE OF CONTENTS

	Page no.
Declaration	i
Certificate	ii
Abstract	iii-iv
Acknowledgement	v
List of abbreviations and symbols used	vi-vii
Table of contents	viii-xi
List of figures	xii-xvi
List of tables	xvii-xix
List of publications	xx
CHAPTER 1 - INTRODUCTION	**1-19**
1.1 Introduction	1-6
1.2 Segregation/Identification techniques of plastics	6-9
1.3 Recycling techniques for polymer waste	10-14
1.4 Additive Manufacturing	14-17
1.5 Novelty of the present work	18

1.6 Organization of the thesis 18-19

CHAPTER 2 - LITERATURE REVIEW 20-30

2.1 Literature review related to filament fabrication and 3D printing 20-30

CHAPTER 3 - PROBLEM FORMULATION AND OBJECTIVES 31-32

3.1 Need of the current research work 31

3.2 Observations from literature review 31-32

3.3 Objectives of the research 32

CHAPTER 4 - MATERIALS AND METHODOLOGY 33-49

4.1 Selection of base matrix and reinforcement material 34

4.2 Melt Flow Index (MFI) 34-35

4.3 Selection of Orthogonal Array (OA) 35-36

4.4 Fabrication of fused filaments using Twin Screw Extruder (TSE) 36-37

4.5 Tensile testing using Universal Testing Machine (UTM) 37

4.6 Flexural testing 38

4.7 Field Emission Scanning Electron Microscopy (FESEM) 38-39

4.8 Electron Dispersive Spectroscopy (EDS) 39

4.9 Porosity analysis using Tool Maker's microscope 39-40

4.10 Thermal analysis using Differential Scanning Calorimetry (DSC) 40

4.11 3D printing via Fused Filament Fabrication (FFF) 40-44

4.12 Pilot experimentation 44-48

4.13 Optimization of mechanical properties using Minitab 48

4.14 Analysis of Variance (ANOVA) 49

CHAPTER 5 - RESULTS AND DISCUSSIONS **50-91**

5.1 Melt Flow Index (MFI) Results 50-51

5.2 Tensile Testing of Fused Filaments Prepared using Twin Screw Extrusion 52-56

5.3 Optimization of mechanical properties of fused filaments using Minitab 56-58

5.4 Analysis of Variance (ANOVA) of fused filaments 58-60

5.5 Field Emission Scanning Electron Microscopy (FESEM) of fused filaments 60-61

5.6 Energy Dispersive Spectroscopy (EDS) Analysis 61-62

5.7 Microscopic analysis of fused filaments 63-64

5.8 Porosity analysis of fused filaments 64-66

5.9 Differential Scanning Calorimetry (DSC) of filaments 66-68

5.10 Tensile Testing of 3D printed samples 68-72

5.11 Optimization of mechanical properties of 3D printed tensile samples using Minitab 72-74

5.12 Analysis of Variance (ANOVA) of 3D printed tensile samples 74-76

5.13 FESEM analysis of 3D printed tensile samples 76-77

5.14 EDS of 3D printed tensile sample 77-78

5.15 Flexural testing of 3D printed samples 79-82

5.16 Optimization of flexural samples using Minitab 83-85

5.17 Analysis of Variance (Anova) of 3D printed flexural samples 85-87

5.18 FESEM analysis of 3D printed flexural samples 87-88

5.19 Energy-Dispersive Spectroscopy (EDS) of flexural sample 88-89

5.20 Multi-Response optimization of tensile and flexural testing for almond skin and wood powder 89-91

CHAPTER 6 - CONCLUSIONS **92-93**

Scope of future research work **94**

References **95-106**

LIST OF FIGURES

Figure No.	Figure Name	Page No.
Figure 1.1	Chemical structure of Polylactic Acid	1
Figure 1.2	Experimental set up of LIBS	7
Figure 1.3	Froth floatation process	8
Figure 1.4	Magnetic density separation setup	8
Figure 1.5	Setup for tribo electric separation	9
Figure 1.6	Different recycling techniques	10
Figure 1.7	Summary of recycling techniques	13
Figure 1.8	Shows comparison of conventional and additive manufacturing	14
Figure 1.9	Schematic diagram of Fused Filament Fabrication setup	17
Figure 4.1	Flow chart for methodology adopted in the present research	33
Figure 4.2	Melt Flow Index setup	35
Figure 4.3	Schematic diagram of Twin Screw Extruder	37

Figure No.	Figure Name	Page No.
Figure 4.4	UTM setup for tensile testing	37
Figure 4.5	UTM setup for flexural testing	38
Figure 4.6	FESEM setup	39
Figure 4.7	DSC setup	40
Figure 4.8	Fused Filament Fabrication setup	41
Figure 4.9	Tensile specimen according to ASTM D638-type IV	41
Figure 4.10	Flexural specimen according to ASTM D790	42
Figure 4.11	Repetier-Host V2.1.6 interface window	42
Figure 5.1	Stress strain curve of fused filament for 94% 2° recycled PLA + 6% almond skin	55
Figure 5.2	Stress strain curve of fused filament for 94% 2° recycled PLA + 6% wood powder	56
Figure 5.3	Mean S/N ratio plot for PS of filaments reinforced with almond skin	58
Figure 5.4	Mean S/N ratio plot for %BE of filaments reinforced with almond skin	58
Figure 5.5	Mean S/N ratio plot for PS of filaments reinforced with wood powder	58

Figure No.	Figure Name	Page No.
Figure 5.6	Mean S/N ratio plot for %BE of filaments reinforced with wood powder	58
Figure 5.7	FESEM image of filaments reinforced with almond skin with (a) maximum and (b) minimum PS	61
Figure 5.8	FESEM image of filaments reinforced with wood powder with (a) maximum and (b) minimum PS	61
Figure 5.9	EDS image of filaments reinforced with almond skin having maximum PS	62
Figure 5.10	EDS image of filaments reinforced with almond skin having minimum PS	62
Figure 5.11	EDS image of filaments reinforced with wood powder having maximum PS	62
Figure 5.12	EDS image of filaments reinforced with wood powder having minimum PS	62
Figure 5.13	Photomicrographs at break x-section of almond skin reinforced filaments	63
Figure 5.14	Photomicrographs at break x-section of wood powder reinforced filaments	64
Figure 5.15	Porosity analysis of filaments reinforced with almond skin	65
Figure 5.16	Porosity analysis of filaments reinforced with wood powder	66
Figure 5.17	DSC analysis for varying almond skin proportions	67
Figure 5.18	DSC analysis of filaments reinforced with wood powder having maximum & minimum porosity	67

Figure No.	Figure Name	Page No.
Figure 5.19	Stress-Strain diagram of 3D printed tensile sample reinforced with Almond Skin	71
Figure 5.20	Stress-Strain diagram of 3D printed tensile sample reinforced with Wood Powder	72
Figure 5.21	Mean effect plots for S/N ratio for PS of 3D printed tensile specimens reinforced with almond skin	73
Figure 5.22	Mean effect plots for S/N ratio for %BE of 3D printed tensile specimens reinforced with almond skin	73
Figure 5.23	Mean effect plots for S/N ratio for PS of 3D printed tensile samples reinforced with wood powder	74
Figure 5.24	Mean effect plots for S/N ratio for %BE of 3D printed tensile samples reinforced with wood powder	74
Figure 5.25	FESEM of 3D printed tensile samples reinforced with almond skin having (a) maximum (b) minimum PS	77
Figure 5.26	FESEM of 3D printed tensile samples reinforced with wood powder having (a) maximum (b) minimum PS	77
Figure 5.27	EDS of fractured tensile sample having maximum PS reinforced with almond skin	78
Figure 5.28	EDS of fractured tensile sample having maximum PS reinforced with wood powder	78
Figure 5.29	Stress-Strain diagram of 3D printed flexural sample reinforced with almond skin	82
Figure 5.30	Stress-Strain diagram of 3D printed flexural sample reinforced with wood powder	82
Figure 5.31	Mean effect plots for S/N ratio for PS of 3D printed flexural samples reinforced with almond skin	84

Figure No.	Figure Name	Page No.
Figure 5.32	Mean effect plots for S/N ratio for %BE of 3D printed sample reinforced with almond skin	84
Figure 5.33	Mean effect plots for S/N ratio for PS of 3D printed flexural sample reinforced with wood powder	85
Figure 5.34	Mean effect plots for S/N ratio for %BE of 3D printed flexural sample reinforced with wood powder	85
Figure 5.35	FESEM of 3D printed flexural samples reinforced with almond skin having (a) maximum (b) minimum PS	88
Figure 5.36	FESEM of 3D printed flexural samples reinforced with wood powder having (a) maximum (b) minimum PS	88
Figure 5.37	EDS of 3D printed flexural sample reinforced with almond skin having maximum PS	89
Figure 5.38	EDS of 3D printed flexural sample reinforced with wood powder having maximum PS	89

LIST OF TABLES

Table No.	Table Name	Page No.
Table 1.1	Applications of different plastic polymers	4
Table 4.1	Control log for the experimentation	36
Table 4.2	Parameters fixed for FFF setup	43
Table 4.3	DOE for printing based on Taguchi L9 OA	43
Table 4.4	Selected MFI parameters	45
Table 4.5	Selected parameters for TSE	46
Table 4.6	Selected parameters for 3D printing	48
Table 4.7	Analysis of Variance (ANOVA)	49
Table 5.1	MFI of 2° recycled PLA with and without reinforcements	50
Table 5.2	Tensile testing results for 94% 2° recycled PLA + 6%wt. almond skin	52
Table 5.3	Tensile testing results for 94% 2° recycled PLA + 6%wt. wood powder	53
Table 5.4	S/N ratio for PS and %BE of filaments	57
Table 5.5	ANOVA analysis for PS of filaments reinforced with Almond Skin	59

Table No.	Table Name	Page No.
Table 5.6	ANOVA analysis for %BE of filaments reinforced with Almond Skin	59
Table 5.7	ANOVA analysis for PS of filaments reinforced with Wood Powder	59
Table 5.8	ANOVA analysis for %BE of filaments reinforced with Wood Powder	60
Table 5.9	Tensile testing results of 3D printed samples reinforced with almond skin	70
Table 5.10	Tensile testing results of 3D printed samples reinforced with wood powder	70
Table 5.11	S/N ratio for PS and %BE of 3D printed tensile samples reinforced with almond skin	73
Table 5.12	S/N ratio for PS and %BE of 3D printed tensile samples reinforced with wood powder	73
Table 5.13	ANOVA for PS of 3D printed tensile samples reinforced with almond skin	75
Table 5.14	ANOVA for %BE of 3D printed tensile samples reinforced with almond skin	75
Table 5.15	ANOVA for PS of 3D printed tensile samples reinforced with wood powder	75
Table 5.16	ANOVA for %BE of 3D printed tensile samples reinforced with wood powder	76
Table 5.17	Flexural testing results of 3D printed samples reinforced with almond skin	80
Table 5.18	Flexural testing results of 3D printed samples reinforced with wood powder	81
Table 5.19	S/N ratio for PS and %BE of 3D printed flexural samples reinforced with almond skin	83

Table No.	Table Name	Page No.
Table 5.20	S/N ratio for PS and %BE of 3D printed flexural samples reinforced with wood powder	84
Table 5.21	ANOVA for PS of 3D printed flexural samples reinforced with almond skin	85
Table 5.22	ANOVA for %BE of 3D printed flexural samples reinforced with almond skin	86
Table 5.23	ANOVA for PS of 3D printed flexural samples reinforced with wood powder	86
Table 5.24	ANOVA for %BE of 3D printed flexural samples reinforced with wood powder	87
Table 5.25	Input and output parameter constraints for 3D printed samples reinforced with almond skin	90
Table 5.26	Suggested parametric levels for 3D printed samples reinforced with almond skin	90
Table 5.27	Input and output parameter constraints for 3D printed samples reinforced with wood powder	91
Table 5.28	Suggested parametric levels for 3D printed samples reinforced with wood powder	91

LIST OF PUBLICATIONS FROM THE THESIS

RESEARCH PUBLICATIONS

Sr. No.	Title	Journal	Impact factor/SJR	Status
1	Fabrication and Characterization of Almond Skin Powder Reinforced PLA Based Composite Filaments for Fused Filament Fabrication	Journal of Polymer & Composites (ESCI)	Impact factor: 6.018	Published
2	Mechanical Assisted Blending of Secondary Recycled PLA with Almond Skin for Fused Filament Fabrication	Lecture Notes in Mechanical Engineering (Scopus)	-	Published
3	Investigating Mechanical, Morphological, and Thermal Properties of Secondary Recycled Polylactic Acid Reinforced with Wood Dust for Three-Dimensional Printing Applications	Smart and Sustainable Manufacturing Systems (Scopus)	SJR: 0.252	Published

CHAPTER 1

INTRODUCTION

1.1 INTRODUCTION

Polymers are human-made long-chain molecules composed of repeating monomer units [1]. These characteristics are similar to those found in natural rubbers, which is why polymers are widely used in making everyday materials like plastics, synthetic fibers, packaging and elastomers. Polymers are macromolecules compose of repeated structural unit, typically connects by covalent chemical bond. Term "polymer" originates from the Greek words *poly* (many) & *mer* (parts), indicating their molecular structure of multiple repeating units, or monomers [1]. Behaviour of polymers can be tailored by controlling the type of monomers, degree of polymerization and molecular architecture, giving them a versatility unmatched by many other materials enabling their utilization in different fields. Due to their versatility, polymers have become indispensable materials in modern society [2-4]. The ability to tailor properties such as tensile strength, flexibility, conductivity and biodegradability through chemical design and processing makes polymers highly adaptable for diverse industrial and biomedical applications. Polymers are having different types of structure for example Figure 1.1 shows Polylactic Acid which belongs to group of poly-α-hydroxy acid, a type of linear aliphatic thermoplastic polymer.

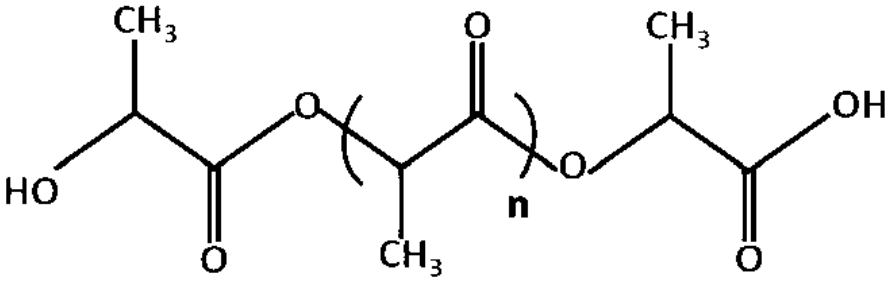

Figure 1.1 Chemical structure of Polylactic Acid [5]

Recent research emphasizes the role of advanced polymeric materials, including nanocomposites, conducting polymers and biodegradable polymers, in addressing global challenges such as environmental sustainability, renewable energy and healthcare. For instance, biodegradable polymers are being developed to reduce polymer pollution and for use in food packaging industry, while polymer nanocomposites are utilized for lightweight, high-strength materials in aerospace and automotive sectors [6-7]. Moreover, polymers have revolutionized medicine through drug delivery systems, tissue engineering, scaffolds and biosensors [8]. This

growth can be attributed largely to their easy processability, which allows them to be moulded, shaped and fabricated into a wide range of products using relatively simple and cost-effective techniques such as extrusion, injection moulding, blow moulding and thermoforming. Unlike metals, which often require high-temperature processing, or wood, which involves extensive mechanical treatment and has limitations in shape and durability, polymers can be processed at lower temperatures and with greater versatility. Polymers can also be classified based on their properties and applications. For example, some polymers exhibit elastic and rubbery behaviour like elastomers, while others may be opaque, strong, or stiff, making them suitable for structural or packaging purposes [9-10].

Polymers are also cost-effective to produce and offer excellent processability, which means they can be easily moulded into a wide variety of shapes and forms to meet specific requirements [11-12]. These advantages make Polymers indispensable in different sectors [13-14]. Their versatility and adaptability ensure that they remain one of the most important classes of engineering materials in the modern world [15-16].

Unlike organic materials such as wood or paper, which can be broken down by microorganisms, the strong covalent bonds and chemical inertness of most polymers do not allow them to decompose easily under natural environmental conditions. Despite offering too many to be countless benefits, the most prevalent issue with Polymers is that it degrades slowly. As a result, Polymers can persist in the environment in their original form for hundreds of years, leading to significant challenges in polymer waste (PW) management and environmental sustainability [17]. This durability, while beneficial for applications requiring long service life, has become one of the most critical drawbacks of Polymers, as their accumulation contributes to soil, water and marine pollution. Landfilling is the most common PW disposal method used worldwide [18]. Waste material buried in landfills, where they may persist for hundreds of years due to their resistance to natural degradation. Although this method is inexpensive, landfilling leads to long-term environmental and health issues such as soil contamination, groundwater pollution and accumulation of non-degraded plastic waste [19-20].

The rapid increase of PW has given rise to several critical socio-environmental complications. One of the most immediate concerns is the reduction in geographic space due to the excessive dependence on landfills, which are rapidly reaching their capacity and occupying land that could otherwise be used for agriculture, housing or ecological conservation [21]. Furthermore, the improper disposal of plastics contributes to widespread terrestrial and marine

pollution, where plastic debris contaminates soil, rivers and oceans, ultimately disrupting natural ecosystems. This accumulation of plastic waste has an adverse effect on biological life, as many species ingest or become entangled in plastic materials, leading to injury, suffocation, or death. Microplastics, formed by the breakdown of larger plastics, further infiltrate freshwater resources and enter food chain, creating potential health risks to human and wild life [22-26]. Collectively, these socio-environmental impacts make PW one of the most pressing challenges of modern society.

These problems arise mainly from wide applications of polymers leading to their extensive use especially in the packaging industry [27]. However, most packaging materials are designed for single-use or a very short service span, such as plastic bags, food wrappers, bottles and disposable containers. Once discarded, these items quickly accumulate in the waste stream because they are produced in enormous volumes [28]. The petrochemical sector in India is the primary source of polymer manufacturing, including ethylene, synthetic fibres and surfactants, which account for 20% of the country's overall chemical industry and are predicted to grow by 14% in the coming years. Due to higher household use of polymers, municipal waste is the major and direct source of PW following which demand for landfilling is also increasing [29]. In 2018, global plastic production reached 359 million tons, representing an almost 20-fold increase over the past 50 years [30]. According to the Central Pollution Control Board (CPCB, India), the country produced approximately 26000 ton of plastic waste/day during 2019–2020 and out of that around 60% is recycled, while the remaining 40% ends up contaminating soil, water bodies, or in landfills. Managing plastic solid waste (PSW) has become essential for conserving natural resources and safeguarding the environment. It helps reduce the quantity of waste sent to landfills, lowers the need for producing new plastics from fossil fuels and minimizes pollution caused by improper disposal [31-33]. Recycling also supports the concept of a circular economy, where discarded plastic materials are reprocessed and reused in manufacturing, thereby extending their lifecycle and reducing environmental impact [34-37]. As a result, improving recycling efficiency and public participation in waste segregation has become a global priority in addressing the plastic pollution challenge.

Classification of polymers is very important from the their point of view [38] and those classifications of polymers are essential for understanding the recyclability and reusability potential of different plastic materials in waste management and recycling processes. Among the different types of polymers, thermoplastics play a dominant role due to their versatility and

ability to replace a large fraction of materials. In contrast, thermosetting polymers are formed from monomers that create highly cross-linked polymer networks through irreversible chemical reactions, resulting in rigid and durable structures. Table 1.1 presents the most commonly used thermoplastics and thermosetting polymers along with their typical applications. Elastomers are highly elastic polymers capable of returning to their original shape after deformation. This property makes them suitable for variety of applications, including automotive components like tires, seals & hoses, construction materials like expansion joints and sealants and medical devices including gloves and tubing. They are also used in consumer products such as footwear soles and sports equipment, as well as in industrial and electronic applications for insulation and vibration-damping components. Their combination of flexibility, durability and chemical resistance makes them essential across various sectors.

Table 1.1 Applications of different plastic polymers [13-14]

Thermoplastics	**Applications**
PP (Polypropylene)	Syringes, packaging containers, ropes and carpets
PC (Poly Carbonate)	Helmets, optical applications, CDs and telecom hardware
PVC (Polyvinyl Chloride)	Water pipes, Intravenous fluid bags, electrical wires and cable and plastic bottles
HDPE (High Density Polyethylene)	Utensils, pipes, chemical containers and toys
LDPE (Low Density Polyethylene)	Computer hardware's tray packaging, optical disc driver and battery casings
PET (Poly Ethylene Terephthalate)	Films for Packaging , yarn for carpets and cosmetic jars
PLA (Polylactic Acid)	Packaging materials for Decomposing, cloth fibres, biomedical implants

Polystyrene	Computer components, TV casings and insulating walls
ABS (Acrylonitrile Butadiene Styrene)	Luggage bags, mobile cases, keyboards and Draining pipes
PA6 (Polyamide)	Electrical circuit breakers, tyres, gears and bearings
Thermosetting	**Applications**
Bakelite	Utensil handles, parts of washing machine, Jigs & fixtures and decorative items
Faturan	Prayer beads & Umbrellas
Silicon	Thermal/electrical insulations, Adhesives, electronic chips and solar cells
Polyester	Touch screen, flexible circuits and clothing
Phenol Formaldehyde	Circuit boards, switches, brake linings and high strength composites
Polyurethane	Refrigerator, freezers, bedding, Furniture, Adhesive, coating, Building insulation
Melamine	Utensils and dinnerware, dry boards, plywood and sound insulation
Urea Formaldehyde	Cotton blend, wrinkle resisting fabric, wall/agriculture cavity fillers
Epoxy	Adhesives, protective coating and sealant materials

Vinyl Ester	Chemical processing, marine industry and wind turbine blades

To effectively manage plastic waste and reduce its environmental impact, plastic recycling has become a critical global priority, offering a sustainable approach to reuse materials while conserving natural resources. Plastic recycling has become essential, as it not only reduces the accumulation of waste but also promotes long-term environmental and economic sustainability But plastic recycling majorly depends on the types of plastic as only collection of PW never ensures the type of plastic. So, prior to recycling of plastic, issue of compatibility between the plastics has be resolved as all the plastics are having different melting points [39]. Blending of two or more than two different plastics reduces the base properties e.g. brittleness of HDPE will increase if blended with polypropylene (PP) [40]. Hence, segregation/identification of plastics is one of the important aspect of waste recycling.

1.2 SEGREGATION/IDENTIFICATION TECHNIQUES OF PLASTICS

- Laser-induced breakdown spectroscopy (LIBS)
- Froth flotation method
- Magnetic density separation
- Tribo electric separation
- X-ray fluorescence
- Fourier transformed infrared technique (FTIR)
- The hyper spectral imaging (HSI) technology

1.2.1 Laser-induced breakdown spectroscopy (LIBS)

LIBS technique primarily used for 6-different polymers such as LDPE, HDPE, PP, PET (Polyethylene Terephthalate), PS (Polystyrene) and PVC (Polyvinyl chloride) [41]. This technique is analysing constituent's hydrogen & carbon available in polymers based on pulsed laser sources [42-43]. Plasma emission produced by laser is recorded for spectral investigation of polymers. Nd: YAG 1.06 μ m of required wavelength is used for calibration by striking laser beam on the surface of waste plastic [43]. Figure 1.2 depicts experimental setup of LIBS.

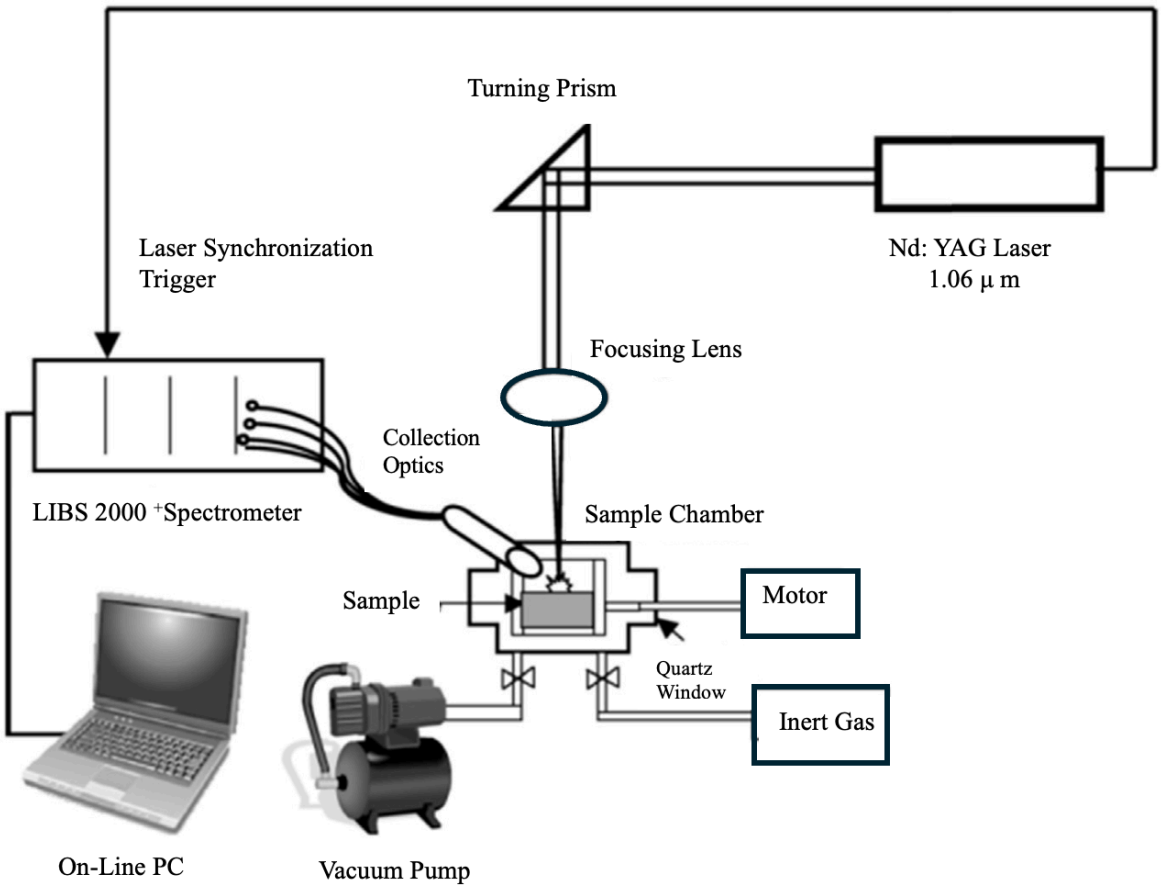

Figure 1.2 Experimental set up of LIBS [43]

1.2.2 Froth flotation method

It is one the separation method for the identification of polymers for segregation. It is low cost and simplest method amongst all other techniques also utilized in processing and mineral industry [44]. Many researchers used this method for PVC and PET separation and they can be separated upto 95%-100% [45]. In this technique, pine oil and methyl isobutyl carbinol (MIBC) as froth agent and calcium lignin sultanate as wet agent are used. MIBC and pine oil gives best result in the recovery of PET and PVC, respectively [41].

In electromagnetic feeder, material and hot water were mixed followed by alkaline treatment which happened in different container. Pulp will form after this process which further supplied to vibrating screen for washing in cold water. Cold water and wet material together fed in to the tank which initially having presence of surfactants to treat it chemically. Products of different streams may get separated and extract in predefined time. This type of process usually requires large space for installation [46-47]. Schematic process of froth floatation process shown in Figure 1.3.

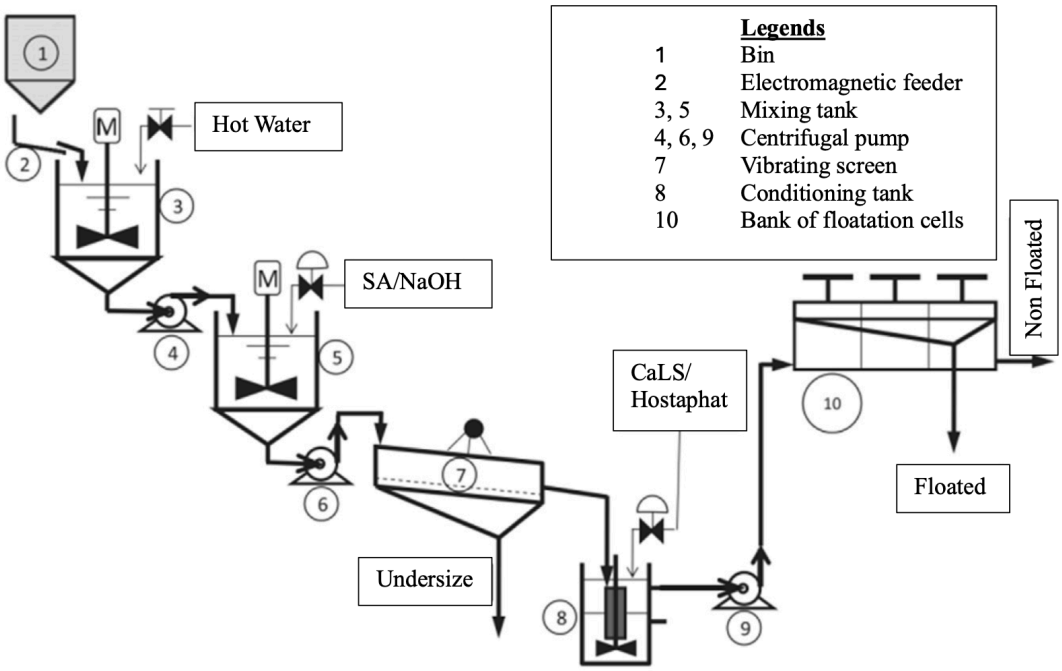

Figure 1.3 Froth floatation process [39]

1.2.3 Magnetic density separation

This process is carried out after manual segregation of polymers. This method is depend upon variation in densities of materials [48]. This method is generally applicable on PP, HDPE and LDPE mixed with metals etc. Magnetic liquid is flowing in this setup moving from left to right with pressure difference and flowing back. To make material surface hydrophilic, boiling water wets int material first for a minute removing heavy plastic particles [49]. Through 1m openings, wet particles fed into box of stainless steel and air gets discharged for the prevention of system from turbulence. When the lid gets opened, particles starts rising up and flows into separation channel. P1, P2, P3 and P4 showing the different separated layers of plastics. Figure 1.4 shows magnetic density separation setup.

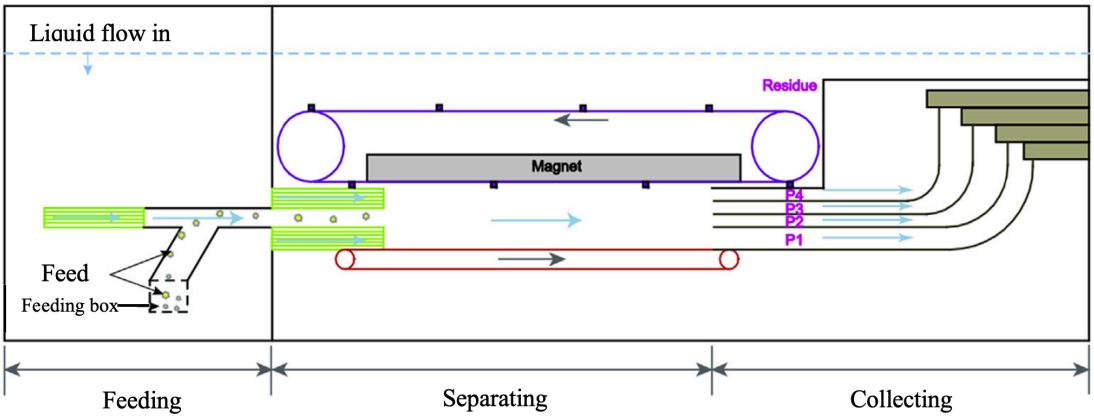

Figure 1.4 Magnetic density separation setup [50]

1.2.4 Tribo electric separation

This method is also called as free fall tribo-electric separation method used for segregation and purify plastic waste material [51]. This method is mainly utilized for the segregation of granular mixture of waste. In this process, two-different materials were fed rotates at same speed, then that material experiences particle to particle force and particle to cylinder force. Charge started appearing when materials gets rubbed against each other. Force acting on particle surface starts segregation due to high electrostatic force. For example teflon is negatively charged whereas PVC takes positive charge when rub against each other. This type of technique can be utilized in the separation of all types of materials. Figure shows the functioning of Tribo electric separation. This method is limited to to 2-4mm particle size material separation [52]. Figure 1.5 depicts setup for tribo electric separation.

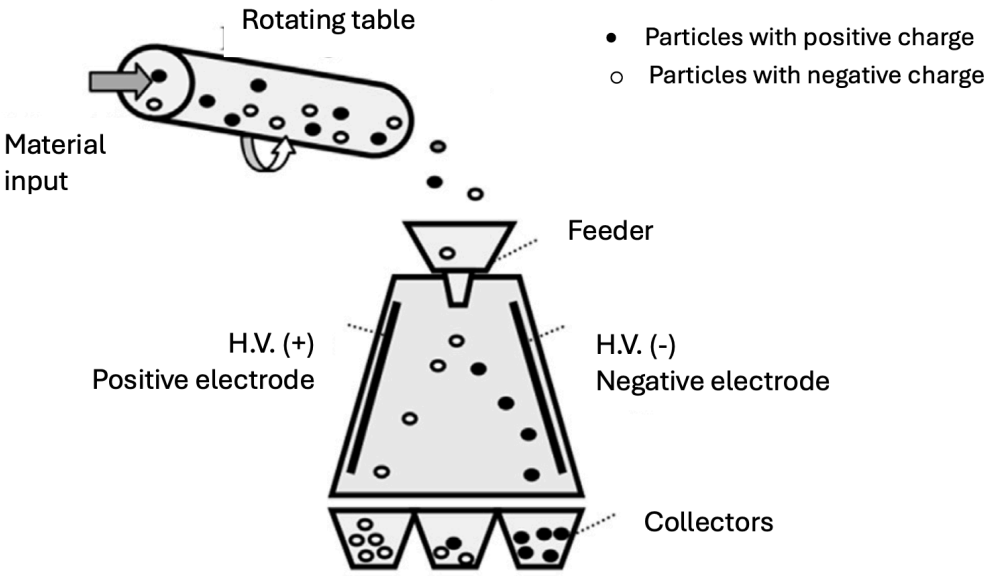

Figure 1.5 Setup for tribo electric separation [51]

1.2.5 X-ray fluorescence

This method is a qualitative method covers variety of material to analyze their chemical composition such as metals, cement and polymers etc. Time needed for measuring particles is depending on how many elements need to be analyzed and can range from seconds to 30 minutes. This method depends on x-rays to irradiate the specimen. X-ray tubes are commonly used, though in some cases synchrotron radiation or radioactive sources may also be employed [53]. The element being analyzed emits fluorescent x-rays with various energy levels (similar to colours in visible light. By detecting and measuring these emitted energy colours, element composition of the sample can be found [41].

1.3 RECYCLING TECHNIQUES FOR POLYMER WASTE

In order to minimize the production of plastic waste and mitigate it's adverse effects on the environment, the 3R approach Reduce, Reuse and Recycle is being widely used by different developing and developed countries. According to this approach, the management of any product, regardless of its material composition, should follow a structured life cycle framework: (i) prevention of waste generation, (ii) reduction of waste at the source, (iii) re-use of products or components, (iv) recycling and (v) disposal through landfilling, considered as the last resort. Recycling, in particular, is a crucial step wherein waste materials are processed and re-utilized either for the fabrication of new products or for other valuable applications, often by improving or modifying their inherent properties. Extensive research indicates that polymer recycling, a key aspect of material sustainability, is generally divided into four types: primary, secondary, tertiary and quaternary recycling, having different methodology, efficiency and end-use potential [54–57]. Implementing these recycling strategies not only conserves natural resources but also reduces environmental pollution and supports the circular economy. Figure 1.6 shows different recycling techniques.

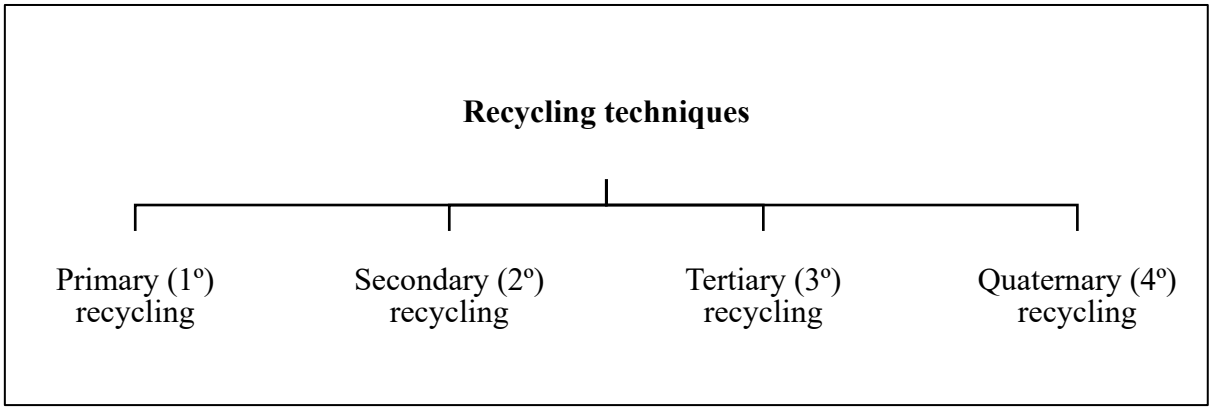

Figure 1.6 Different recycling techniques

1.3.1 Primary (1º) recycling

Primary recycling, also called closed-loop recycling [58], involves uncontaminated waste from industrial production or manufacturing scrap into new products of the same quality as the original material where properties are near to virgin polymers [59-60]. Primary recycling is limited to clean, homogeneous scrap and maintains material properties, making it the most efficient form of recycling with minimal degradation. To improve the properties and functionality of waste materials, clean scrap is sometimes added to collected refuse. In most cases, primary recycling is employed to manage PW generated from household activities.

However, the use of this recycling approach in municipal applications is often constrained due to the high level of contamination present in municipal solid waste. Collection of clean scrap is a foundational step in primary recycling, ensuring that downstream processes such as mechanical or chemical recycling can produce materials with consistent performance and longer life cycles [61-62].

1.3.2 Secondary (2º) recycling

Secondary recycling, also referred to mechanical recycling [63-64], involves reprocessing of waste plastic into new plastic products through physical methods without altering the chemical structure of the polymer. In this process, industrial plastic waste is collected, cleaned, sorted, shredded, melted and remoulded to usable items. Secondary recycling is important because it reduces waste by expanding the range of materials that can be reused, saves natural resources by using "new" sources from waste and is often more efficient than chemical recycling processes. Secondary recycling is now the main method used worldwide to process large volumes of plastic waste, thanks to the broad availability of recycling machinery.

Methods of Secondary (2º) Recycling

Secondary recycling relies on mechanical and physical processes. Steps involved in this method are as follows [65]:

a) Melting and Extrusion: Cleaned flakes or granules are melted in extruders depending upon the application, either single screw extruder or twin screw extruders can be used [5]. This approach uses a hopper to help feed material into the barrel in the shape of granules. The material is melted by the barrel's heater and forced forward toward the die by the screw. For the material to exit the die and form wire, a pressure of up to 500 psi is needed. Below are schematic diagram of a twin screw extruder:
b) Pelletizing: Extruded strands are cooled (water baths or air quenching) and chopped into uniform pellets.
c) Molding and Product Manufacture: Pellets are reprocessed into end-user items.

1.3.3 Tertiary (3º) recycling

In this form of recycling, the monomers of various polymeric materials are recovered from PW through the depolymerization process [41]. In other words, this approach regenerates

the fundamental raw materials used to synthesize new plastics, thereby making a significant contribution to energy sustainability, since most polymers are petroleum-derived products [66]. This method, commonly referred to as chemical recycling, involves depolymerization of PW either by chemical means (solvolysis) or through thermal processes (thermolysis). Furthermore, the process can be conducted in the absence of air (pyrolysis) or under controlled atmospheric conditions (gasification) [67]. Petroleum based products are generally obtained from polymers. If energy sustainability is required, tertiary recycling can be used because primary/secondary recycling both are not contributing in sustainability. In this process, waste plastic is converted into smaller molecules as chemical intermediates through heat and/or chemical treatment.

1.3.4 Quaternary (4^{o}) recycling

This type of recycling is primarily applied to plastic waste that cannot be recycled through conventional methods, such as materials from medical applications or packaging of hazardous substances and is particularly suitable for thermosetting polymers [68]. Repeated reuse of polymers leads to a gradual deterioration of their properties, eventually resulting in disposal in landfills, which contaminates the soil and releases toxic gases. With advancements in modern incineration technologies, many researchers have suggested that energy can be recovered from plastic waste through combustion, thereby reducing waste volume; this approach is therefore also referred to as energy recovery recycling. During incineration, the chemical energy stored in the long-chain polymer structures is converted into thermal and electrical energy [69]. However, since most plastics are derived from petroleum, incineration typically produces gases such as CO_2, SO_x and NO_x [70-71]. Various techniques can be employed to minimize the release of harmful pollutants, including filtration, addition of ammonia to the combustion chamber, flue gas cooling, acid neutralization and repeated flue gas treatment [72]. The recycling methods discussed above are summarized schematically in Figure below, providing an overview of the different approaches used to manage PW. Figure 1.7 explain the summarised recycling process.

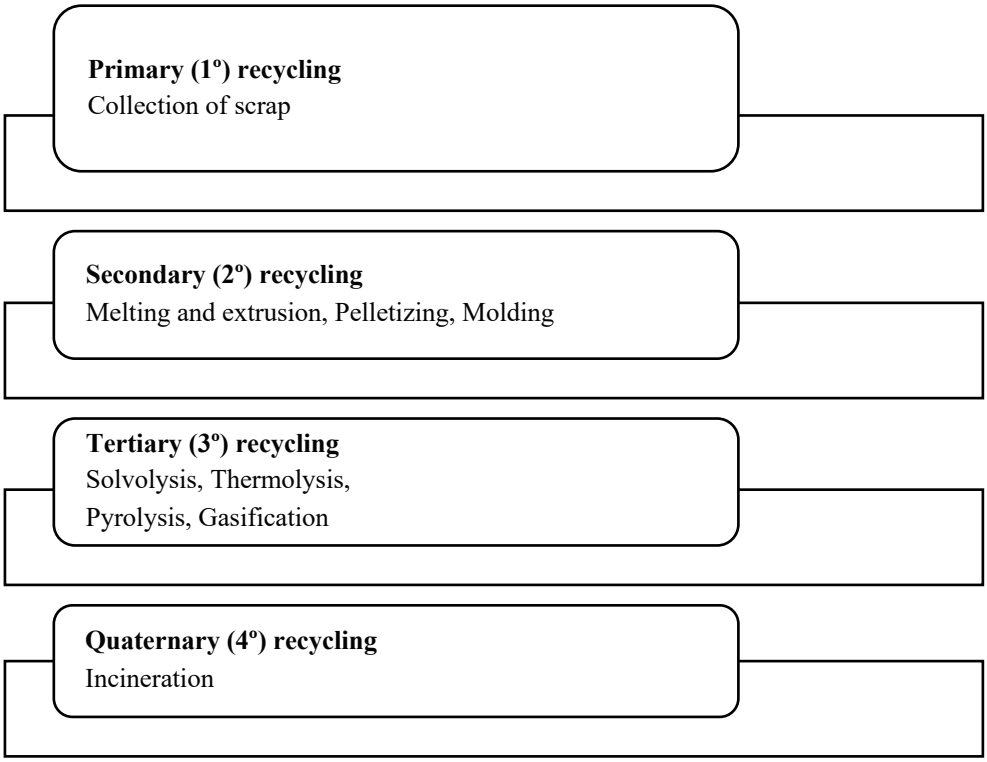

Figure 1.7 Summary of recycling techniques

While various recycling techniques have been developed to manage polymer waste and promote material reuse, recycling alone cannot entirely address the growing global demand for high-performance materials and sustainable production. As industries continue to expand and technology advances, there is an increasing need not only to recycle existing materials but also to manufacture new products that exhibit superior mechanical, thermal and aesthetic properties with minimal environmental impact.

In the present era of modernization and rapid technological advancement, industries across the world are striving to produce high-quality finished goods that possess enhanced mechanical, thermal and aesthetic properties increasing the demand for products that are cost-effective and environmentally sustainable. To meet this rising demand, the manufacturing sector must adopt faster, more precise and resource-efficient production methods. However, conventional manufacturing techniques like drilling, milling, machining and cutting are subtractive, meaning they remove material from a larger block to achieve the desired shape. This approach leads to substantial material wastage, higher production costs and increased energy consumption. Additionally, these traditional methods often involve multiple stages of processing and finishing, which makes the entire production cycle longer and less flexible for customization. Consequently, it becomes difficult to meet global industrial needs solely through

conventional manufacturing due to its limitations in speed, efficiency and sustainability. This challenge has paved the way for advanced manufacturing technologies like additive manufacturing or 3D printing which enables the production of intricate and custom made components with minimal material loss, reduced production time and improved environmental performance. Figure 1.8 explains the comparison between conventional and additive manufacturing.

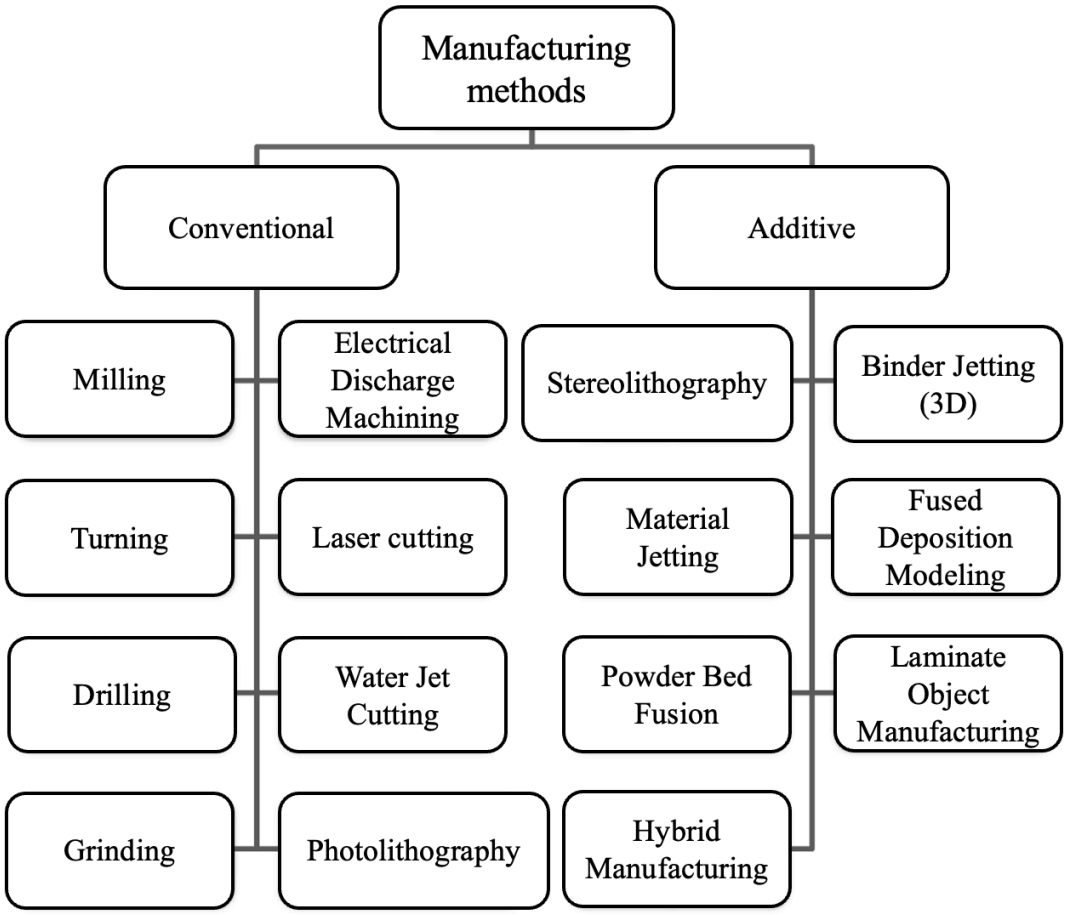

Figure 1.8 Shows comparison of conventional and additive manufacturing [73]

1.4 ADDITIVE MANUFACTURING

The limitation of conventional manufacturing techniques has accelerated the shift toward advanced and digital manufacturing technologies under the framework of Industry 4.0. Among these, additive manufacturing (AM) also known as 3D printing [74] emerged as transformative solution has been widely used now a days in countless industries helps in quick production and reducing wastage [75]. Unlike conventional processes, AM starts from loading of filaments onto spool which furthers deposited layer by layer directly from digital models to

make 3D objects. Moreover, AM offers faster prototyping, customization and design flexibility, aligning perfectly with modern industrial demands for efficiency, sustainability and innovation.

Owing to these unique capabilities, additive manufacturing has found wide-ranging applications across diverse industrial sectors.. In the aviation and automotive industries, AM is used to fabricate lightweight and higher strength components which enhances overall performance. Compared to the aerospace industry, the shipping sector has adopted additive manufacturing more slowly, but its use is steadily growing. Today, warship components are being For example, study by Islam et al. (2024) discusses the utilization of polymer AM in automotive applications, highlighting its potential to manufacture complex parts with reduced material waste [76]. In the biomedical area, AM enable the production of custom made implants and prosthetics for single patients. Research by Alghamdi et al. (2021) provides a comprehensive review of the advancements in polymer AM for medical applications, including the development of patient-specific devices [77].

Furthermore, the integration of recycled polymers into AM processes has gained significant attention as a sustainable manufacturing approach. A study by Habiba et al. (2024) explores the use of recycled materials like PLA, Polyethylene Terephthalate (PET) and Acrylonitrile butadiene Styrene (ABS) in AM, emphasizing the environmental benefits and material efficiency of this practice [78]. following are the various additive manufacturing techniques used for various application:

1.4.1 Selective Laser Sintering (SLS)

SLS is leading additive manufacturing method which generates high quality finished parts directly from computer aided design (CAD) files saves significant time [79]. This technique is using carbon dioxide laser beam for the fabrication of models, selectively. Initially, The SLS machine takes 2D information about each layer of the object and uses this information to determine where the laser should aim and move. The laser beam scans across the powder bed, heating the material to its sintering temperature so that the particles fuse along the defined path. Once the first layer is solidified, the build platform lowers by thickness of one layer and fresh coat of powder spread over the surface[80]. This layer-by-layer method continues until the entire component is completely built. Additionally, parts produced through SLS can be recycled by crushing them back into powder for reuse. A huge types of materials can be used in SLS for example polymers, ceramics, metals and combination of them [81].

1.4.2 Stereolithography (SL)

Stereolithography (SL) is a layer-by-layer fabrication method that closely related to gel-casting, as both depends on photopolymerization of ceramic powder suspensions dispersed in solution of monomers. In the SL process, a UV light source solidifies the liquid suspension to form the desired shape. The efficiency of photopolymerization is majorly influenced by the characteristics of the monomer, the selected photo-initiator and the manner in which light travels through the suspension. Photon transport within the suspension is affected by particle-induced scattering as well as absorption by photo-initiators and added inert dyes [82].

In the process of SL, the component is formed on a build platform which is repeatedly immersed in a liquid monomer. When light is projected onto the surface, the exposed region undergoes photopolymerization and gets solidifies. After the solidification of each layer, thin film of monomer deposited over the previous one and the cycle continues layer by layer until the entire part is fabricated [83]. The manufacturing data is obtained from CAD or similar design software and then converted into sequential layers using STL.. Once the layer-by-layer fabrication is complete, the component is removed from remaining raw liquid to form ceramic green body, which is subsequently prepared to obtain the final product [83-87]. Stereolithography offers many benefits, including its ability to fabricate parts with variety of shapes and sizes, along with high precision and rapid production rates. The materials commonly employed in SL includes epoxy resins, acrylate-based resins and thermoplastic elastomers [75].

1.4.3 Laminated Object Manufacturing (LOM)

This method integrates both additive and subtractive manufacturing approaches. The feedstock is supplied in the form of sheets, which are fused together using heat, pressure and a thermally coating. Excess material from each layer is removed by using a CO_2 laser. A key limitation of this technique is the significant material waste it generates and the resulting components often exhibit direction-dependent properties. It is suitable for use with paper, composite materials and certain metals [88].

1.4.4 Fused Filament Fabrication (FFF)

FFF is one of the widely used and cost-effective 3D printing technologies [89] The process begins by loading a spool of thermoplastic filament through heating system [90]. Once the nozzle reaches the designated temperature, the extruder pushes the filament through hot nozzle,

where it melts. Printer then precisely moved the nozzle along the X-Y plane, depositing molten material onto the print bed. Within milliseconds, the material solidifies. After each layer is completed, the print bed lowers slightly and the process continues layer by layer until the digital CAD model is transformed into a physical 3D object. FFF is a popular and accessible type of additive manufacturing (3D printing) technology used to create three-dimensional objects from digital designs [91]. The initial step involves creating a 3D CAD model of the specimens using SolidWorks 2014. This CAD file is then processed in Slice3r, where it is converted into STL format and subsequently used to generate G-code. Once the G-code is ready, Repetier-Host V2.1.6 software is employed to control the 3D printing process, as illustrated in Figure 4.11. Repetier-Host reads the G-code and directs the 3D printer to carry out the printing process. The printer then fabricates the model by sequentially depositing layers through extrusion, forming the final object layer by layer. A key feature of the printer is the ability to manually change the feedstock filaments at any desired point during the printing process. It is equipped with two separate nozzles, one designated for model material and other one for support material, each responsible for extruding their respective filaments. Further, various parameters such as bed temperature, nozzle temperature, air gap, layer thickness and raster width etc. are required to be fixed. The materials most frequently used in the FFF process include PLA, investment-casting wax, ABS, PC, Polyphenylsulfone (PPSF), Polypropylene (PP), Polyethylene (PE), Polyether Ether Ketone (PEEK) and Nylon (PA) etc. [92]. Figure 1.9 Fused Filament Fabrication setup.

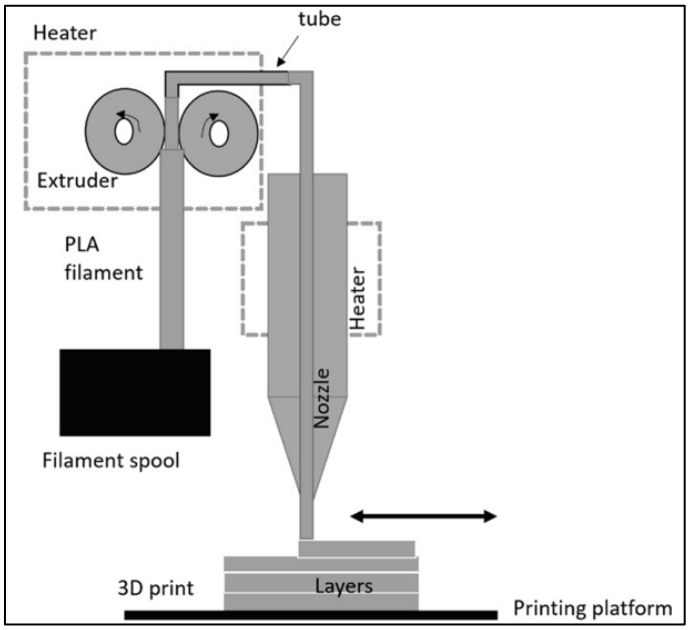

Figure 1.9 Schematic diagram of Fused Filament Fabrication setup [92]

1.5 NOVELTY OF THE PRESENT WORK

The literature review showed that most of the research work was conducted on mechanical, thermal, morphological properties of virgin polymers reinforced with different materials. However, there is limited research focusing on morphological, mechanical properties of polymers reinforced with industrial waste materials at varying weight proportions. A review of the literature indicates that while extensive research has been conducted on virgin polymer, there is a significant gap regarding sustainable composites that pair a recycled polymer matrix with industrial waste reinforcements. This study addresses this limitation by evaluating a novel, dual-waste approach utilizing recycled polymers reinforced with various industrial waste materials such as almond skin, rice husk, nutshell powder, cellulose, and wood powder are thus leveraged as unique, eco-friendly, and cost-effective alternatives to conventional synthetic fillers.

These waste materials to be used as reinforcements are abundantly available as by-products of agricultural, processing industry and wood-processing industries, making them environmentally safe. Unlike many commonly used natural fillers that may require additional processing or chemical treatment, almond skin and wood powder may be used with minimum processing which reduces overall production costs.

The novelty of the current research rests in using secondary recycled PLA reinforced with industrial wastes such as almond skin and wood powder for sustainable and circular 3D printing applications. Further comparative analysis of composites made from 2ºPLA+almond skin and 2ºPLA+wood powder allows to investigate how waste reinforcement material affects mechanical properties, printability and morphological properties in fused filament fabrication (FFF). Adding waste materials into 2º PLA matrix, also a complete sustainable manufacturing in terms of circular economy and environment impact etc. overall, current research work is an innovative idea to produce eco-friendly high performance via 3D printing which further may get enters to the stream of waste materials. 3D printed composite parts prepared using 2º PLA reinforced with almond skin and wood shows the potential to be utilized in the fabrication of lightweight and high strength automobile components.

1.6 ORGANIZATION OF THE THESIS

Present research work is divided into the following six-chapter:

Chapter 1 highlights the brief introduction about the polymer and additive manufacturing along with applications. It also highlights the different types of polymers along with their applications. It also highlights the various recycling methods and different types of additive manufacturing. The aim of the present research work and a brief introduction of the thesis has been explained.

Chapter 2 includes the work done by different researchers in the field of feedstock filaments and FFF. Literature review has been divided into two parts where first part reviewed the work done by the researchers related to the Feedstock filaments and in the second part, literature review was done related FFF for printing to tensile and flexural specimens etc. to examine their properties.

Chapter 3 explain the problem formulation and need of the research based on a literature review. This chapter depicts various objectives used in the present work.

Chapter 4 outlines the detailed methodology followed in conducting the experiments for the present work. It also includes the various techniques, testing procedures and equipment utilized in the current work.

Chapter 5 explains a the experimental result and related discussions. It identifies key factors contributing to improved material properties as determined through Taguchi experimentation and ANOVA analysis.

Chapter 6 presents the key conclusions derived from the research and outlines potential directions for future work. The chapter concludes with the list of references.

CHAPTER 2

LITERATURE REVIEW

A detailed review of literature was carried out and presented in this chapter which helps in identifying the research objectives. The review of literature includes work done on fused filaments for 3D printing and FFF in printing tensile and flexural specimens.

2.1 LITERATURE REVIEW RELATED TO FILAMENT FABRICATION AND 3D PRINTING

Abbas et al. has carried out investigation of thermal and mechanical properties of composites by reinforcing bio-additives arginylgly-cylaspartic acid (RGD) in 3 different polymer which are poly(lactic-co-glycolic acid) (PLGA), polycaprolactone (PCL) and PLA in different weight %age i.e. 5% and 10%. Filaments have were prepared using TSE followed by FDM. From thermogravimetric analysis (TGA), it has been observed that the addition of bio-additives leads to changes in thermal properties of the base polymers, with all bioactive materials exhibits a 1-step degradation process. In general, an increase in bio-additive content resulted in a reduction in the degradation temperature. Author has observed maximum tensile strength of 42.36 MPa by using PLA/RGD10% as compared to other composite polymers [93]

Billah et al. has fabricated various filaments by reinforcing ABS with 20 wt.% glass fiber and short carbon fiber to examine their mechanical stiffness and thermal behavior using Differential Scanning Calorimetry (DSC). The filaments have been fabricated at uniform barrel temperature of 200 °C and an 50 rpm extrusion speed. The results showed that the mechanical stiffness of ABS reinforced with short carbon fiber increased by 272%, while that of ABS reinforced with glass fiber improved by 84% compared to unreinforced ABS. Additionally, ABS composites containing short carbon fiber exhibited significantly higher thermal stiffness than both glass fiber reinforced ABS and neat ABS [94].

Bhandari et al. has compared tensile properties of PETG/SCF (polyethylene terephthalate-glycol (PETG)) and PLA/SCF 3D printed parts prepared using extrusion-based printing. Authors found that PETG/SCF and PLA/SCF parts shows the low inter layer tensile strength as compared to neat PLA and PETG in 3D printed parts [95].

Cao et al. has examined the impact of reinforcing 30 V% carbon fiber (CF) on tensile properties of the 3D printed PLA tensile specimens made through FDM. Reinforcing the CF,

reduction in tensile strength of PLA part from 54.51MPa to 49.41MPa has been observed. However, the Young's modulus enhanced from 1.04 GPa to 1.26 GPa and the Break Elongation increased from 6.26% to 7.81% of the PLA-CF when compared with the pure PLA part. The significantly higher Young's modulus of the carbon fiber compared to PLA results in increasing Young's modulus of the PLA - CF composite, making it stiffer than the pure PLA specimen [96].

Ismail et al. has prepared PLA composites reinforced with glass fiber in different concentrations of 1.02%, 2.39%, 4.98% and pure PLA using 3D printing via fused deposition modelling (FDM) to investigate their tensile properties. It has found that with increasing glass fiber concentration, tensile strength increases but upto 2.39 wt% of glass fiber, afterwards, tensile strength decreases upon increasing glass fiber content because composite becomes brittle. The SEM images revealed that with an increased glass fiber content, the average line width of the deposited material also increased, while the layer height remained consistent throughout the samples. [97].

Kalimithu et al. has created composite filaments using PLA matrix by reinforcing 5% and 10% loading of tamarind shell powder (TSP) using twin screw extruder at 190° C temperature, 40mm/s speed and 1.74mm diameter. Author has observed that tensile strength of PLA composite filaments by reinforcing 10 wt% TSP was higher than tensile strength of 5 wt% reinforcement of TSP. Further, author concluded that PLA/TSP composites may be used in biomedical application [98].

Kumar et al. has investigated mechanical properties of 3D printed onyx reinforced with glass fibre using tensile testing, hardness testing and ANOVA. FFF was used to deposit polymer layers and continuous filament fabrication was used to print the fibre layer. L9 orthogonal array was used involving 3 parameters each at 3 levels such as infill pattern, roof layer, infill orientation. Maximum tensile strength and hardness was observed for sample 9 with honeycomb pattern, 6 roof layers and 45° infill orientation. Increasing layers of fibers in 3D printing enhance mechanical properties significantly as improvements shown in durability and strength. ANOVA results confirms that roof layer is the most influential parameter which significantly affects tensile strength and hardness [99].

Kumar et al. has investigated various properties of 2° PLA reinforced almond skin powder (AS) composite filaments prepared using different TSE parameters i.e. temperature,

load and torque. AS was reinforced in different proportions of 3 %wt., 6 %wt. and 9 %wt. MFI results indicate that increasing the reinforcement content beyond 9 %wt. results in nozzle clogging during extrusion. Therefore, a 6 %wt. proportion was selected for the effective utilization of industrial waste. The 2° PLA + 6 %wt. almond skin powder composite filament achieved its maximum Peak Strength of 43.85 MPa under a load of 12.5 kg, torque of 0.1 Nm and an extrusion temperature of 195 °C. Porosity analysis shows that less porosity percentage in the filaments results in better mechanical properties [100].

Kumar et al. has carried out investigation of mechanical characterization of Multi-walled-CNT reinforcement based High Density Polyethylene (HDPE) nanocomposites developed fused filament fabrication (FFF) 3D printing. Author developed nanocomposites using 0.5, 1, 3 and 5 by wt% MWCNT as reinforcement in HDPE matrix. Author observed decrease in Melt Flow Index (MFI) when MWCNT content increase in nanocomposites due to increase in viscosity which leads to reduced flow of material through nozzle. Further, from differential scanning calorimetry (DSC) results, it has been observed that tensile, flexural modulus and strength improves with increased content of MWCNT At higher loadings, MWCNTs tend to form network structures that hinder crystal growth and restrict the development of large, uniform crystallites, leading to a reduction in the degree of crystallinity [101].

Kariz et al. has examined influence of addition of wood on PLA-based filaments utilized for 3D printing and fabricated 6 types of filament with wood loadings ranging from 0 to 50 wt.% and found that filament density decreased as the wood content increased. The highest tensile strength of 57MPa has been achieved with 10wt.% wood content, which declined to 30 MPa when the wood content reached 50 wt.%. Moreover, higher wood content led to rougher surface textures due to increased void formation [102].

Kartal et al. has developed PLA-based composite filaments by incorporating waste beach sawdust (WBS) using a single screw extruder to examine various mechanical properties, including flexural, tensile and impact strength. The WBS has been added in different percentage of 5%, 10%, 15%, 20% to the PLA matrix for filament fabrication. Tensile testing was performed using a Universal Testing Machine. The authors found that when the WBS increases from 0% to 5%, the tensile strength decreased slightly from 56.03MPa to 52.78MPa. However, with further increases in WBS percentage, the tensile strength dropped more significantly [103].

Kozień et al. explored the development of ceramic-reinforced PLA composite filaments for fused deposition modeling (FDM) applications by incorporating boron carbide (B4C) and silicon carbide (SiC) particles into the polymer matrix to examine the printability, rheological and thermal properties . The ceramic fillers were added in different weight percentages, and the composite filaments were fabricated using a commercial extrusion system. It was observed that filaments containing lower ceramic concentrations exhibited better dimensional consistency and smoother surface morphology, while higher filler loadings required multiple extrusion cycles to improve filament uniformity. In terms of printability, SiC-filled PLA composites showed successful extrusion and printing up to 20 wt.% after double extrusion. Rheological analysis indicated shear-thinning behavior at lower ceramic contents, whereas highly filled composites demonstrated near-Newtonian flow characteristics. Thermal characterization through TGA and DSC revealed that the suitable processing temperature range for the developed composite filaments was between 200 °C and 270 °C. The study confirmed that ceramic-reinforced PLA filaments can be effectively utilized in FDM printing to enhance thermal and functional performance for advanced engineering applications [104].

Lau et al. has examined tensile properties of kenaf fiber reinforce PLA 3D printing filament composite by adding 5 %wt., 10 %wt., 15 %wt., 20 %wt. in PLA. Filaments have been prepared at 190°C temperature and at speed of 15rpm via twin screw extrusion. Prepared filaments were taken for testing their tensile properties and they have observed that PLA/15 %wt. kenaf fiber possesses maximum ultimate tensile stress as compared to 5 %wt., 10 %wt., 20 %wt. kenaf fiber reinforced PLA [105].

Leon et al. has developed a novel material to enhance the adhesive properties in additive manufacturing by blending the thermoplastic polymer ABS with thermoplastic polyurethane (TPU). Filaments were produced using a single-screw extruder operating at a screw speed of 60 rpm and an extrusion temperature of 230°C, with TPU content varied between 10 and 30 wt.% in the ABS matrix. These filaments were then used to study the mechanical properties of 3D-printed tensile specimens. FTIR analysis revealed that increasing the TPU content improved interlayer adhesion and the best yield strength was observed at 30 wt.% TPU [106].

Lourenço et al. investigated Kahili ginger (KG) fiber-reinforced PLA composites for sustainable FDM 3D printing applications using alkaline and alkaline/silane fiber treatments. Author prepared filaments using single screw extruder and the extrusion process was carried out using a fixed temperature profile of 180°C, 185°C, 190°C while maintaining a screw speed

of 3.5 rpm. The extruded filaments exhibited a uniform circular cross-section with a consistent diameter of 1.75 mm. Composite filaments containing 5, 10, and 15 wt.% KG fibers were successfully fabricated, although 15 wt.% filaments showed significant defects and poor printability. 3D printing was performed using FFF technology and the best print quality was achieved at 5 wt.% fiber loading, while 10 wt.% composites exhibited improved tensile strength and superior compressive performance compared to neat PLA. Flexural properties also increased, particularly for alkaline-treated composites, indicating enhanced rigidity and interfacial bonding. Overall, alkaline-treated KG/PLA composites shows enhanced mechanical performance and good printability, highlighting their potential as eco-friendly reinforcement materials for 3D printing applications [107].

Makannavar et al. has conducted the study to evaluate the tensile properties of graphite reinforced Acrylonitrile Butadiene Styrene (ABS) composites produced by twin screw extrusion for making of filament for FDM-3D printing. Author observed that components exhibiting enhancement in ultimate tensile strength of graphite filled ABS when compared with virgin ABS components [108].

Masood et al. has developed a novel composite by incorporating iron (Fe) powder into polyamide to produce filaments for FDM. They utilized 2 separate Fe particle size of fine and coarse and observed that increasing the filler content enhanced both the thermal conductivity and the melt flow rate (MFR) of the composite. Since Fe acts as an effective heat retainer, the study revealed that thermal conductivity is strongly dependent on particle size, with fine Fe particles exhibiting higher thermal conductivity than coarse ones [109].

Memis et al. has conducted a study to develop PLA reinforced with 5% iron (Fe) composite filaments. Laboratory type filament extruder was used to prepare filaments to investigate various mechanical properties. They observed that Fe-reinforced PLA-based filament exhibits a 49.60% improvement in tensile strength and 21.15% increase in hardness as compared to pure PLA filament, along with a 4-times increase in surface roughness. The particle shape, size and uniform distribution observed in the scanning electron microscopy of the PLA filament fractured surface are consistent with pure PLA materials [110].

Maqsood et al. has prepared composite using four groups of samples using PLA, continuous-carbon fiber/PLA (CCF/ PLA), short-carbon fiber/PLA (SCF/PLA) and CCF-SCF/PLA to examine their flexural, tensile properties. These samples were prepared to increase

mechanical performance of thermoplastic components. Authors found that the CCF reinforced PLA samples shows the highest young's modulus and tensile strength which is 27.93GPa & 245.4MPa, respectively. Strength of CCF/PLA samples was 460% more than strength of both SCF/PLA and virgin PLA samples and 7.84% more when compares with CCF-SCF/PLA samples. The CCF/PLA samples exhibits the higher average flexural strength at 168.88MPa, exceeding another composite representing increase of 121% compared to PLA/SCF, 103% compared to pure PLA, & 44.6% compared to CCF-SCF/PLA samples. Additionally, the SCF/PLA composites with CCF achieves highest mean flexural modulus of 10.85GPa [111].

Minhaz et al. examined the development of secondary recycled PLA composites reinforced with stubble waste powder (SWP) for sustainable FFF-based consumer products. In this study, author fabricated 3D printed samples using FFF as per ASTM D 695 standard. Optimized printing conditions, including 100% infill and 80 mm/s printing speed, produced samples with a compressive strength of 59.93 MPa, showing an 89.11% improvement over virgin PLA where these compressive properties of the composite are suitable for interior automotive components such as gear knobs. Morphological analysis confirmed good interfacial bonding with reduced porosity (15.24%), grain size number (GSN) of 5 and low surface roughness (Ra = 11.33 nm). The results highlighted that infill percentage was the most influential parameter affecting compressive strength, demonstrating the potential of recycled PLA-SWP composites for eco-friendly automotive applications. Author suggested that the infill percentage is the only significant parameter for compressive strength with 95% significance level [112].

Petousis et al. has investigated effectiveness of Titanium Nitride (TiN) as reinforcement into PLA thermoplastic matrix and prepared nanocomposite using material extrusion (MEX) 3D printing. 3D printed samples then taken for mechanical testing, thermal properties, morphological properties and structural properties of the nano-composites. Author observed improvement in the flexural strength and tensile strength by 51.5% and 43.4% respectively for 4wt% TiN content nano- composite and also reported that the addition of TiN can give better mechanical properties of PLA while using MEX 3D printing because nanoparticles fills void spaces in matrix causing solid composite with higher strength. SEM images shows defect free structure with better interlayer fusion. Thermal analysis indicates that adding TiN to the PLA, at all loadings, does not significantly affect the material's thermal behavior [113].

Rodriguez-Pacheco et al. has developed filaments for FDM by reinforcing zine carbonate basic (ZCB) in PLA matrix via extrusion. Author has used ZCB in various weight fractions like 10%, 20%, 30%, 40% and 50% to reinforce in PLA matrix. Author observed nozzle clogging at different weight %ages except 10% ZCB. The ration of 10% has been chosen as it represents the highest %age of ZCB that can be extruded [114].

Ryder et al. has developed a new technique to produce filaments by the chemical blending of ABS with Stainless steel (SS420) by varying weight proportion of SS420 with 10, 15 and 23%. to investigate different mechanical properties such as tensile, thermal and morphological properties. The author found that filaments prepared at 15% wt. SS420 and ABS have superior mechanical properties as compared to filaments prepared without reinforcement. Sharp reduction in mechanical properties has been observed upon further increase in wt.% of SS 420 in the base material [115].

Santos et al. has examined mechanical properties of polymer composites prepared through fused filament fabrication (FFF). Composite was prepared using PLA filament as matrix material and vegetable yarns such as jute, ramie, sisal as reinforcement with diameters ranges from 0.5mm to 2mm. Author observed the specimens reinforced with sisal fiber showed 28.6% improvement in maximum strength as compared to pure PLA matrix using 48.2% fiber content which attributed to low resistance gains and low adhesion [116].

Saleh et al. has prepared the filaments and 3D printed samples from PLA reinforced with recycled carbon fiber (rCF) with different compositions 3wt%, 5wt%, 8wt% and 15wt% using single screw extruded and FDM printer, respectively. Author observed homogenous distribution of rCF in PLA matrix. While the addition of rCF tends to increase the tensile modulus**,** it may slightly reduce ductility and tensile strength**,** particularly at higher filler concentrations due to fiber agglomeration and void formation. SEM images confirmed a uniform distribution of recycled carbon fibers (rCF) within the PLA matrix, indicating effective dispersion of the reinforcement throughout the composite. Thermal analysis revealed an improvement in thermal stability, with the degradation on set temperature increasing by approximately 8°C when compared with neat PLA [117].

Schmitz et al. has investigated the influence of material composition and electrical conductivity on ABS-based composites. They prepared three filament formulations: ABS with 5wt.% carbon black (CB), ABS with 5wt.% carbon nanotubes (CNT) and hybrid composites

containing a total of 5 wt.% additives with a 75:25 CNT-to-CB ratio. Test specimens have been printed in 3 orientations - horizontal with ±45° raster angle, horizontal concentric & perpendicular concentric to evaluate the effect of reinforcement type on electrical conductivity. The results showed that electrical conductivity was strongly dependent on the presence of CNTs, increasing notably with their inclusion. Specifically, ABS with 5 wt.% CB exhibited conductivity values around 10^{-12} $S \cdot cm^{-1}$, while the hybrid composites and ABS with 5wt.% CNT showed enhanced conductivities ranging between 10^{-8} and 10^{-5} $S \cdot cm^{-1}$ [118].

Singh et al. has examined different mechanical and rheological properties of the feedstock filaments prepared via reinforcing almond skin from 0%wt. to 5%wt. in the base PLA. It was found that filament prepared by reinforcing 5%wt. almond skin in base PLA has better mechanical strength as compared to filament prepared by reinforcing almond skin powder at 9 %wt. It was also noticed that with rise in weight proportion of reinforcement after 10 %wt. MFI decreased which results in nozzle clogging [119].

Sharma et al. has explored 4D printing applications of polyvinylidene fluoride (PVDF) composites reinforce with barium titanate ($BaTiO_3$) and graphene (Gr), using a D33 meter to evaluate their 4D functional properties. Feedstock filaments were produced using a twin-screw extruder (TSE) with varying weight proportions of $BaTiO_3$ and graphene to study their mechanical and rheological behavior. The optimal performance was achieved with the composition PVDF (78 wt.%), Gr (2 wt.%) and $BaTiO_3$ (20 wt.%), which exhibited superior mechanical and rheological properties compared to other formulations with $BaTiO_3$ (0–25 wt.%) and Gr (0–5 wt.%) [120].

Shubmugam et al. has fabricated PLA based composite filaments by reinforcing 25 wt.% orange peel powder (OPP) using twin screw extruder at 160°C temperature for use in 3D printing. Author examined thermal properties of the composite filaments and found that adding OPP in PLA matrix increases thermal stability at higher temperatures [121].

Stoof et al. has conducted experiments to evaluate mechanical properties of PLA composite reinforces with hemp and harakeke fibres in varying proportions from 0 to 30 wt.%. Feedstock filaments with a diameter of 3 mm were prepared for 3D printing. Results showed that the highest tensile strength of 38MPa has been achieved for the PLA composite containing 10 wt.% hemp, while the second-highest tensile strength of 37 MPa was observed for the PLA

composite with 20 wt.% harakeke. Additionally, the maximum Young's modulus, exceeding 4 GPa, was recorded for PLA composites reinforced with 20–30 wt.% harakeke [122].

Suvanjumrat et al. has examined the effect of adding parawood powder in PLA matrix on mechanical properties of 3D printed specimens. Experimental findings showed that increasing the wood powder content from 5% to 10% w/w leads to a reduction in specimen strength because increased amount of wood content leads to increase in viscosity of the polymer. However, blending wood powder at a 15% w/w ratio results in the highest observed strength among the tested samples [123].

Tambrallimathy et al. has examined the characteristics of two different polymers by incorporating filler materials to enhance their mechanical performance. Polycarbonate and ABS were blended with varying amounts of graphene (Gr) as a filler, ranging from 0.2% to 0.8% by weight, to produce feedstock filaments for FDM. The study revealed the inclusion of graphene leads to a notable improvement in Young's modulus, thermal behavior and glass transition temperature due to effective dispersion and strong interfacial bonding within the composite. Furthermore, the inclusion of 0.8wt.% graphene resulting in 7.6% rise in glass transition temperature (Tg) and 3.8% enhancement in thermal degradation resistance [124].

Thirugnanasamabandam et al. has investigated and compared the mechanical properties of 3D printed wood flour reinforced PLA (WPLA), PLA reinforced with ceramic (CPLA) and functionally grade structural material (FGSM). It has been observed by the author that the FGSM laminate showed higher tensile and compressive strength compared to WPLA, but observed as decreased when compared to CPLA. This improvement is attributed to enhanced interfusion between layers in multilayer structure contributing to superior tensile performance. Its flexural strength improved by **1**07.8% over WPLA and was 16.39% lower than that of CPLA, indicating excellent performance to WPLA and near-comparability with CPLA which was because of contribution of weak WPLA in FGSM [125].

Trivedi et al. has investigated the effect of different weight %age of crystalline nano cellulose (CNC) like 0%, 1%, 3% and 5% on the crystallinity, morphology mechanical as well as dynamic properties of 3D-printed PLA-based bionano-composites. Further, study found that incorporation of CNCs significantly enhanced the crystalline behavior**,** mechanical and dynamic mechanical properties of bionano-composites. Notably, flexural and tensile strengths reaches peak at 1wt% CNC, showing improvements of 39.4% and 64.17%,

respectively, compared to virgin PLA. Furthermore, impact strength consistently increased with higher CNC content, with the maximum value of 16.92 kJ/m² observed at 5 wt% CNC, representing a 53.95% increase over pure PLA. The Tg of bio-nanocomposites persisted mainly unaffected by inclusion of CNC in PLA matrix. SEM results shows homogeneous dispersion of CNC particles in PLA matrix and indicates their strong interfacial bonding [126].

Wang et al. has prepared PLA composite filaments by reinforcing carbon fiber (CF) in ratio of 100 wt% PLA, 5wt% CF and 95 wt% PLA, 10 wt% CF and 90wt% PLA using twin screw extruder for use in 3D printing. Author investigated mechanical properties such as impact strength, bending strength, tensile strength and fracture elongation which were measured as 3.27 kJ/m2, 65.7 MPa, 56.06 MPa and 6.16% respectively which was found to be declining upon further increase in CF content to 10 wt% [127].

Yang et al. has examined influence of carbon nanotube (CNT) content on MFI and mechanical performance of PLA/CNT composites. The CNT content was varied from 0 to 8 wt.% in PLA and it was observed that inclusion of 6wt.% CNT results in 64.12% increase in tensile strength. However, notable decrease in MFR was recorded from 29.38 g/10 min for pure PLA to 6.91 g/10 min with 8 wt.% CNT. This reduction was attributed to the nucleation effect between CNT and PLA strengthens inter molecular interactions and consequently lowers MFI [128].

Zhang et al. has carried out investigation for examining degradation behaviour and mechanical performance of PLA/cellulose nano fiber (CNF) 3D printed composites. Tensile modulus of composites has been 18.4% more than virgin PLA, whereas strength was 7.4% lower because of CNF has higher tendency of agglomeration in the PLA matrix causing inferior interfacial bonding between PLA and CNF. At 37 °C, tensile strength of the PLA/CNF shows 8.9% decrease caused by decrease in molecular weight over degradation period of 14days. Author observed that aggregated flakes of CNF are embedded in the matrix of PLA causing poor interfacial bonding between PLA and CNF leading to internal defects [129].

Zhao et al. has performed a study to examine tensile properties of pure PLA, short glass fiber (SGF)/PLA composites, CNT-SGF/PLA composites. FDM 3D printing was used to process these composites. According to the experimental results, author observed that composites of SGF/PLA and CNT-SGF/PLA shows higher tensile strength and young's

modulus values because of better interface adhesion. Author also observed that FDM Raster Angles did not have much impact on tensile properties of samples [130].

CHAPTER 3

PROBLEM FORMULATION AND OBJECTIVES

3.1 NEED OF THE CURRENT RESEARCH WORK

To reduce the effect of waste polymer on environment and economy, recycling is one of the most important aspect which not only ensures the optimum use of materials but also shows the sustainable manufacturing approach. However, recycled polymers undergo degradation in their base properties after few cycles of recycling. So, further, addition of reinforcement into the polymers is one of the ways to improve properties of the composites.

The review of literature shows that extensive research was conducted on thermal, morphological, mechanical properties of virgin polymers reinforced along with materials such as carbon fiber, cellulose nanofibers (CNF), kenaf fiber, glass fiber, multi-walled carbon nanotubes (MWCNT), vegetable yarns, SS and titanium nitride (TiN). However, there is limited research focusing on morphological, mechanical properties of secondary recycled polymer reinforced with industrial waste materials such as wood powder, almond skin and rice husk etc. at varying weight proportions for a sustainable manufacturing perspective. This gap requires more focus and deeper examination industrial waste reinforcements into recycled polymers.

3.2 OBSERVATIONS FROM LITERATURE REVIEW

Most investigations show that adding reinforcements, such as glass fibers, improves various mechanical properties including tensile strength, stiffness, Young's modulus and flexural properties at an optimum weight-based filler loading. However, beyond a specific reinforcement threshold, these mechanical properties can degrade due to the agglomeration of filler particles within the base matrix. Further, nano materials such TiN and MWCNT improves thermal stability and strength but these nano material often increases viscosity which affect MFI of the composite leading to problem while 3D printing.

Further from the literature review, SEM results shows that homogeneous distribution of reinforcement materials lead to increased strength of the polymer composites whereas on the other hand, agglomeration of reinforcement materials may reduces tensile strength, enhances voids formation and increases brittleness which reduces the overall performance of the composites. Performance of the composites is entirely depends upon the type and quantity of reinforcement materials such as adding glass fibres into polymer matrix increases tensile

strength but also increase the brittleness of the composite at higher amounts by weight. From the review of literature, it was observed that most of the research was carried out using virgin polymers to make 3D printed composite materials. Very limited studies are available on the use of waste materials as reinforcement which highlights the significant research gap. So in the current study, secondary recycled Polylactic Acid (2ºPLA) has been utilized as matrix material whereas industrial waste such as almond skin and wood powder utilized as reinforcement materials to study their effect on mechanical properties. Therefore, a research gap exists in the development of sustainable 3D printed composites using secondary recycled PLA reinforced with industrial waste materials particularly in understanding of their rheological, mechanical, thermal and morphological properties for automotive applications.

3.3 OBJECTIVES OF THE RESEARCH

Main research objectives of proposed have been mentioned below:

1. To prepare and study the rheological properties of PLA based matrix reinforced with almond skin and wood powder.
2. To prepare and investigate the properties (mechanical, thermal and morphological) of composite feedstock filament for 3D printed applications.
3. To prepare and analyse the properties of multi-layered tensile and flexural specimen printed by Fused Filament Fabrication and its process optimization.

CHAPTER 4

MATERIALS AND METHODOLOGY

To achieve the objectives of this study, the following methodology was adopted.

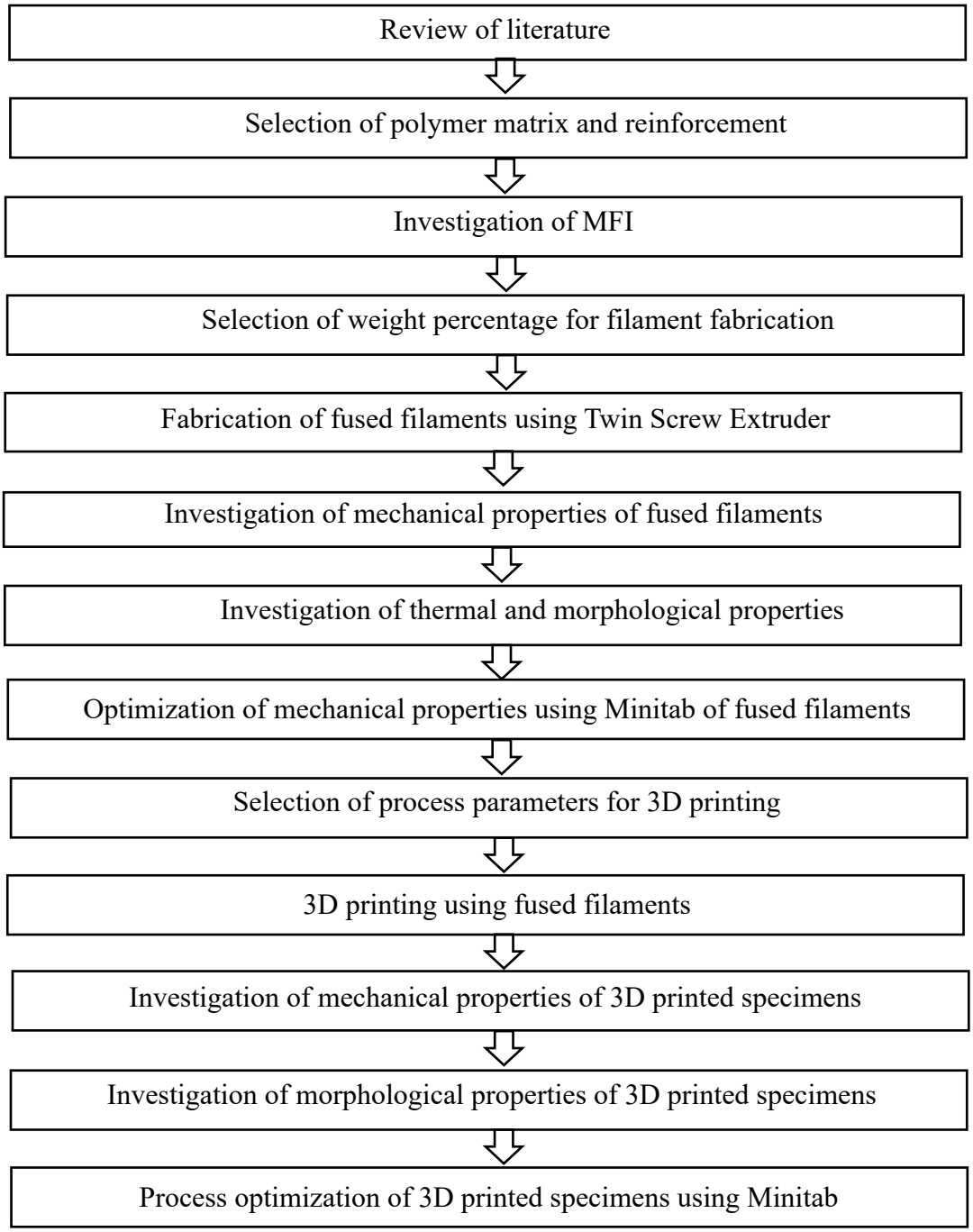

Figure 4.1 Flow chart for methodology adopted in the present research

4.1 SELECTION OF BASE MATRIX AND REINFORCEMENT MATERIAL

PLA is widely used because it can be easily processed polymer with good mechanical properties which makes it suitable for 3D printing, packaging, automobile interior components etc. 2°PLA, purchased from the local market (Batra Polymers, Ludhiana, Punjab), was used as the base material for fabricating composite filaments. After the procurement of 2°PLA, further, the next step was to select the reinforcement material and its wright percentage to be added in the base matrix. In the current study, industrial waste materials which are almond skin and wood powder have been selected. Almond skin, obtained as waste from an almond oil manufacturing industry, was selected as the reinforcing material. To eliminate moisture, the AS was oven-dried at 50°C for five hours. Industrial waste wood powder taken from a local saw mill was chosen as a reinforcement material. The wood powder sieved to achieve particles of 50 μm in size before being reinforced into the 2° PLA to form fused filament composites. Mustard oil was not preferred for mixing because of its high viscosity which can affect the uniform dispersion and may adversely affect the homogeneity of the composite. Therefore, a small amount of linseed oil was used to mix 2° PLA and wood powder, as even a low quantity of linseed oil improved the dispersion of wood powder particles within the 2° PLA matrix. Above mentioned industrial waste reinforcement materials promotes circular economy by converting waste into useful products. This approach is a sustainable approach of making feedstock filaments which are further suitable for FFF.

4.2 MELT FLOW INDEX (MFI)

The MFI represents the rate of flow of a polymer melt measured in g/10 min and is used to assess the ease of polymer flow under controlled temperature, load and diameter of nozzle [100] according to the American Society for Testing and Materials (ASTM) D1238 standard, with the MFI setup as shown in Figure 4.2 [131–132]. MFI reading have been taken under fixed conditions using a 2.16 kg load and 190°C for 10 minutes [100, 132]. Prior to producing fused filaments, MFI investigation was carried out through two separate mixtures of 2º PLA with almond skin powder (3%, 6% and 9% by weight) and the with wood powder (3%, 6% and 9% by weight). MFI of 2º PLA was also calculated for the comparison with the composites. Before investigating MFI, materials were cleaned, mixed and then fed into preheated barrel of the apparatus maintaining 190°C temperature under standard testing load of 2.16 kg. Once the composite starts coming through the nozzle in wire form as shown in figure below of the apparatus, it is allowed to flow for 10mins and then collected to measure its weight. Results were calculated in gm/10min under required temperature and load.

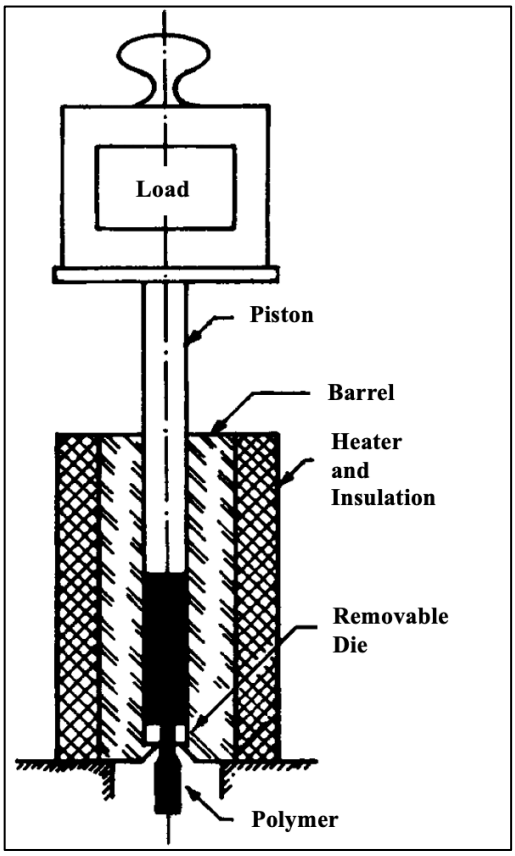

Figure 4.2 Melt Flow Index setup [133]

4.3 SELECTION OF ORTHOGONAL ARRAY (OA)

In the current study, selection of the OA is one of the very important aspect of the study while design of the experiments which analyses the significance of process parameters. As current study involves 3-control log parameters which are torque (0.1Nm, 0.2Nm, 0.3Nm), load (7.5kg, 10kg, 12.5kg), temperature (175ºC, 185ºC, 195ºC), each have 3-levels and the Taguchi's design of experiments balances the accuracy with minimum no. of experiments. Using an OA within Taguchi's experimentation allow the impact of different parameters efficient investigation, making it impactful tool in robust design [134]. Full-factorial design requires L27 means 27 experiments which is very costly and time consuming, therefore L9 OA has selected as it works with 3-factors at 3-levels reducing no. of experiments to nine only. L9 OA has factors in 3-column and testing parameters in rows. As per Taguchi's design, L9 OA has 8 Degree of Freedom (DOF) because DOF is given by n-1where n is the no. of levels which means each factors has 2-DOF. Below Table 4.1 shows design of experiments as per L9 OA where each parameter is assigned with individual column showing different test conditions.

Table 4.1 Control log for the experimentation

Sample No.	Torque (Nm)	Load (Kg)	Temperature (°C)
1	0.1	7.5	175
2	0.1	10	185
3	0.1	12.5	195
4	0.2	7.5	185
5	0.2	10	195
6	0.2	12.5	175
7	0.3	7.5	195
8	0.3	10	175
9	0.3	12.5	185

4.4 FABRICATION OF FUSED FILAMENTS USING TWIN SCREW EXTRUDER (TSE)

Composition of reinforcement and matrix material was selected based on MFI investigation of the composites using different compositions of almond skin and wood powder. Next step was to fabricate fused filaments using TSE according to control log of parameters given in table 1 to examine its various mechanical, thermal and morphological properties. Diameter of the TSE nozzle was 0.8mm. Total 18 fused filaments have been fabricated 9-for 2° PLA + AS and 9-for 2° PLA + WP using a TSE by feeding 2° PLA + almond skin and 2° PLA + wood powder separately into a heated barrel equipped with intermeshing twin crews. The rotating screws facilitated feeding, melting and intensive mixing of the materials, after which the pressurized melt was extruded through a die to obtain a continuous filament. Following Figure 4.3 is the schematic diagram of TSE.

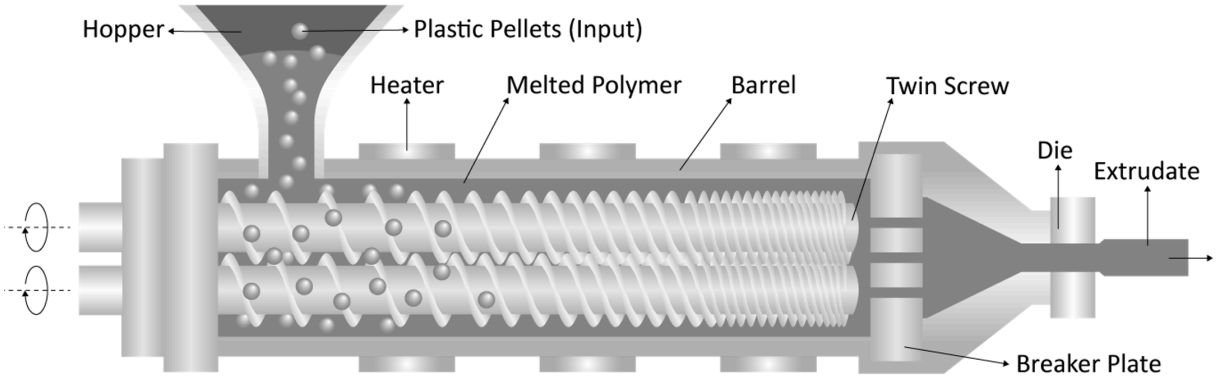

Figure 4.3 Schematic diagram of Twin Screw Extruder [134]

4.5 TENSILE TESTING USING UNIVERSAL TESTING MACHINE (UTM)

UTM was used to for tensile testing of as fabricated fused filaments to investigate their mechanical properties. UTM comprises of load cell, lower and upper jaws, strong loading frame etc. Each sample was fixed between lower and upper jaws aligned properly to avoid bending stress. Distance between the lower and upper jaws was kept at 60mm as shown in figure given below and maximum load carrying capacity of UTM used for tensile testing was 5KN. UTM was used to investigate various mechanical properties which are Peak Strength (PS), Break Strength (BS), % Break Elongation (%BE) and % Elongation at Peak (%PE) and further calculating Modulus of Toughness (T) and Modulus of Elasticity (E). Initially, fused filaments which were fabricated in the form of wire have been used for determining different mechanical properties. Values for PS, BS, %BE and %PE were recorded for further calculation and analysis. Later on 3D printed samples were also tested under UTM as show in Figure 4.4 given below.

Figure 4.4 UTM setup for tensile testing

4.6 FLEXURAL TESTING

Flexural specimens have been prepared using 3D printing as per ASTM D 790 standards to investigate their mechanical properties. Flexural testing was done on UTM having 3-point bending fixtures which has one loading nose positioned centrally and two static supports as shown in Figure 4.5. During this testing, sample was horizontally placed on static supports as shown in Figure 4.5 after ensuring their alignment and then load nose touches the midpoint of the sample placed on static supports. After that UTM applies the load on sample at constant speed. As the load increases, sample experiences the bending and reading were noted down at different levels. This flexural testing was carried out to evaluate the resistance to fracture.

Figure 4.5 UTM setup for flexural testing

4.7 FIELD EMISSION SCANNING ELECTRON MICROSCOPY (FESEM)

FESEM analysis (JEOL JSM-7610F-PLUS) was conducted to study the morphology of sample's surface by taking high resolution images and the setup is shown in Figure 4.6. FESEM is used to check the structure of surface of the sample. In the current study, to identify agglomeration and distribution of particles, interlayer bonding, cracks, voids spaces and surface structures, FESEM micrographs have been taken at different magnifications. Initially, after conducting tensile testing on fused filaments, fractured surface of the broken samples have been brought taken for their microstructural analysis under FESEM. Similarly, fractured 3D printed samples after tensile testing and flexural testing were also tested under FESEM for microstructural analysis. Prior to microstructural analysis using FESEM, gold coating was carried out on samples because prepared samples are non-conductive in nature. When non-conductive samples were brought under electron beam of FESEM, charge occurs on the surface

of samples which results in image distortion and bad resolution. Gold coating prevents samples from surface charge which improves conductivity which helps in obtaining high resolution and clear FESEM image. FESEM analysis was done on fractured surfaces of the samples revealing void spaces and cluster of voids etc.

Figure 4.6 FESEM setup

4.8 ELECTRON DISPERSIVE SPECTROSCOPY (EDS)

FESEM utilized in the current research work has been integrated with EDS. EDS was used for the elemental composition of the samples. After taking microstructural micrographs using FESEM, EDS was carried along with mapping of surface of the samples. When beam of electrons impinges on the sample's surface, it generated x-rays which are useful to identify the elemental composition of the sample. Further, mapping of samples was done which gives coloured images of element distribution depicting how these elements have been spatially distributed on the fractured surface of samples.

4.9 POROSITY ANALYSIS USING TOOL MAKER'S MICROSCOPE

Porosity analysis was carried out using Tool Maker's microscope at 100x magnification according to ASTM B276. Porosity analysis was done on the fused filaments available in the form of wire at their break cross-sections. In the current study, porosity analysis was carried out on all the samples of fused filaments prepared from 2º PLA + almond skin and 2º PLA + wood powder to investigate the porosity present within the samples generated while their fabrication.

Tool maker's microscope measures the area of pores which was used to calculate the porosity percentage.

4.10 THERMAL ANALYSIS USING DIFFERENTIAL SCANNING CALORIMETRY (DSC)

DSC is used to find thermal properties such as the heat capacity(J/g), glass transition temperature(Tg), solidification and melting temperatures and the overall thermal response of polymer based composite samples. In this study, DSC analysis (Perkin Elmer DSC 6000) shown in Figure 4.7 was carried out by heating and cooling the composite samples repeatedly under controlled air flow of 50mL/min. Samples were heated at 10°C/min to investigate endothermic reactions and cooled at 10°C/min to examine exothermic transitions. The heat absorbed or released during these transitions was recorded to estimate the heat-carrying capacity and thermal behaviour of the materials. All measurements were carried out under continuous, controlled heating and cooling cycles. The DSC equipment evaluates the sample's thermal transitions by comparing it with a reference material, using two separate crucibles one for the sample and the other for the reference as illustrated in Figure below.

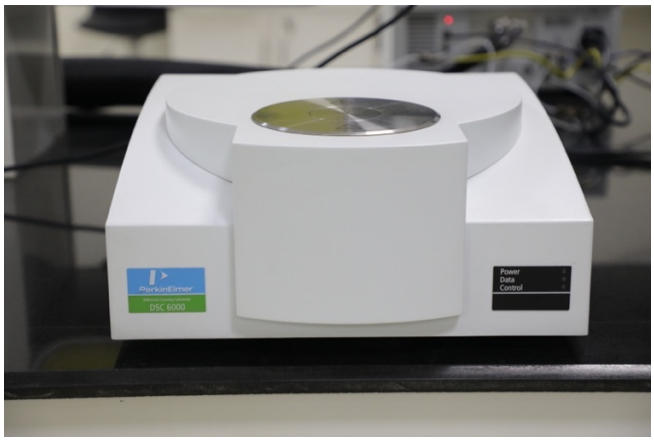

Figure 4.7 DSC setup

4.11 3D PRINTING VIA FUSED FILAMENT FABRICATION (FFF)

FFF is one of the most cost-effective 3D printing method [89]. The process begins by loading a spool and ending at depositing layers of filament via heating system [90]. Fused filament fabrication is a method which is working on utilizing filament which further deposits on the bed of 3D printer in solid form. FFF is known for its versatility in different fields like medical, automobile and intricate products. Computer Aided Drafting (CAD) model of the component is used to convert it into live physical component using 3D printing.

Feedstock filaments prepared with the help of Twin Screw Extruder (TSE) have been utilized for the 3D printing of tensile and flexural specimens for further testing. FFF model Accuraft 250D was used for the printing of tensile specimen (as per ASTM D 638 type IV) and flexural specimen (as per ASTM D 790 standards) as shown in Figure 4.8 [135-136]. Tensile testing is a fundamental mechanical test used to determine the strength, ductility and mechanical behaviour of materials under uniaxial tensile stress whereas flexural testing is used to determine the maximum stress a material can withstand before failure in bending.

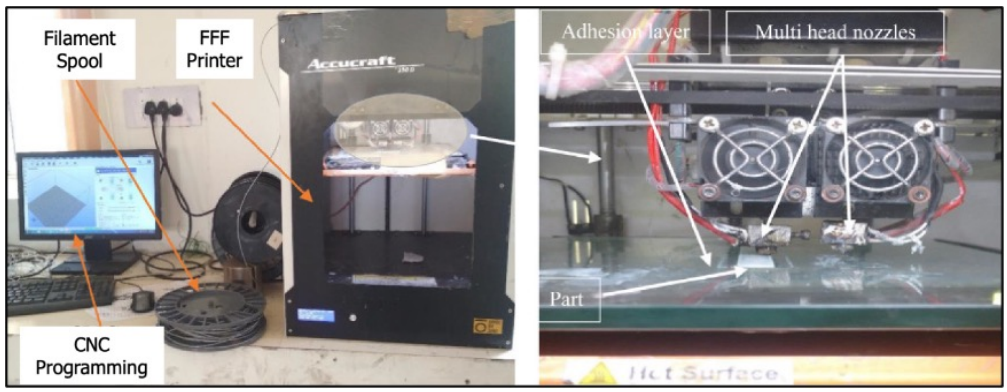

Figure 4.8 Fused Filament Fabrication setup

The initial step involves creating a 3D CAD model of the tensile and flexural specimens using Creo and schematic diagrams for tensile and flexural specimens are shown in Figure 4.9 and 4.10. Figure 4.9 shows tensile specimen according to American Society for Testing and Materials (ASTM) D638-type IV and Figure 4.10 shows flexural specimen according to ASTM D790.

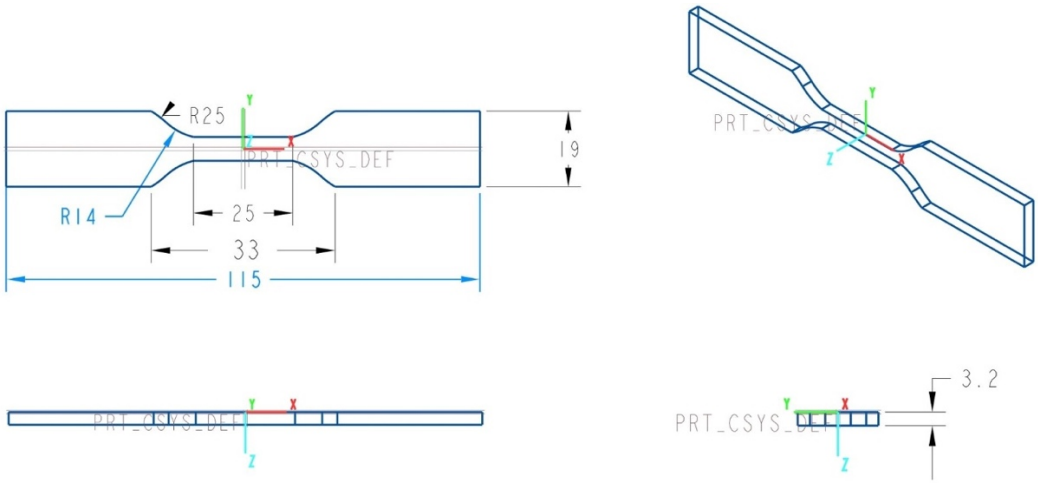

Figure 4.9 Tensile specimen according to ASTM D638-type IV

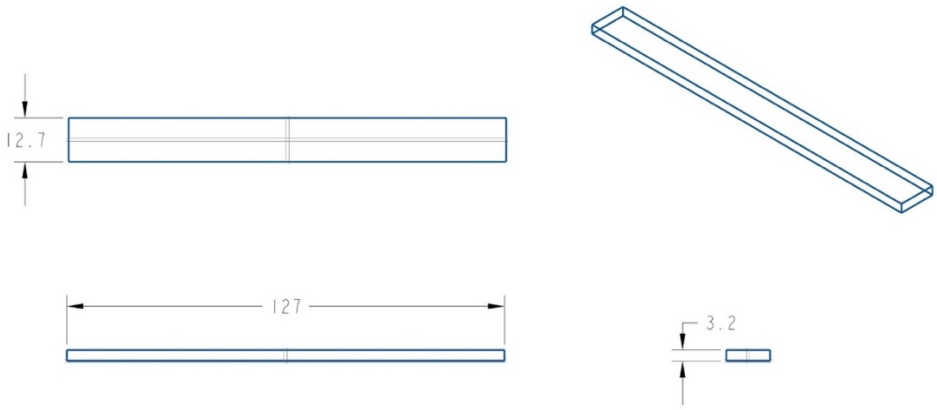

Figure 4.10 Flexural specimen according to ASTM D790

This CAD file is then processed in Slice3r, where it is converted into STL format and subsequently used to generate G-code. Once the G-code is ready, Repetier-Host V2.1.6 software is employed to control the 3D printing process, as illustrated in Figure 4.11. Repetier-Host reads the G-code and directs the 3D printer to carry out the printing process. The printer then fabricates the model by sequentially depositing layers through extrusion, forming the final object layer by layer. A key feature of this printer is the ability to manually change the feedstock filaments at any desired point during the printing process. It is equipped with two separate nozzles, one designated for model and second for support materials, each responsible for extruding their respective filaments.

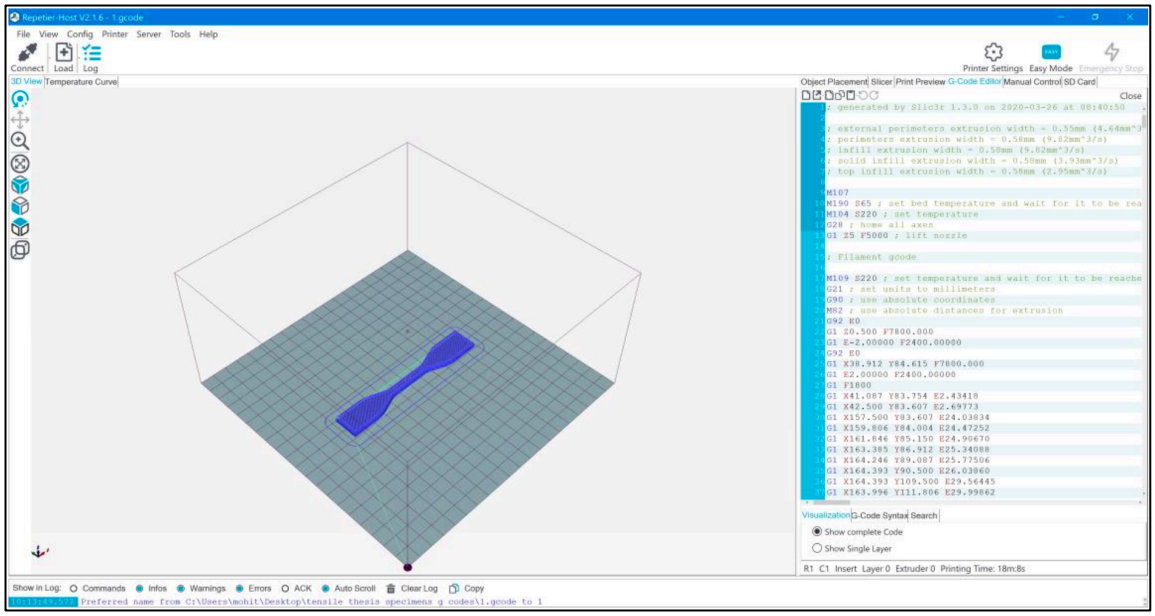

Figure 4.11 Repetier-Host V2.1.6 interface window

Further, various parameters such as bed temperature, nozzle temperature, air gap, layer thickness and raster width etc. are required to be fixed. Parameters fixed for FFF in this experimentation are mentioned in Table 4.2

Table 4.2 Parameters fixed for FFF setup

Parameter	Value
Layer thickness(mm)	0.8
Nozzle Temperature	190°C
Bed Temperature	90°C
Infill pattern	Honeycomb
Raster width (mm)	0.254
Air Gap (mm)	0

Prior to printing the parts using FFF, three input parameters infill density, raster angle and infill speed were selected. Infill density is selected as 50%, 70%, 90%, raster angle is selected as 45°, 60°, 90° and infill speed was selected as 40 mm/s, 60 mm/s, 80 mm/s. To avoid repetitions of the experiments, design of experiment (DOE) of Taguchi L9 orthogonal array (OA) was used for printing [134] as mentioned in the Table 4.3 given below:

Table 4.3 DOE for printing based on Taguchi L9 OA

Sample No.	Infill Density (%)	Raster Angle (°)	Infill Speed (mm/s)
1	90	45	40
2	90	60	60
3	90	90	80
4	70	45	60
5	70	60	80
6	70	90	40
7	50	45	80
8	50	60	40
9	50	90	60

After the selection of the FFF parameters, Repetier-Host V2.1.6 software utilized to execute the printing as shown earlier in the Figure 4.11. Software directs 3D printer to execute printing through G-codes. The process begins by loading the G-code file into the software followed by the next step to run the job. When nozzle & bed attains required temperature, then the 3D printer will starts printing to fabricate the specimens.

4.12 PILOT EXPERIMENTATION

Initially, pilot experimentation has been conducted to investigate the Melt Flow Index (MFI) of 2°PLA at and result showed that there was a smooth flow of melt through the nozzle at 190°C, 200°C and 210°C under 2.16kg load. At 190°C temperature, it was observed that flow of melt through the nozzle was smooth retaining optimum viscosity and uniform filament wires have been obtained. Upon further increase in temperature to 200°C and 210°C, viscosity of melt flow gets decreases due to which melt is coming out of the nozzle in the form of liquid due to which melt was not able to get solidify. Hence, 190°C temperature and 2.16kg load was selected for further study. Further 2°PLA + almond skin and 2°PLA + wood powder under different condition such as temperature and varying weight proportions of materials. MFI is the effective tool to find the impact of varying weight proportions of reinforcement materials on the melt flow of composite for the fabrication of fused filaments. Initially, all procured materials were dried below the glass transition temperature of 2° PLA to remove the moisture. Initially, MFI of 2°PLA was carried out and found that material is flowing easily through nozzle. During this pilot experimentation, three different temperature values were selected for the trials which are 190°C, 200°C and 210°C under 2.16kg of fixed load. For the pilot experimentation, 1% to 12% reinforcement by weight has been selected for 2° PLA matrix. All compositions were investigated with three repetitions as three different temperature values were taken.

The main motive behind conducting this pilot experimentation was that how increasing the reinforcement content affects the flow of composite while melting during the fabrication of fused filaments. It has been found that upon exceeding temperature from 190°C to 200°C and further to 210°C, composite gets flowing very easily as melting temperature of 2° PLA is near to 190°C. Upon increasing the temperature, viscosity of the melt gets too high allows material to flow rapidly which delays the solidification of the melt when coming outside from the nozzle. Hence 190°C was considered as the suitable temperature to carry out the further pilot experimentation. Further when MFI was conducted by adding 1% to 12% of almond skin and wood powder separately by taking temperature as 190°C and 2.16 kg of load. Further, it has

been observed that at low concentration of the composite, i.e. 1% and 2%, MFI values of 2° PLA + almond skin (1% and 2%) and 2° PLA + wood powder (1% and 2%) were very near to the MFI of 2° PLA which indicates that viscosity remains stable when compared with 2° PLA which did not impact the flow of melt significantly. Further, it has been observed that MFI gets decreasing upon increasing reinforcement content and there was drastic drop in MFI values at higher reinforcement content such as 10% to 12% which increases viscosity of the melt interrupting the flow of composite through the nozzle leads to the nozzle clogging. Further change in composition gives similar MFI values.

At last, 3%, 6% and 9% by weight reinforcement of almond skin and wood powder, separately were selected to provide balanced approach in results. Table 4.4 shows the selected MFI parameters.

Table 4.4 Selected MFI parameters

Selected compositions	2° PLA + 3%, 6% and 9% almond skin by weight 2° PLA + 3%, 6% and 9% wood powder by weight
Temperature	190°C
Load	2.16 kg

Further after selecting the composition, next step was to fabricate the fused filaments using twin screw extruder (TSE) for 3D printing where extrusion temperatures of 175°C, 185°C, and 195°C were finally selected for filament fabrication. It has been observed from the literature that many parameters of TSE are impacting the material properties while fabricating fused filaments such as speed, load, torque and temperature. Speed of the screw was kept stable during the process to avoid shear rate of the material ensuring comparable viscosity and uniform mixing of melt. TSE nozzle diameter was 0.8 mm. The TSE equipment allows to keep torque on higher side such as 0.4 Nm or more than that also but maximum torque was avoided because it can cause resistance in melt flow and risk of clogging of nozzle. Trials shows non uniform flow of melt when torque was kept above 0.3 Nm. Therefore, 0.1 Nm, 0.2 Nm and 0.3 Nm values for toque were selected to ensure stable process. Load was taken as second parameter during pilot experimentation where load was taken as 5kg, 7.5kg, 10 kg, 12.5kg and 15kg. At 5kg load, melt is not easily flowing which results in variation in diameter of filament and void

formation at higher reinforcement compositions whereas at higher load of 15 kg, excessive barrel pressure leading to uncontrolled flow of material from the TSE nozzle. Hence, intermediate values of 7.5 kg, 10 kg, 12.5 kg load were selected for the further process. Though, 2º PLA based composite materials can be fabricated within 170ºC to 210ºC temperature. Temperature near to 170ºC causes high viscosity melt which requires high torque to flow especially at high additions of reinforcements. Whereas temperature near or above 200ºC burnt the reinforcement material which are almond skin and wood powder results in inconsistent flow of melt. Finally the intermediate temperature of 175°C, 185°C, 195°C were selected for the fabrication of fused filaments. Parameter selected for TSE process are shown in Table 4.5.

Table 4.5 Selected parameters for TSE

Selected parameters	**Values**
Torque	0.1 Nm, 0.2 Nm, 0.3 Nm
Load	7.5 kg, 10 kg, 12.5 kg
Temperature	175°C, 185°C, 195°C
Nozzle diameter	0.8 mm

Further using above parameter of TSE, fused filaments have been prepared to investigate its mechanical properties, these prepared filaments were tested on UTM at 5 KN of constant load. using all combinations of parameters, filaments have been prepared to tested under UTM undergoes 3-cycles of testing and average of those three values were taken to avoid error. During tensile testing using UTM, pilot experimentation was done by taking 60mm distance between the jaws.

Before finalizing the 3D printing parameters, pilot experimentation was done to find most significant parameters. To investigate the printability of the 2º PLA based filaments prepared from almond skin and wood powder, flexural and tensile samples were prepared using fused filament fabrication (FFF). Pilot experimentation for 3D printing was carried out where infill density is 50%, 60%, 70%, 80% and 90%, raster angle is 30º, 45º, 60º, 75º and 90º, infill speed is 40mm/s, 50mm/s, 60mm/s, 70mm/s, 80mm/s. At very low infill density, 3D printed

component may get empty which reduces the strength of components and shows lower mechanical properties. High density value of 90% may fill 3D printed component more densely which can further leads to improved mechanical properties. For the further investigation and to remove the redundancy in experimentation, 50%, 70% and 90% infill density was selected.

Further at lower raster angle, warpage of the components was observed and raster angle of 45º and 60º shows consistent printability. On the other hand, larger raster angle of 90º, it deposition of the material is perpendicular and gives uniform pattern of the surface. Hence, raster angles of 45º, 60º and 90º were selected.

Further when infill speed was taken into account, it has been observed that lower infill speed resulted in smooth printed surface as the material gets sufficient time for cooling. Mid-range speed of 60mm/s, reduces build time along with better print quality. Higher infill speed give weak bonding between layer due insufficient cooling time. Therefore, speeds of 40mm/s, 60mm/s and 80mm/s were selected for further experimentation as they effectively represent low, medium and high-speed conditions.

During the pilot experimentation, nozzle temperature was kept at 190ºC because lower extrusion temperatures results into insufficient melting and cause material stagnation within the barrel and subsequent nozzle clogging. Further, different 3D printing parameters were tried during pilot experimentation and it was observed that honeycomb structure gives highest Peak Strength when compared with triangular and rectilinear pattern because it provides uniform load distribution due to shape of its geometry as stresses pass along the straight lines.

Airgap was kept 0mm because it gives maximum contact rea between adjacent rasters. Bed temperature was taken 90ºC because during the experimentation, it was found that deposited material was properly stick to the bed surface and reduces warpage. During the trials, when bed temperature was taken 100ºC, excessive layer adhesion damages the surface of deposited material and on the other hand, when bed temperature was taken as 70ºC to 80ºC, warpage and lifting of material from corners has been observed, hence bed temperature was considered as 90ºC for further experimentation.

Further layer thickness was considered as 0.8 mm because it gives fast printing speed along good surface finish during printing. Raster width was selected as 0.254 mm. At last, parameters fixed for 3D printing were 0.8 mm layer thickness, 190°C nozzle temperature, 90°C

bed temperature, honeycomb infill pattern, 0.254 mm raster width and 0 mm airgap. Finally the selected parameters are shown in Table 4.6 as shown below.

Table 4.6 Selected parameters for 3D printing

Selected parameters	Values
Infill density	50%, 70% and 90%
Raster angle	45º, 60º and 90º
Infill speed	40mm/s, 60 mm/s and 80 mm/s

4.13 OPTIMIZATION OF MECHANICAL PROPERTIES USING MINITAB

After conducting the mechanical testing of the used filaments, optimization of the resulted mechanical properties has been optimized using Minitab software. This software analyzes the experiment-based data to understand the effect of parameters used in the fabrication of the filaments. Minitab is a statistical tool used in analyzing Taguchi's OA based parameters comprises of stages: (i) optimization of parameters used in filament fabrication and (ii) process parameter optimization for 3D printed samples. Using this software Main Effect Plots were taken which shows how the mean response of mechanical properties changes across the parameters and examine the effect of each parameter on response. Further, signal to noise (S/N) ratio was calculated for each combination of parameter. Taguchi's method use the S/N ratio to examine the robustness of the samples. Signal depicts mean value of the response and noise means variability by uncontrolled parameters. In the current study, 'Larger the Better' approach was used to maximize the strength of samples. Taguchi's method help in defining deviation between experiment value and targeted value [137]. This deviation is converted into a S/N ratio, which is a statistical tool for measuring performance. S/N ratio determines the inverse of the coefficient of variation, i.e. it determines the ratio μ/σ, where μ defines the process means (signal) and σ (noise) the process standard deviation. After optimizing the fused filament, using optimized parameters, fused filaments have been prepared and used for 3D printing via FFF. Further mechanical properties of the 3D printed samples was optimized to identify the best suitable 3D printing samples.

4.14 ANALYSIS OF VARIANCE (ANOVA)

Analysis of Variance (ANOVA) was used in the present research in order to statistically evaluate the impact of process parameters and compositions of reinforcement on the performance of 3D printed specimens. In this study, ANOVA was used to identify the most significant parameters during both filament fabrication and 3D printing. Since many input parameters like infill density, raster angle, infill speed and reinforcement percentage were considered simultaneously, ANOVA helped in finding the contribution of all parameters towards the overall performance of the specimens. The p-values helped determine whether a factor was statistically significant, while the percentage contribution shows how much each parameters influenced the mechanical properties. For fused filaments, ANOVA revealed which extrusion settings mainly affected filament strength. For 3D printed samples, it highlighted the importance of parameters such as infill density, raster angle and infill speed. In simple terms, ANOVA helped identify which factors matter the most and how strongly they impact the final mechanical performance**.**

The ANOVA Table 4.7 represents the statistical variation in the experimental data and determines the significance of process parameters on the response characteristics. It divides the total variation into variation between and within repetitions. Sum of Squares (SS) represents data variation, Degree of Freedom (DOF) indicates independent observations, Mean Square (MS) is the ratio of SS to DOF, and the F-ratio determines the significance of the considered parameters.

Table 4.7 Analysis of Variance (ANOVA)

Source of Variation	**Sum of Squares (SS)**	**Degree of Freedom (DOF)**	**Mean of square (MS)**	**F- ratio**
Between the repetitions	SSbetween	i-1	$\frac{SS_{between}}{i-1}$	$\frac{MS_{between}}{MS_{within}}$
With in the repetition	SSwithin	j-1	$\frac{SS_{within}}{i-1}$	
Total	SST	Rxn-1	$\frac{SS_T}{Rxn-1}$	

CHAPTER 5

RESULTS AND DISCUSSIONS

In this results part, detailed evaluation of the prepared composite was done using multiple characterisation techniques. The MFI was initially analysed to assess the flow behaviour of the prepared materials. This was followed by tensile testing of the extruded filaments to determine their mechanical integrity prior to printing. Optimisation studies using Minitab was then carried out to find the most significant parameter affecting mechanical properties. Subsequently, tensile and flexural testing of the 3D-printed samples was conducted to examine the impact of printing on final strength. DSC analysis was employed to study thermal transitions and crystallisation behaviour of composites. Finally, morphological properties were investigated using FESEM and EDS for reinforcement dispersion, interfacial bonding and fracture characteristics. The detailed results of each of these analyses are presented and discussed in the following sections.

5.1 MELT FLOW INDEX (MFI) RESULTS

MFI is a key measure used to analyse polymer rheological behaviour where polymer flows when heated to its melting point subjected to a standardized load. The results of melt flow rate performed as per ASTM D 1238 standard with different weight %age of reinforced material was presented in Table 5.1. Further, The MFI of 2° PLA reinforced with almond skin and reinforced with wood powder was investigated using reinforcement of 3%, 6% and 9% by weight selected using pilot experimentation. Total 7 combinations of the experimentation were taken into account for MFI calculations where 1 for 2° PLA, 3 for 2° PLA + almond skin and 3 for 2° PLA + wood powder. Table 5.1. Initially MFR of 2° PLA was examined (average of three repetitions) [138] and it was found to be 33.85 gm/10min. As observed from the Table 5.1, MFI for 2ºPLA is quite high which usually not pose any problem as it will help to operate twin screw extruder and FFF setup at high production rate.

Table 5.1 MFI of 2° recycled PLA with and without reinforcements

Sr. No	**Specimen**	**MFR (gm/10min)**			**Average MFI (gm/10min)**
1	2° PLA	33.75	33.85	33.95	33.85

Sr. No	Specimen	MFR (gm/10min)			Average MFI (gm/10min)
2	2° PLA + 3% almond skin	29.4	30.7	31.1	30.40
3	2° PLA + 6% almond skin	22.2	24.5	23.8	23.50
4	2° PLA + 9% almond skin	14.9	17	16.1	16
5	2° PLA + 3% wood powder	32.7	31.44	33.3	32.48
6	2° PLA + 6% wood powder	27.4	30.2	28.44	28.68
7	2° PLA + 9% wood powder	14.6	16	15.9	15.50

From the above Table 5.1, it was observed that MFI of 2° PLA + 3% almond skin and 2° PLA + wood powder was found to be 30.40 gm/10min and 32.48 gm/10min, respectively, which means at 3% reinforcement, there was a slight MFI decrease when compared to MFI of 2° PLA. This indicates the slight increase in viscosity reduces the melt flow again slightly. This was because of poor polymer reinforcement interaction due to which reinforcement material is not able to alter the rheological properties of composite. When reinforcement reaches to 2° PLA + 9 %wt. almond skin and 2° PLA + 6% wood powder, MFI was drastically reduces to 16 gm/10min and 15.50% gm/10min, respectively, indicating very high viscosity. Due to increase in viscosity, flow of metal was restricted leading to the clogging of the nozzle of the MFI setup.

When 6%wt. of almond skin and 6%wt. of wood powder was used as reinforcement in the matrix of 2° PLA, material coming out through the nozzle was uniform and continuous. MFI of his composition was 23.5 gm/10min 28.68 gm/10min, respectively, which give balanced melt flow rate. This result indicated that interaction of the polymer and reinforcement was sufficient to ensure their bonding. From these results, finally 2° PLA + 6%wt. almond skin composition was selected to fabricate fused filaments using twin screw extruder. It gives smooth flow of composite when coming out through the nozzle along with proper melting and uniform wire formation.

5.2 TENSILE TESTING OF FUSED FILAMENTS PREPARED USING TWIN SCREW EXTRUSION

The fused filament wires have been prepared using TSE by taking 94% 2° recycled PLA + 6% almond skin and 94% 2° recycled PLA + 6% wood powder by weight as per the parameters given in Table 4.1. Tensile testing was carried out on Universal Testing Machine (UTM) to investigate different mechanical properties like Break Strength (BS), Peak Strength (PS), percentage Elongation at Peak (%PE), percentage Break Elongation (%BE), Modulus of Elasticity (E) and Modulus of Toughness (T) of filaments. Tensile testing results were shown in Table 5.2 and Table 5.3.

Table 5.2 Tensile testing results for 94% 2° recycled PLA + 6%wt. almond skin

Sample No.	PS (MPa)	BS (MPa)	%PE	%BE	E (GPa)	T (MPa)
1	39.82	34.18	3.72	4.3	0.6423	1.2248
2	40.36	38.18	2.65	3.2	0.9138	1.0181
3	43.85	40	4.07	2.8	0.6464	0.9333
4	43.1	41.56	3.2	3.7	0.8081	1.2814
5	39.33	37.12	2.7	3	0.8740	0.9280
6	28.8	25.02	3.12	3.9	0.5538	0.8132
7	27.2	23.74	4.26	4.7	0.3831	0.9298
8	16.82	14.98	3.72	5.2	0.2713	0.6491

Sample No.	PS (MPa)	BS (MPa)	%PE	%BE	E (GPa)	T (MPa)
9	20.23	18.69	3.1	4.4	0.3915	0.6853

Table 5.3 Tensile testing results for 94% 2° recycled PLA + 6%wt. wood powder

Sample No.	PS (MPa)	BS (MPa)	%PE	%BE	E (GPa)	T (MPa)
1	31.81	27.09	6.02	7.19	0.3170	1.6231
2	18.8	14.9	4.43	5.65	0.2546	0.7015
3	11.92	8.12	2.85	3.07	0.2509	0.2077
4	26.89	24.11	7.92	8.86	0.2037	1.7801
5	15.22	11.26	3.75	4.22	0.2435	0.3960
6	12.89	9.89	2.83	3.09	0.2733	0.2547
7	27.76	23	5.12	6.79	0.3253	1.3014
8	20.14	16.78	3.81	4.56	0.3172	0.6376
9	13.51	9.62	1.58	2.01	0.5130	0.1611

It has been observed from the Table 4.1 and 5.2 that, at low torque (0.1 Nm) and high temperature (195 °C) conditions, sample 3 has highest Peak Strength (43.85 MPa) amongst all the fabricated filaments which may be due lower mechanical stress during fabrication and better

heat carrying capacity of the melt during processing, resulting in strong intermolecular molecular bond between reinforcement and base matrix whereas at high torque (0.3 Nm) and least temperature (175 °C) conditions, sample 8 possesses the minimum Peak Strength (16.82 MPa). Further from Table 4.1 and Table 5.2, it was observed that upon increasing torque (Nm), PS is decreasing for all the specimens because of improper bonding between reinforcement material and the matrix material at higher load (kg) conditions. Whereas at low torque conditions, composite gets enough time for proper interbonding between reinforcement and matrix material which further helps in exhibiting ductile behaviour of the fused filaments. Further Table 5.2shows that sample 8 has the highest %BE which was 5.2% at 10kg load, 0.3 Nm torque and 175°C temperature. This may be happened due to lower load and speed condition because material gets sufficient time for proper bonding between matrix material and reinforcement. Hence, sample 8 has the maximum ductility among all the samples under specific parametric conditions of TSE. Further it has been observed from Table 5.2 that sample 3 has the minimum %BE (2.8%) under 12.5kg load, 0.1Nm torque and 195°C temperature. On the other hand, From Table 4.1 and 5.3, It was observed that with increase in load (7.5 kg to 12.5 kg), mechanical properties of fused filaments starts reducing abruptly. This could be due to increased load causing filament coming through the twin-screw extruder exhibits inferior properties, may be due to uneven blending of reinforcement in the base material. Further from Table 4.1 and Table 5.3, increasing torque (Nm), PS and %BE both starts decreasing. The reason behind decreasing mechanical properties might be under higher loading conditions, composite material gets solidifies at faster rate leads to poor mechanical properties. In addition to load and torque, temperature played a vital role in the extrusion process of fused filaments affecting mechanical properties. It has been observed from the Table 4.1 and Table 5.3 that as upon rising the extrusion temperature at low torque, PS, BS, %PE and %BE decreasing. Further analysis from Table 4.1 and Table 5.3 shows that, sample 1 possesses highest PS which is 31.81 MPa at 0.1 Nm torque, 7.5 kg load and 175°C temperature, whereas sample 3 possesses lowest PS which is 11.92 MPa at 0.1 Nm torque, 12.5 kg load and 195°C temperature. Further sample 4 depicts highest %BE which is 8.86 at 0.2 Nm torque, 7.5 kg load and 185°C temperature, whereas sample 9 depicts lowest %BE which is 2.01 at 0.3Nm torque and 12.5kg load. From Table 5.2 and 5.3, it has been observed that PS for almond skin (43.85 MPa) reinforced filaments was higher than and wood powder (31.81 MPa) reinforced filaments under similar parametric conditions.

On the basis of these observations mentioned in Table 5.2 and Table 5.3, stress-strain diagrams have been drawn as shown in the Figure 5.1 and 5.2 respectively. During the analysis of stress-strain diagram, no negative strain was found which ensures that there was no slippage between jaws of UTM while testing. Additionally, Modulus of Toughness and Modulus of Elasticity were also calculated as shown in Table 5.2 and Table 5.3. Modulus of Toughness (T) shows the total energy absorbed by fused filaments per unit volume prior to fracture and depicts the area under stress-strain curve whereas Modulus of Elasticity (E) is defined as resistance of a material to permanent deformation. From Table 5.2 and Table 5.3 it can be corelated that filaments reinforced with almond skin has higher Modulus of Elasticity as compared to filaments reinforced with wood powder which means filaments reinforced with almond skin are having higher resistance to plastic deformation.

$$\text{E (GPa)} = \frac{\text{Peak Strength}}{\text{Elongation at Peak}} \times \text{Original length} \quad (\text{Eq. 6}) \quad [139]$$

$$\text{T (MPa)} = \frac{1}{2} \times \frac{\text{Break Elongation}}{\text{Original length}} \times \text{Break Strength} \quad (\text{Eq. 7}) \quad [139]$$

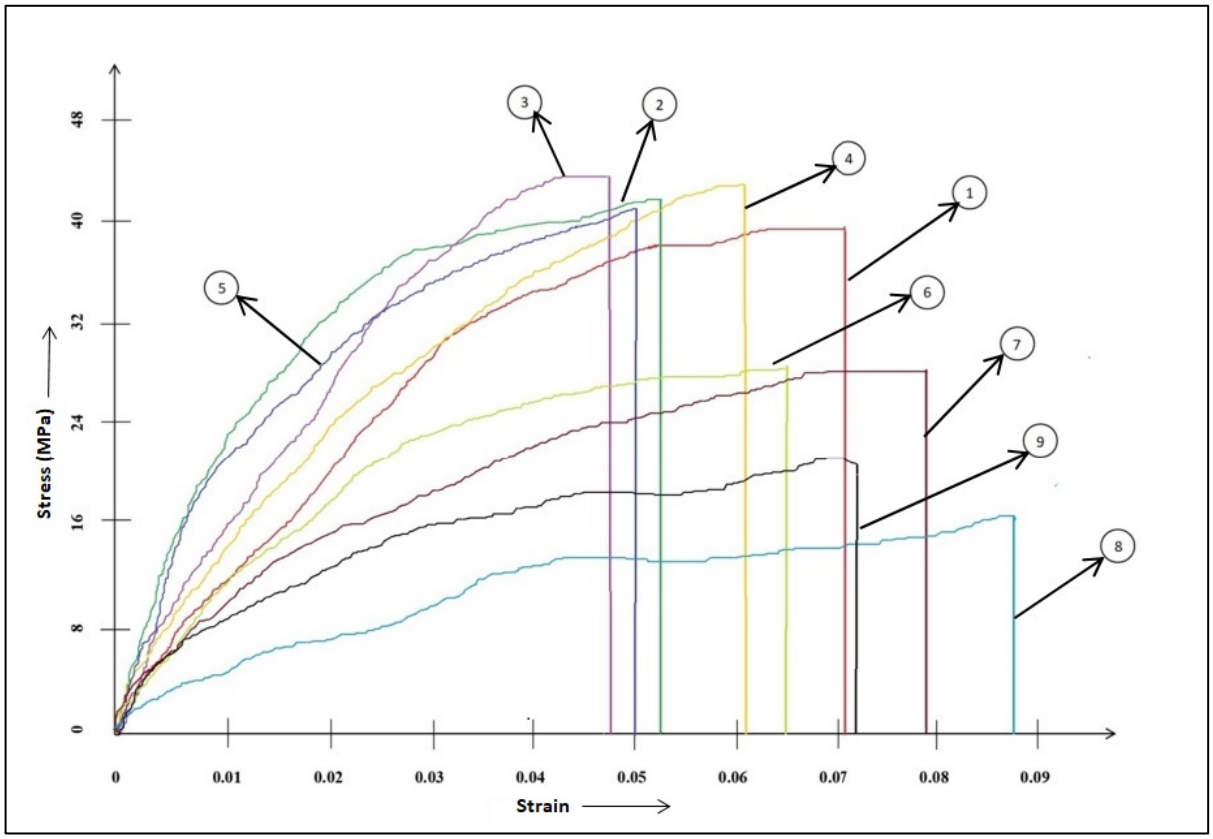

Figure 5.1 Stress strain curve of fused filament for 94% 2° recycled PLA + 6% almond skin

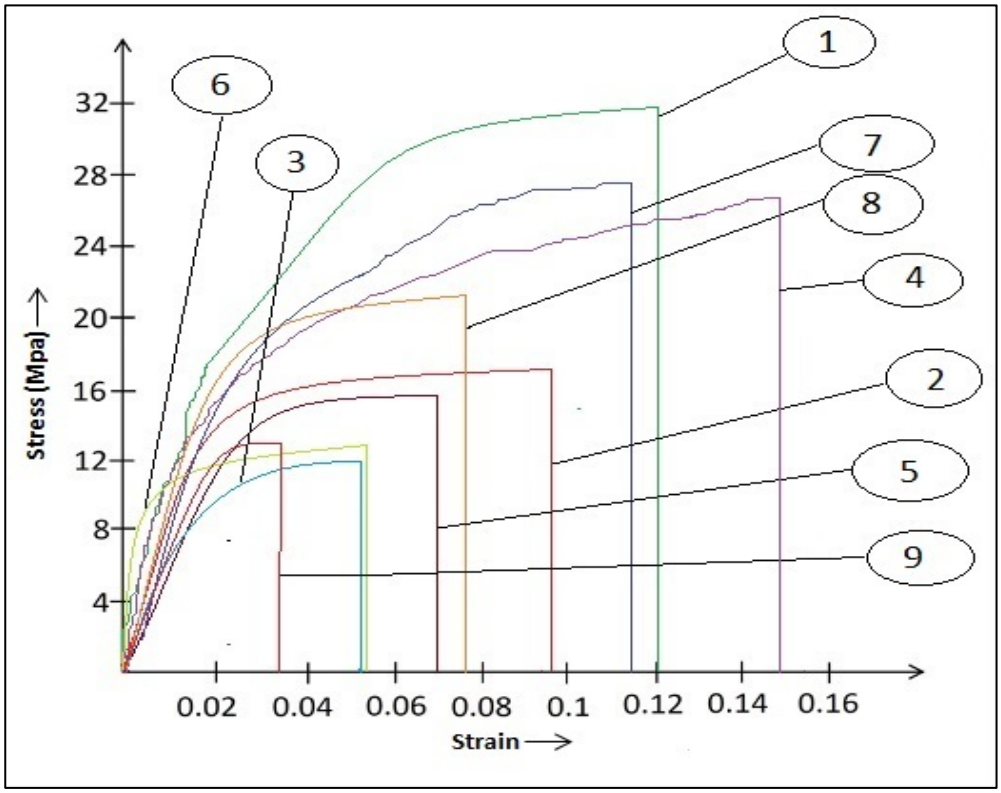

Figure 5.2 Stress strain curve of fused filament for 94% 2° recycled PLA + 6% wood powder

5.3 OPTIMIZATION OF MECHANICAL PROPERTIES OF FUSED FILAMENTS USING MINITAB

Further, to determine the effect of all parameters signal to noise ratio (S/N) curve has been plotted via Minitab software by assuming larger is better. S/N ratio for PS and %BE of filaments reinforced with almond skin and wood powder have been shown in Table 5.4. Based on S/N ratio values, mean effect plots for PS and %BE for fused filaments reinforced with almond skin and wood powder have been obtained using Minitab to examine the effect of individual parameters such as torque, load & temperature on the PS and %BE of fused filaments as shown in Figure 5.3 & 5.4 and 5.5 & 5.6. From Figure 5.3, it has been found that PS enhanced with rise in temperature form 175°C to 195°C. Further, with an increase in torque and load, PS decreases as shown in Figure 5.3. Parametric conditions for maximum PS for almond skin reinforced filaments were 0.1Nm torque, 7.5kg load, 195 °C temperature. Further Figure 5.4 shows %BE of almond skin based filaments increased when torque increases from 0.1 Nm to 0.3 Nm. Further %BE reduces drastically when temperature increases to 195°C from 175°C which shows that material cannot sustain at high temperatures, leads to change in its mechanical properties. %BE also decreases upon increasing load from 7.5kg to 12.5 kg. Parameter

conditions yielding higher %BE for almond skin reinforced 2°PLA filaments have been 0.3Nm torque, 7.5kg load and 175°C temperature.

It has been observed from the Figure 5.5 that increasing load from 7.5kg to 12.5 kg, PS of fused filament falls off abruptly. However, upon increasing torque from 0. 1 Nm to 0.2 Nm, PS of the fused filaments reduces slightly but upon further increase in torque from 0. 2 Nm to 0.3 Nm, PS starts increasing whereas with increase in temperature from 175°C to 195°C, PS reduces slightly. This might be happened because wood powder carries low specific heat capacity which impedes the steady flow of material at elevated temperatures, leading to inferior PS. Parametric conditions for maximum PS for wood powder reinforced filaments were 0.3 Nm torque, 7.5 kg load and 175°C temperature. Further from Figure 5.6, upon increasing torque and load, there was slight decrease in %BE but on the other hand, when load rises from 7.5 kg to 12.5 kg, %BE falls down quickly. Parameter conditions that yields higher %BE for wood powder reinforced 2°PLA filaments were 0.1Nm torque, 7.5kg load and 175°C temperature.

Table 5.4 S/N ratio for PS and %BE of filaments

Sample No.	**2° PLA + 6%wt. Almond Skin**		**2° PLA + 6%wt. Wood Powder**	
	S/N ratio for PS (dB)	**S/N ratio for %BE (dB)**	**S/N ratio for PS (dB)**	**S/N ratio for %BE (dB)**
1	32.00	12.67	30.05	17.13
2	32.12	10.10	25.48	15.04
3	32.84	8.94	21.53	9.74
4	32.69	11.36	28.59	18.95
5	31.89	9.54	23.65	12.51
6	29.19	11.82	22.21	9.80
7	28.69	13.44	28.87	16.64
8	24.52	14.32	26.08	13.18
9	26.12	12.87	22.61	6.06

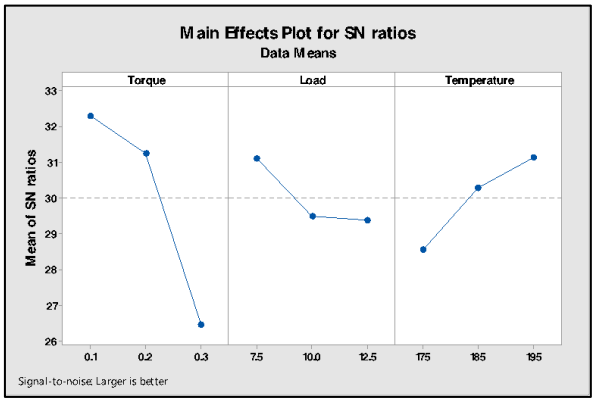

Figure 5.3 Mean S/N ratio plot for PS of filaments reinforced with almond skin

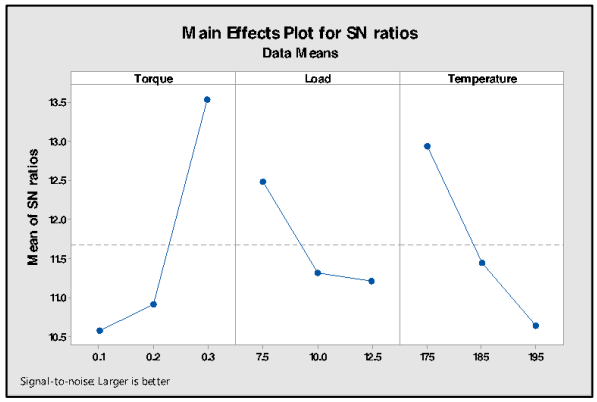

Figure 5.4 Mean S/N ratio plot for %BE of filaments reinforced with almond skin

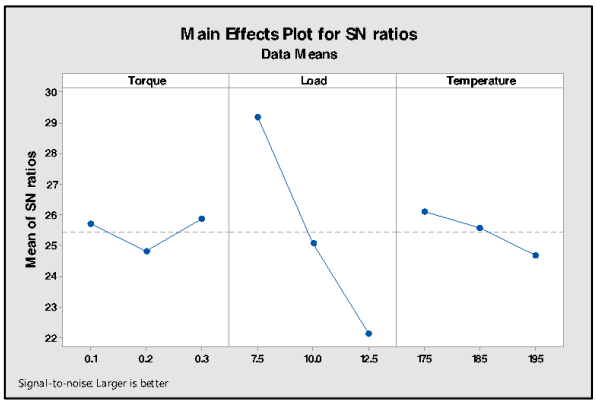

Figure 5.5 Mean S/N ratio plot for PS of filaments reinforced with wood powder

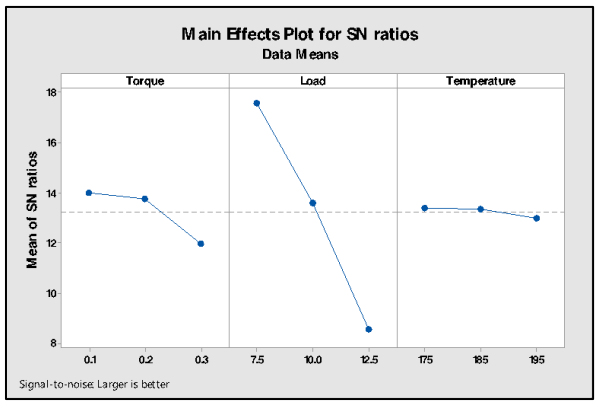

Figure 5.6 Mean S/N ratio plot for %BE of filaments reinforced with wood powder

5.4 ANALYSIS OF VARIANCE (ANOVA) OF FUSED FILAMENTS

Further an analysis of variance (ANOVA) was conducted on the S/N ratio for both PS and %BE of filaments reinforced with almond skin and wood powder to find most dominant parameter affecting PS & %BE and results obtained from the ANOVA represents in Table 5.5, Table 5.6, Table 5.7 & Table 5.8. ANOVA was conducted at 95% confidence level for S/N ratio of PS and %BE. Factors with p-value less than 0.05 were perceived statistically significant. Analysis of variance (ANOVA) was applied using Minitab as ANOVA results highlights the most significant parameters and their %age contributions which affects the PS and %BE of the fused filaments. The results of ANOVA are shown in Table 5.5 & Table 5.6 shows that temperature and torque both have remarkable effect on PS & %BE as P-values were very close or less that 0.05 for filaments reinforced with almond skin. As PS & %BE were important mechanical characteristics of the almond skin reinforced composite filament, %age contribution

using S/N ratios of the factors by applying ANOVA were also determined as shown in Table 5.5 & Table 5.6. It was observed that pre dominant factor which is impacting mechanical properties of the fabricated filaments was temperature (69.203%).

On the basis of ANOVA result findings represented in Table 5.7 and 5.8 for filaments reinforced with wood powder, load comes out as a most significant factor which affects PS of fused filament with 92.939% contribution. However, the impact of temperature on PS can't be ignored, given that p-value of temperature factor was nearly 0.05. From Table 5.8, it has been observed that p-value of load was less that 0.05 considered as the most significant factor that affect %BE with 88.378% contribution.

Table 5.5 ANOVA analysis for PS of filaments reinforced with Almond Skin

Source	**DOF**	**Adj SS**	**Adj MS**	**F-value**	**P-value**	**%age Contribution**
Temperature	2	51.818	51.818	30.26	0.003	69.203
Load	2	4.569	4.569	2.67	0.163	6.10
Torque	2	9.930	9.930	5.80	0.061	13.26
Error	2	8.561	1.712	-	-	11.43
Total	8	74.878	-	-	-	100

Table 5.6 ANOVA analysis for %BE of filaments reinforced with Almond Skin

Source	**DOF**	**Adj SS**	**Adj MS**	**F-value**	**P-value**	**%age Contribution**
Temperature	2	13.248	13.2488	18.77	0.007	48.82
Load	2	2.460	2.4600	3.49	0.121	9.06
Torque	2	7.896	7.8964	11.19	0.020	29.10
Error	2	3.529	0.7058	-	-	13.00
Total	8	27.133	-	-	-	100

Table 5.7 ANOVA analysis for PS of filaments reinforced with Wood Powder

Source	**DOF**	**Adj SS**	**Adj MS**	**F-Value**	**P-Value**	**% contribution**
Torque	2	0.0421	0.0421	0.08	0.786	0.052

Source	DOF	Adj SS	Adj MS	F-Value	P-Value	% contribution
Load	2	74.6792	74.6792	146.05	0.000	92.939
Temperature	2	3.075	3.075	6.01	0.058	3.826
Error	2	2.5565	0.5113	-	-	3.182
Total.	8	80.3538	-	-	-	100

Table 5.8 ANOVA analysis for %BE of filaments reinforced with Wood Powder

Source	DOF	Adj SS	Adj MS	F-Value	P-Value	% contribution
Torque	2	6.076	6.076	3.1	0.138	4.382
Load	2	122.535	122.535	62.6	0.001	88.378
Temperature	2	0.251	0.251	0.13	0.735	0.181
Error	2	9.788	1.958	-	-	7.059
Total.	8	138.649	-	-	-	100

5.5 FIELD EMMISSION SCANNING ELECTRON MICROSCOPY (FESEM) OF FUSED FILAMENTS

Further FESEM characterization of the fused filaments reinforced with almond skin and wood powder with maximum and minimum PS were examined. The FESEM images as shown in Figure 5.7 and Figure 5.8 of 2°PLA reinforced almond skin and wood powder filaments at break x-section have been taken at x500. In case of 2°PLA reinforced almond skin filaments, sample 3 shows minimum voids as shown in Figure 5.7 (a) which in turn gives highest PS at 0.1 Nm torque, 12.5 kg load and 195°C temperature. On the other hand, as shown in Figure 5.7 (b), sample 8 shown maximum voids which leads to minimum PS at 0.3 Nm, 10 kg load and 175°C temperature.

For sample 1, Figure 5.8 (a) shows minimum voids which leads to better mechanical properties with highest PS as observed from Table 5.3 with lower parametric conditions such as 7.5 kg load, 175°C temperature and 0.1 Nm torque whereas for sample 3, Figure 5.8 (b) shows the cluster of many voids spread over the whole break x-section of the filament leads to poor mechanical properties with minimum PS amongst all the sample with higher parametric

conditions of 12.5 kg load, 195°C temperature and 0.1 Nm torque. FESEM analysis shows that samples prepared at higher temperature possesses maximum PS with minimum voids spaces as compared to samples prepared under lower temperature conditions.

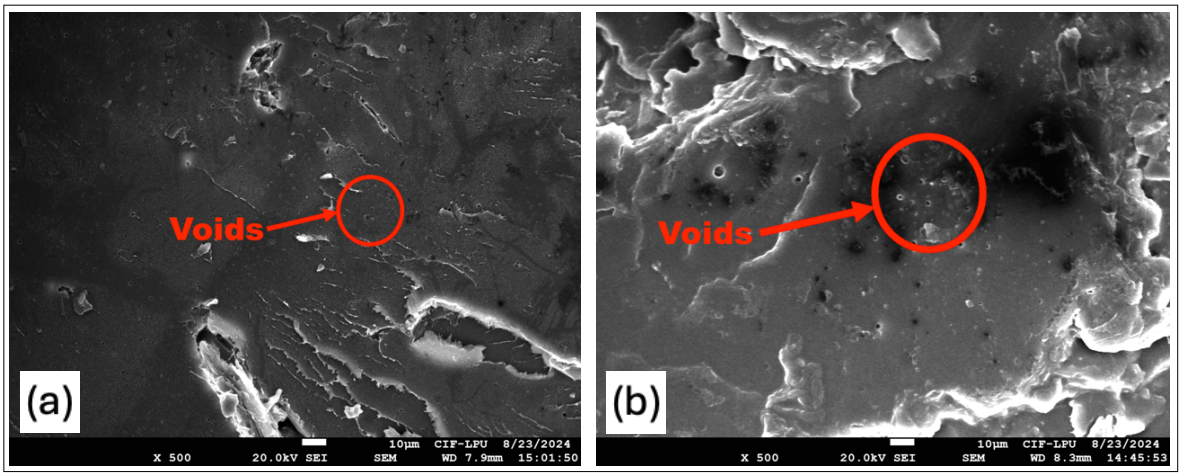

Figure 5.7 FESEM image of filaments reinforced with almond skin with (a) maximum and (b) minimum PS

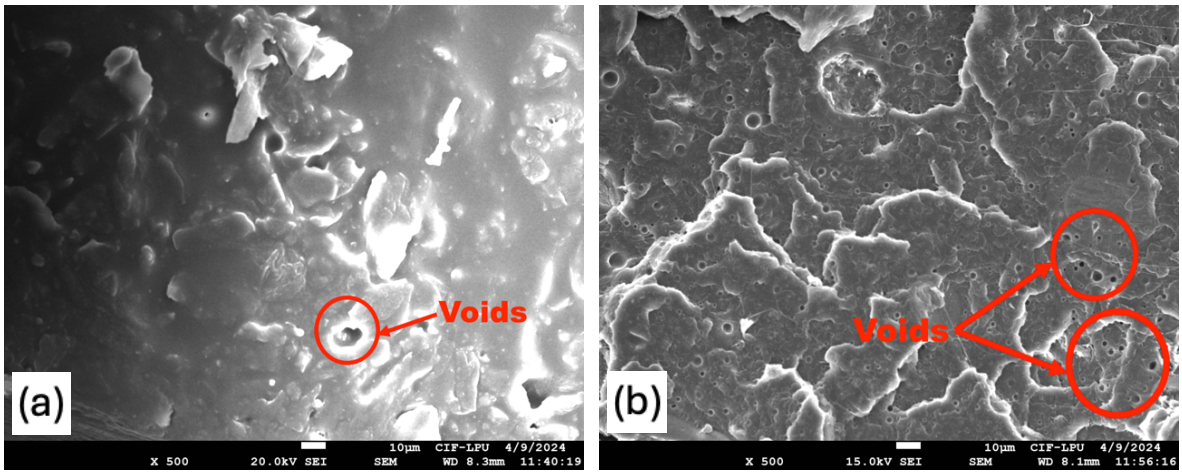

Figure 5.8 FESEM image of filaments reinforced with wood powder with (a) maximum and (b) minimum PS

5.6 ENERGY DISPERSIVE SPECTROSCOPY (EDS) ANALYSIS

EDS was carried out as shown in Figure 5.9, 5.10, 5.11 and 5.12 for the elemental analysis of the sample with maximum and minimum PS on filaments reinforced with almond skin and wood powder. Figure 5.9 of filaments reinforced with almond skin having maximum PS shows 73.06% C, 25.09% O and Na, Ca and Fe were present in very small amount whereas Figure 5.10 for filaments reinforced with almond skin having minimum PS shows 62.06% C and 37.94% O. Further Figure 5.11 of filaments reinforced with wood powder having maximum PS shows 55.38% C, 43.69% O and 0.93% Ni whereas Figure 5.12 of filaments reinforced with

wood powder having minimum PS shows 67.77% C, 32.04% O and Ca, Ni were present in very small quantity of 0.07% and 0.12%, respectively.

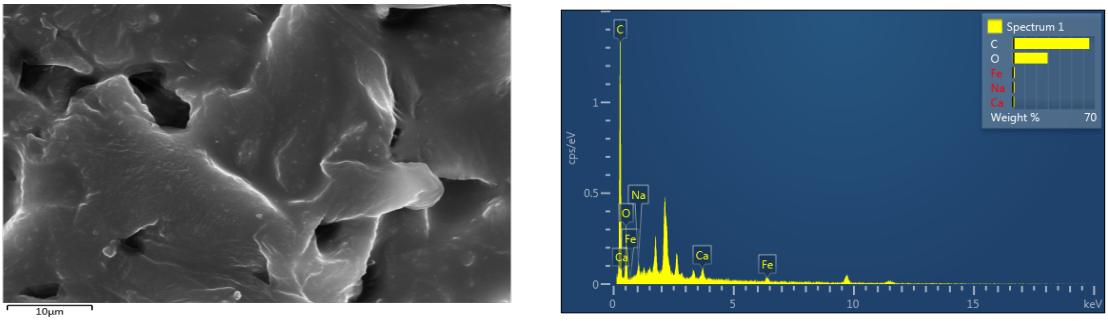

Figure 5.9 EDS image of filaments reinforced with almond skin having maximum PS

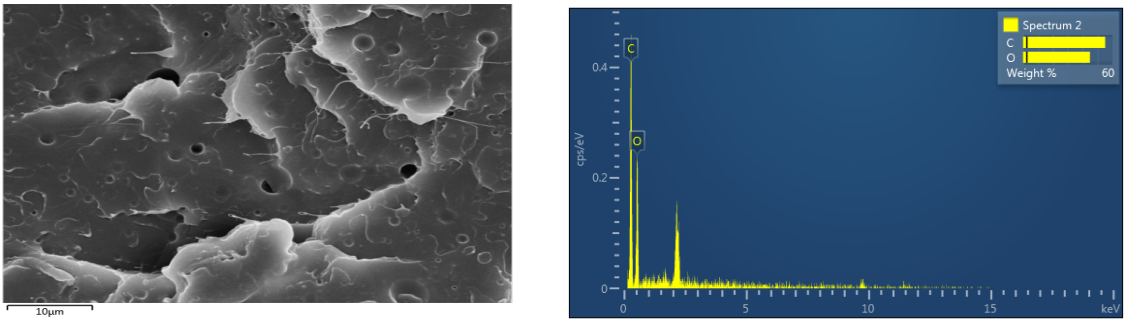

Figure 5.10 EDS image of filaments reinforced with almond skin having minimum PS

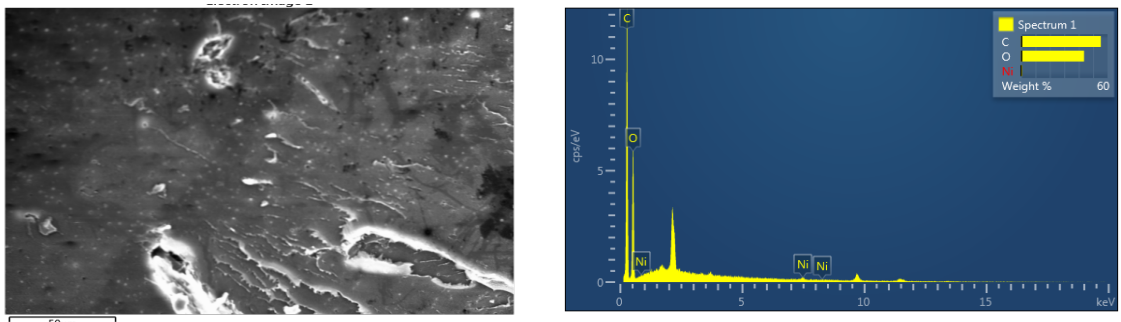

Figure 5.11 EDS image of filaments reinforced with wood powder having maximum PS

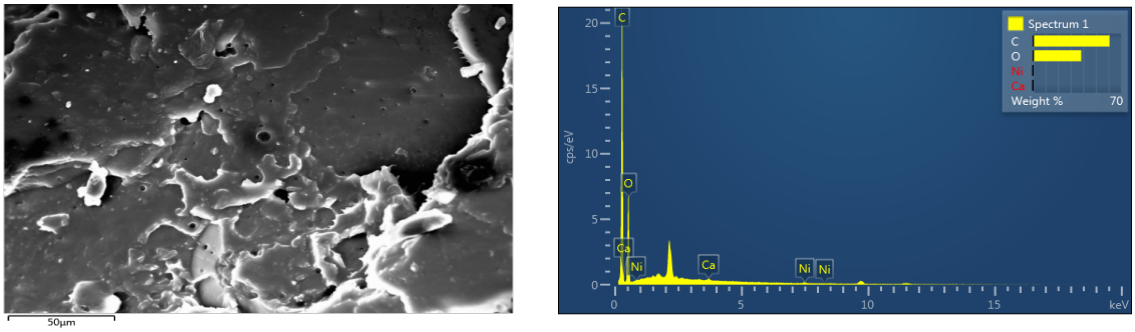

Figure 5.12 EDS image of filaments reinforced with wood powder having minimum PS

5.7 MICROSCOPIC ANALYSIS OF FUSED FILAMENTS

Additionally, optical photomicrographs of the break x-sections for all the filaments were taken at x30 as shown in Figure 5.13 and 5.14. From the analysis of these Figures and Tables 5.2 and 5.3, it has been determined that an increased presence of asperities and voids in the cross-section contributed to the poorer mechanical properties. This observation was considered to examine the role of process parameters for voids. From Figure 5.13, sample 8 shows maximum voids/surface defects which leads to lowest PS (16.82 MPa) in filaments reinforced with almond skin as shown in Table 5.2. Further, from Figure 5.14, sample 3 shows cluster of voids at many places possesses lowest PS value of 11.92 MPa in filaments reinforced with wood powder.

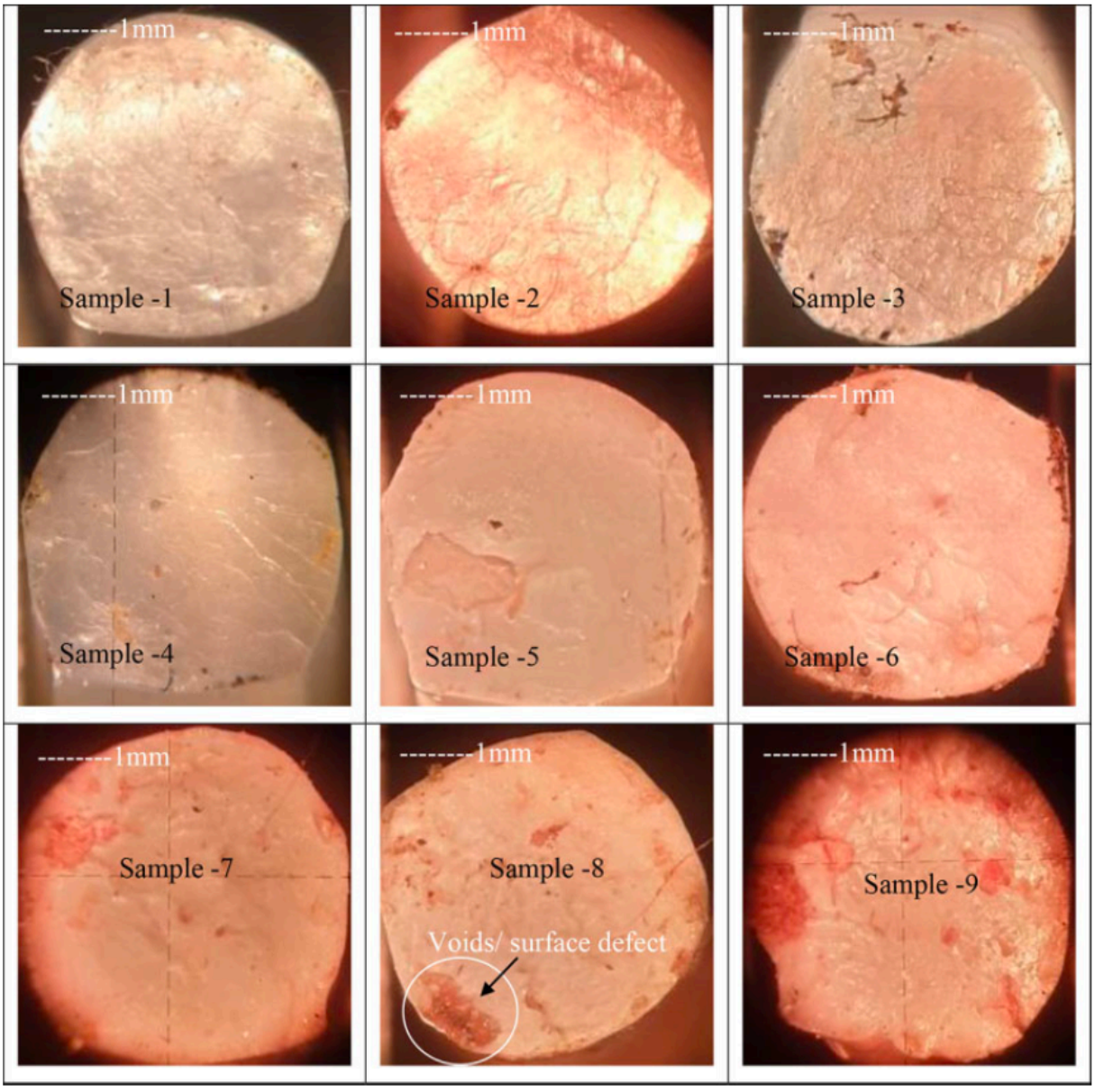

Figure 5.13 Photomicrographs at break x-section of almond skin reinforced filaments

Figure 5.14 Photomicrographs at break x-section of wood powder reinforced filaments

5.8 POROSITY ANALYSIS OF FUSED FILAMENTS

Further Tool Maker was used for porosity analysis of the fused filament reinforced with almond skin and wood powder at break cross-sections at ×100, as per ASTM B276 standards as illustrated in Figure 5.15 and Figure 5.16. It has been observed from Figure 5.15 that sample 3 has lower porosity which is 6.14% as compared to sample 8 which was 34%. Further from Figure 5.16, porosity analysis revealed that Sample 3 exhibited the highest porosity percentage at 17.74%, while Sample 1 had the lowest at 4.96%. That's why sample 1 has superior thermal

and mechanical properties as compared with sample 3. Porosity analysis shows that less porosity %age is responsible for better mechanical strength.

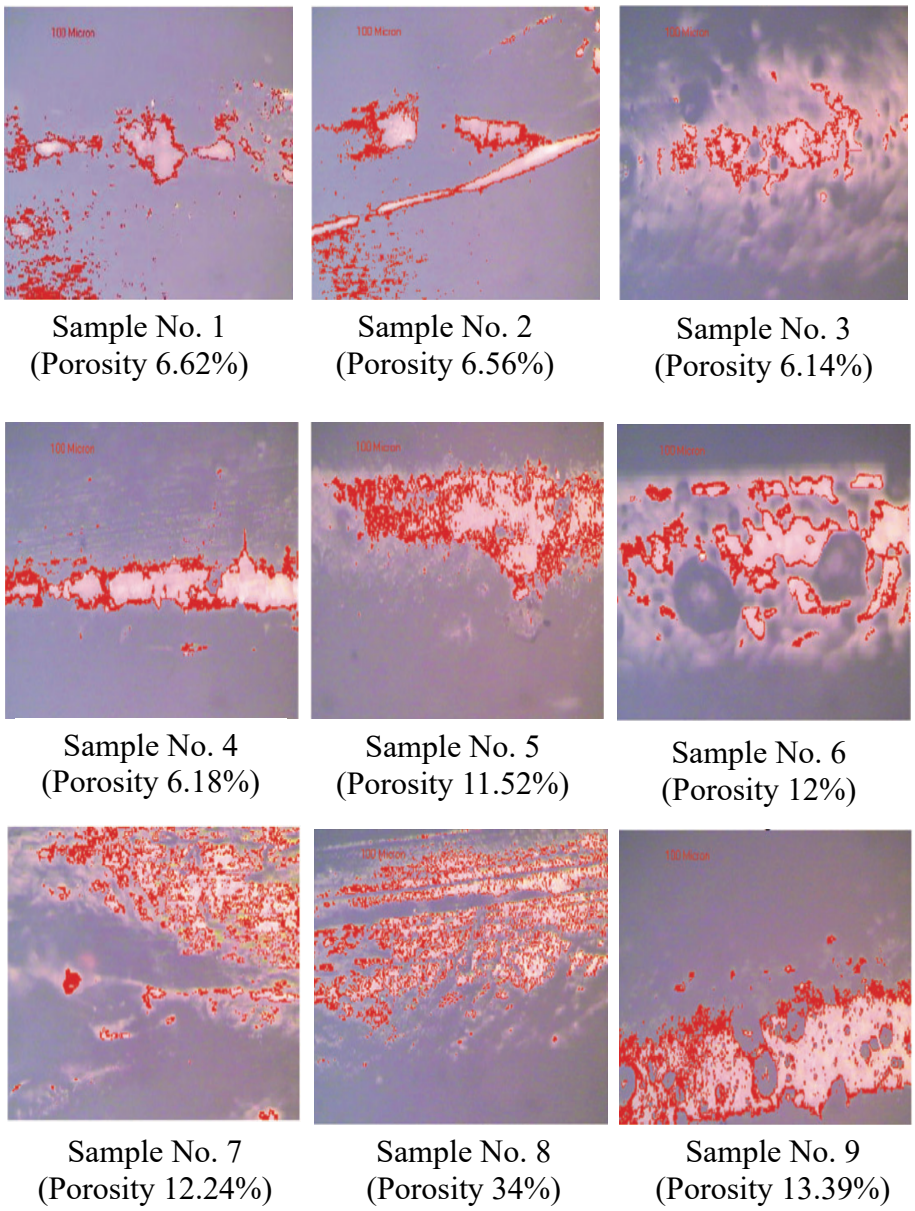

Figure 5.15 Porosity analysis of filaments reinforced with almond skin

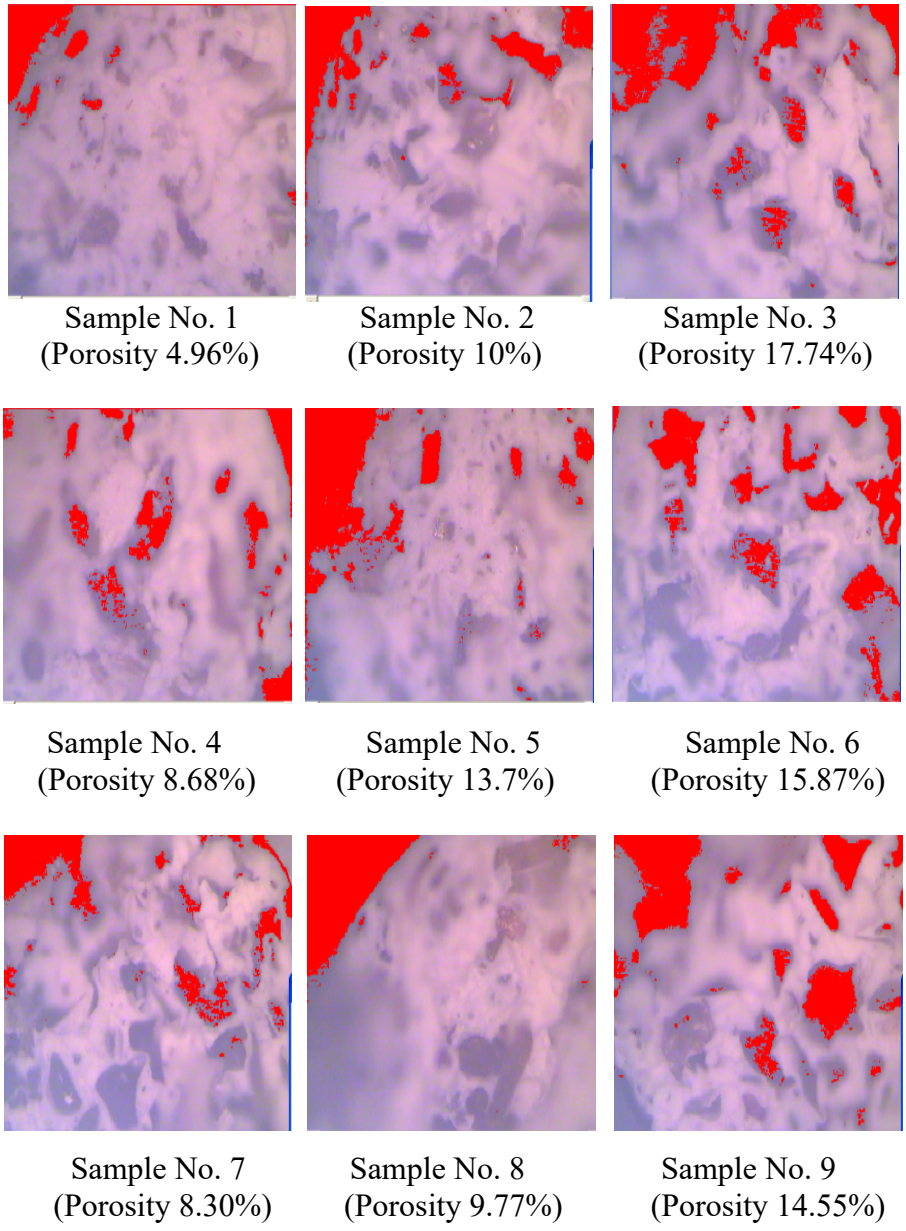

Figure 5.16 Porosity analysis of filaments reinforced with wood powder

5.9 DIFFERENTIAL SCANNING CALORIMETRY (DSC) OF FILAMENTS

To determine the thermal behaviour of fused filament reinforced with almond skin and wood powder, DSC has been used. The thermal analysis was conducted with an airflow rate of 50 ml/min and involved three cycles of heating and cooling to assess both exothermic and endothermic reactions, as depicted in Figure 5.17 and 5.18. Thermal analysis as shown in Figure 5.17 depicts that with change in percentage of reinforcement from 0wt% to 3wt%, glass transition temperature was decreased from 58.31 °C to 57.52 °C while upon further increase in %wt. of almond skin to 6%wt., T_g rises to 59.72 °C while endothermic reaction. While investigating the findings of crystallinity, better result has been found in case of 3%wt. 2° PLA

reinforced with almond skin composites as compared to 0%wt. & 6%wt. almond skin reinforced 2° PLA and further similar results were obtained while observing heat capacity as in case of crystallinity. Further from Figure 5.18, the results revealed that Sample 1, with a heat carrying capacity of 0.86 J/g, outperformed Sample 3, which had a capacity of 0.63 J/g. The DSC results indicated that fused filaments prepared under lower parametric conditions (0.1 Nm torque, 7.5 kg load and 175°C temperature) showing higher PS and BS were more suitable for high-temperature application.

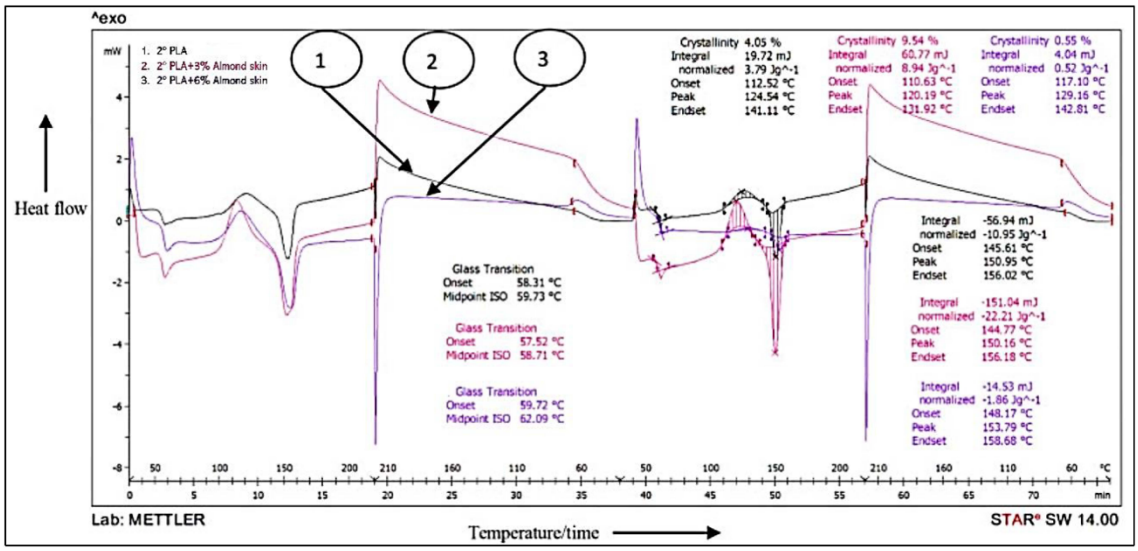

Figure 5.17 DSC analysis for varying almond skin proportions

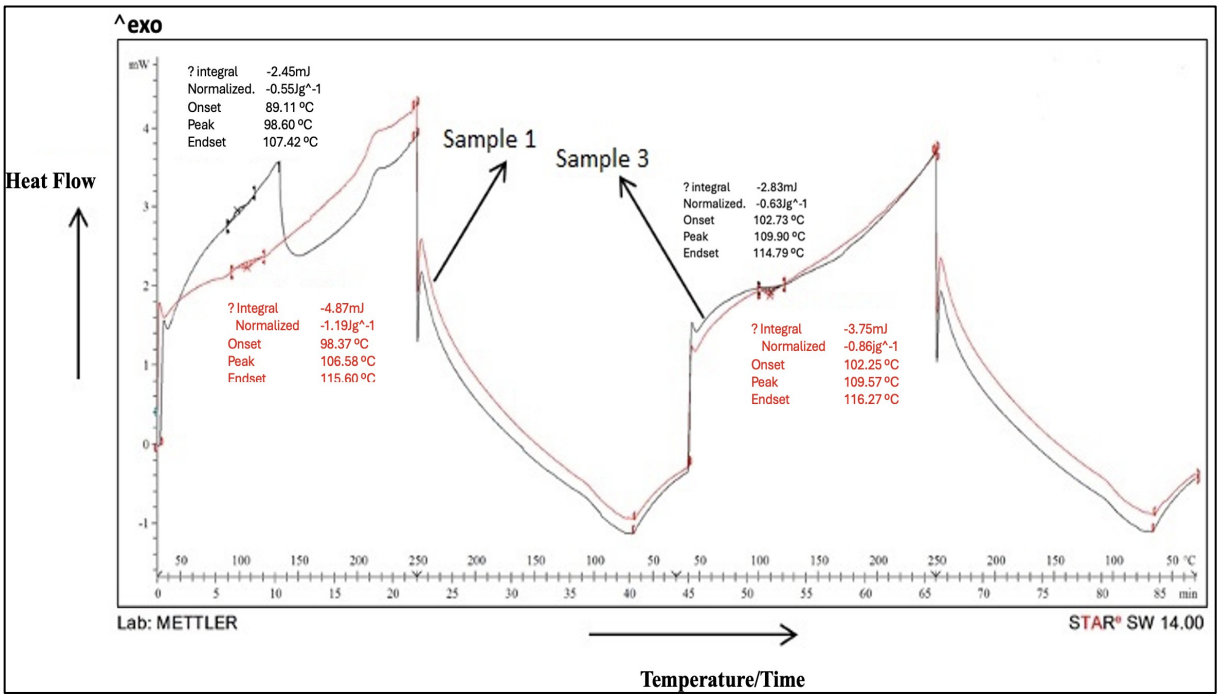

Figure 5.18 DSC analysis of filaments reinforced with wood powder having maximum & minimum porosity

From the above discussion, it has been found that filaments prepared from 2º PLA + 6% almond skin using TSE parameters of 0.1Nm, 12.5kg, 195ºC possesses maximum PS of 43.85Mpa with least porosity of 6.14%. Similarly, filaments prepared from 2º PLA + 6% wood powder using TSE parameters of 0.1Nm, 7.5kg, 175ºC possesses maximum PS of 31.81Mpa with least porosity of 4.96%. Above mentioned TSE parameters were finalized to fabricate fused filaments which were then subsequently used to prepare 3D printed samples according to ASTM standards for tensile and flexural testing to examine their mechanical properties.

5.10 TENSILE TESTING OF 3D PRINTED SAMPLES

The fabrication parameters for 3D printing of flexural and tensile specimens were found through a review of existing literature and confirmed by conducting pilot experiments. 3-different input parameters having 3-different variables were taken into consideration which are Infill Density (50%, 70%, 90%), Raster Angle (45°, 60°, 90°) and Infill Speed (40mm/s, 60mm/s, 80mm/s). The FFF setup has been used in this study is capable of withstanding a maximum temperature of nozzle 270°C**.** A single-nozzle printer was employed, featuring the ability to manually replace the fused filament at any desired point during the printing process**.** Once the total 36 specimens of 2° PLA + 6% almond skin and 18 of 2° PLA + 6% wood powder have been fabricated, 9 each for tensile testing and 9 each for flexural testing according to L9 OA mentioned in the Table 4.6, they are tested on a Universal Testing Machine (UTM) to evaluate their mechanical property in term of tensile and flexural strength.

Tensile testing was carried out on 3D printed specimens using Universal Testing machine (UTM) having load capacity of 500kg to investigate various mechanical properties such as Peak Strength (PS), Break Strength (BS), Elongation at Peak (%PE), Break Elongation (%BE), elastic modulus (E) and Modulus of Toughness (T). Results of tensile testing on all the 3D printed specimens of 2° PLA + 6% Almond Skin and 2° PLA + 6% Wood Powder in terms of strength at break, Peak Strength, Break Elongation, Elongation at Peak, Modulus of Toughness and elastic modulus as shown in Table 5.9 and Table 5.10. It was observed from the Table 5.9 for tensile testing results of 3D printed specimens (2° PLA + 6% Almond Skin) that the maximum Peak Strength (PS) is 32.45 MPa and maximum Break Strength (BS) is 31.22 MPa in sample 1 printed at 90% infill density, 45**°** raster angle and 40 mm/s infill speed which might be due to the higher infill density and lowest printing infill speed as material gets sufficient time for solidification. On the other hand, minimum PS is 16.65 MPa and minimum BS is 15.41 MPa has been found in sample 2 which was printed at 90% infill density, 60**°** raster

angle, speed 60 mm/s. Maximum %PE is 4.68 and maximum %BE is 5.32 was found in sample 3 printed at 90% infill density, 90° raster angle and 80 mm/s whereas minimum % PE is 2.89 and minimum %BE is 3.21 in sample 8 printed at 50% infill density, 60° raster angle and 40 mm/s. It has been observed that maximum elastic modulus (E) is 1.6713 GPa in sample 8 printed at 50% infill density, 60° raster angle and 40 mm/s whereas sample 2 possesses minimum elastic modulus (E) which is 0.2921 GPa printed at 90% infill density, 60° raster angle and 60 mm/s. On the other hand, sample no. 3 possesses maximum Modulus of Toughness (T) which is 0.7219 MPa printed at 90% infill density, 90° raster angle and 80 mm/s whereas minimum Modulus of Toughness (T) which is 0.1556 MPa was observed in sample no. 8 printed at 50% infill density, 60° raster angle and speed 40 mm/s.

Further from Table 5.10, for tensile testing results of 3D printed specimens (2° PLA + 6% Wood Powder), it has been observed that maximum PS is 27.35 MPa and maximum BS is 26.89 MPa for sample no. 1 printed at 90% infill density, 45° raster angle and 40 mm/s infill speed. This may be due to the reason that the 90% infill density provides a nearly solid internal structure with minimal voids and the 45° raster angle creates balanced stress distribution suitable for both tensile loads. On the other hand, 40 mm/s print speed ensures optimal thermal bonding time without introducing defects. These parameters work together to enhance interlayer bonding between layers. The combination minimizes stress concentrators (high infill density), distributes loads effectively (45° raster angle) and ensures strong thermal fusion between layers (moderate print speed). Sample 3 possesses minimum PS (10.31 MPa) and BS (8.67 MPa) printed at 90% infill density, 90° raster angle and 80 mm/s infill speed. Based on the experimental data shown in Table 5.10, reduction of approximately 62% in PS and 68% in BS. The minimum PS and BS observed in Sample 3 is mainly due to the 90° raster angle, which directs the load perpendicular to weak interlayer boundaries. Further from Table 5.9, maximum %PE (4.39%) and %BE (4.5%) has been observed in sample 3 and minimum %PE (2.81%) and %BE (2.87%) was observed in sample 6. Further, it has been observed that maximum elastic modulus (E) is 1.0158 GPa in sample no. 8 printed at 50% infill density, 60° raster angle and 40 mm/s whereas sample no. 3 possesses minimum elastic modulus (E) which is 0.1547 GPa printed at 90% infill density, 90° raster angle and 80 mm/s. Whereas, sample 2 possesses maximum Modulus of Toughness (T) which is 0.5740 MPa printed at 90% infill density, 60° raster angle and 60 mm/s whereas minimum Modulus of Toughness (T) which is 0.1396 MPa was observed in sample no. 8 printed at 50% infill density, 90° raster angle and 60 mm/s.

Both PLA composites one reinforced with 6% almond skin and the other with 6% wood powder exhibited their maximum tensile and flexural strengths when fabricated with a 90% infill density, 45° raster angle and a printing speed of 40 mm/s. These parameters proved optimal for achieving strong interlayer bonding and uniform stress distribution. The almond skin reinforced composite demonstrated superior mechanical performance, showing a 19% higher Peak Strength (32.45 MPa vs. 27.35 MPa) and a 16% higher Break Strength (31.22 MPa vs. 26.89 MPa) compared to the wood powder composite. Based upon Table 5.9 and Table 5.10, Figure 5.19 and Figure 5.20 shows stress vs strain diagram of tensile testing results.

Table 5.9 Tensile testing results of 3D printed samples reinforced with almond skin

Sample No.	Infill Density (%)	Raster Angle (°)	Infill Speed (mm/s)	PS (MPa)	BS (MPa)	%PE	%BE	E (GPa)	T (MPa)
1	90	45	40	32.45	31.22	3.8	3.99	1.2093	0.4735
2	90	60	60	16.65	15.41	4.09	4.71	0.2921	0.5856
3	90	90	80	20.85	18.75	4.68	5.32	0.3292	0.7219
4	70	45	60	28.97	27	3.37	3.88	1.2972	0.3915
5	70	60	80	20.53	18.71	4.1	4.63	0.5894	0.3555
6	70	90	40	30	28.17	3.51	3.73	0.8612	0.5352
7	50	45	80	27.98	24.55	3.53	3.98	0.6311	0.5831
8	50	60	40	21.17	19.65	2.89	3.21	1.6713	0.1556
9	50	90	60	19.33	19.1	3.12	3.61	1.1957	0.2037

Table 5.10 Tensile testing results of 3D printed samples reinforced with wood powder

Sample No.	Infill Density (%)	Raster Angle (°)	Infill Speed (mm/s)	PS (MPa)	BS (MPa)	%PE	%BE	E (GPa)	T (MPa)
1	90	45	40	27.35	26.89	3.71	3.71	0.9541	0.4482
2	90	60	60	15	14.38	3.88	4.02	0.2466	0.5740
3	90	90	80	10.31	8.67	4.39	4.5	0.1547	0.3352
4	70	45	60	23.5	22	3.02	3.21	0.9400	0.3483

Sample No.	Infill Density (%)	Raster Angle (°)	Infill Speed (mm/s)	PS (MPa)	BS (MPa)	%PE	%BE	E (GPa)	T (MPa)
5	70	60	80	12	10.37	3.24	3.5	0.3229	0.2065
6	70	90	40	11.56	10.87	2.81	2.87	0.3029	0.2219
7	50	45	80	24.77	22.09	3.78	3.92	0.5289	0.5523
8	50	60	40	16.93	15.12	2.91	3	1.0158	0.1537
9	50	90	60	11	10.67	3	3.5	0.5323	0.1396

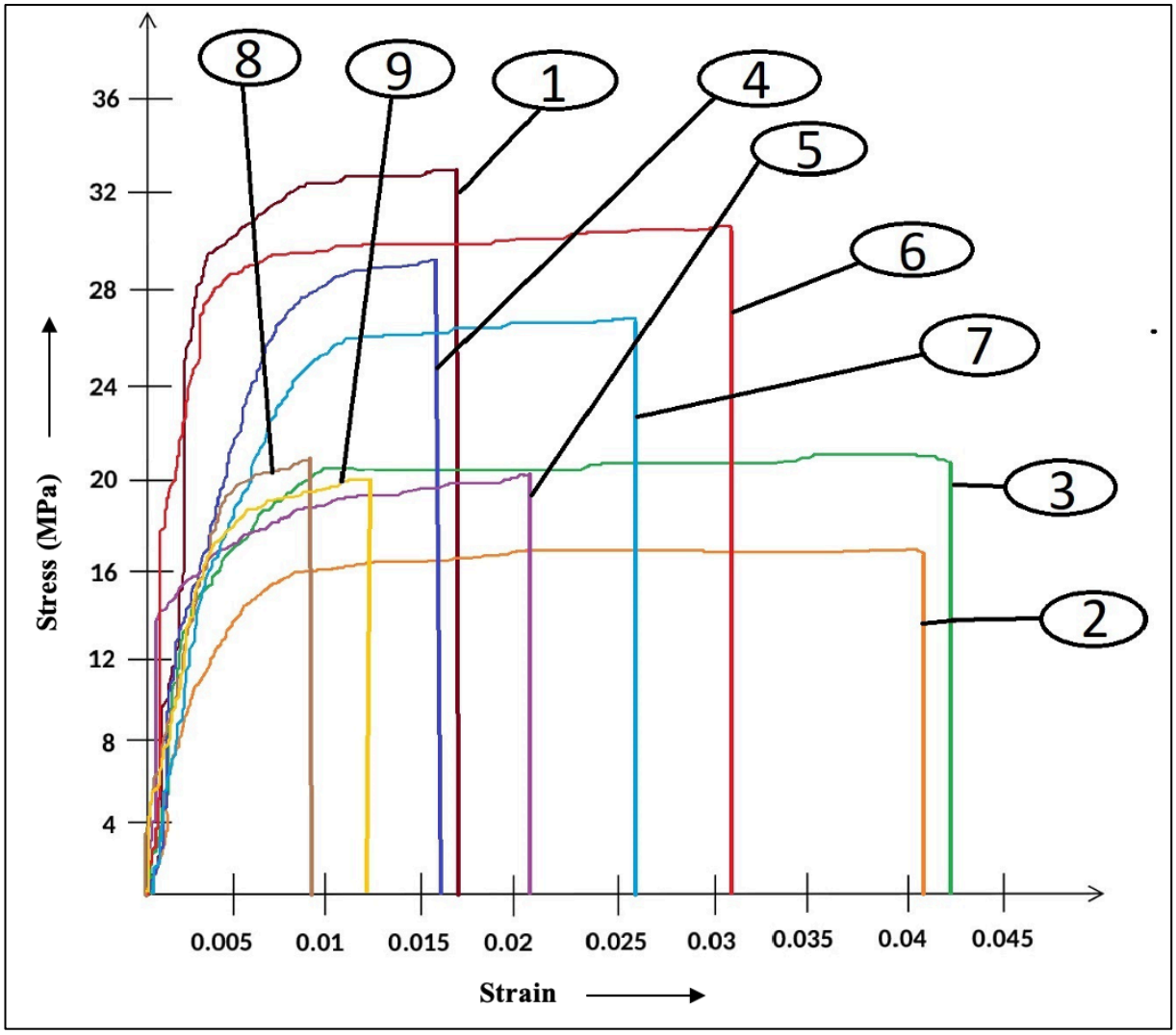

Figure 5.19 Stress-Strain diagram of 3D printed tensile sample reinforced with Almond Skin

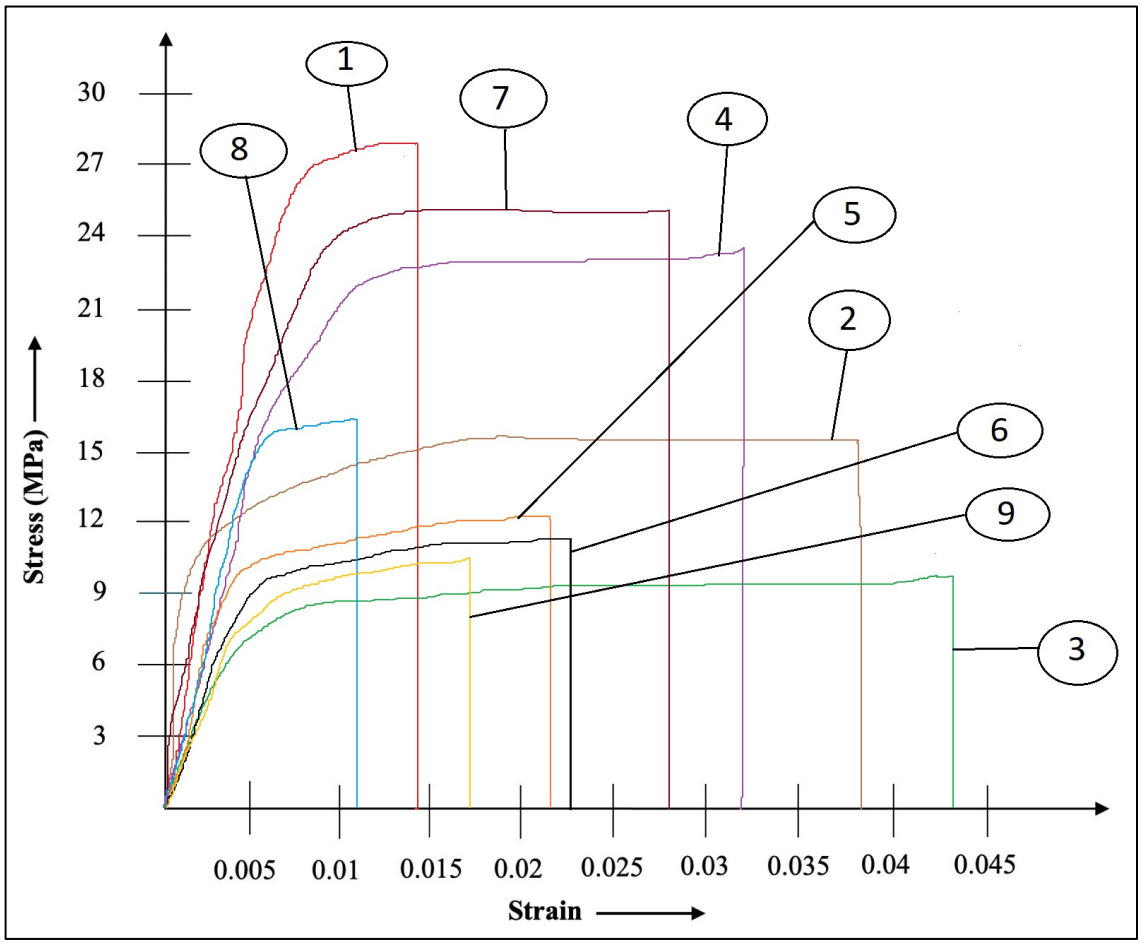

Figure 5.20 Stress-Strain diagram of 3D printed tensile sample reinforced with Wood Powder

5.11 OPTIMIZATION OF MECHANICAL PROPERTIES OF 3D PRINTED TENSILE SAMPLES USING MINITAB

Further, to determine the effect of all parameters signal to noise ratio (S/N) curve has been plotted via Minitab software by assuming larger is better. S/N ratio for PS and %BE of 3D printed tensile specimens prepared from 2° PLA + 6% Almond Skin and 2° PLA + 6% Wood Powder filaments have been shown in Table 5.11 and Table 5.12. Based on S/N ratio values, mean effect plots for PS and %BE have been obtained using Minitab to examine the effect of individual parameters like infill density, raster angle and infill speed on the PS and %BE of 3D printed specimens (both Almond Skin and Wood Powder) as shown in Figure 5.21, Figure 5.22, Figure 5.23 and Figure 5.24. From Figure 5.21 in case of 2° PLA + 6% Almond Skin, it has been observed that for PS, optimized parameters are found to be 70% infill density, 60° raster angle and 40 mm/s infill speed whereas from Figure 5.22, for %BE, optimized parameters are 90% infill density, 90° raster angle and 80 mm/s infill speed. Further from figure 5.23 in case of 2° PLA + 6% Wood Powder, it has been observed that for PS, optimized

parameters are found to be 50% infill density, 45° raster angle and 40 mm/s infill speed whereas from Figure 5.24, for %BE, optimized parameters are 90% infill density, 45° raster angle and 80 mm/s infill speed.

Table 5.11 S/N ratio for PS and %BE of 3D printed tensile samples reinforced with almond skin

Sample No.	S/N ratio for PS (dB)	S/N ratio for %BE (dB)
1	30.22	12.02
2	24.43	13.46
3	26.38	14.52
4	29.24	11.78
5	26.25	13.31
6	29.54	11.43
7	28.94	12.00
8	26.51	10.13
9	25.72	11.15

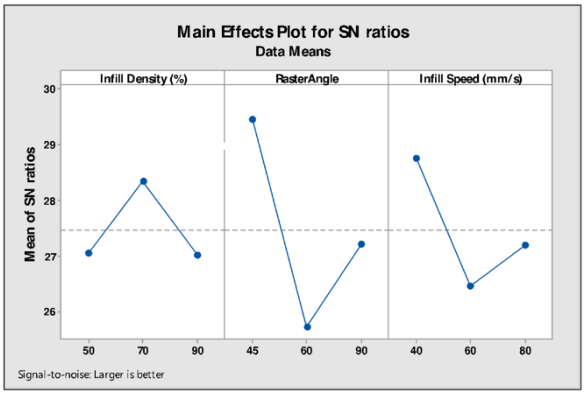

Figure 5.21 Mean effect plots for S/N ratio for PS of 3D printed tensile specimens reinforced with almond skin

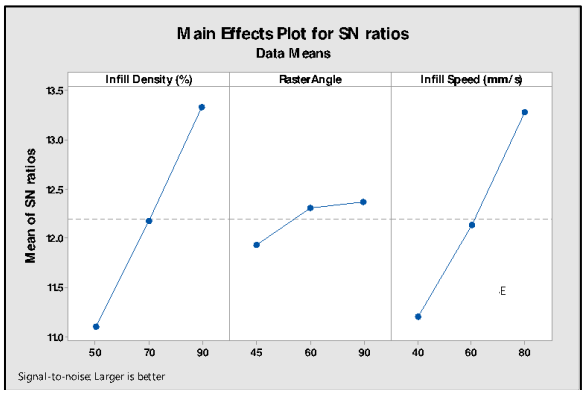

Figure 5.22 Mean effect plots for S/N ratio for %BE of 3D printed tensile specimens reinforced with almond skin

Table 5.12 S/N ratio for PS and %BE of 3D printed tensile samples reinforced with wood powder

Sample No.	S/N ratio for PS (dB)	S/N ratio for %BE (dB)
1	28.73	11.38
2	23.52	12.08

Sample No.	S/N ratio for PS (dB)	S/N ratio for %BE (dB)
3	20.26	13.06
4	27.42	10.13
5	21.58	10.88
6	21.25	9.157
7	27.87	11.86
8	24.57	9.542
9	20.82	10.88

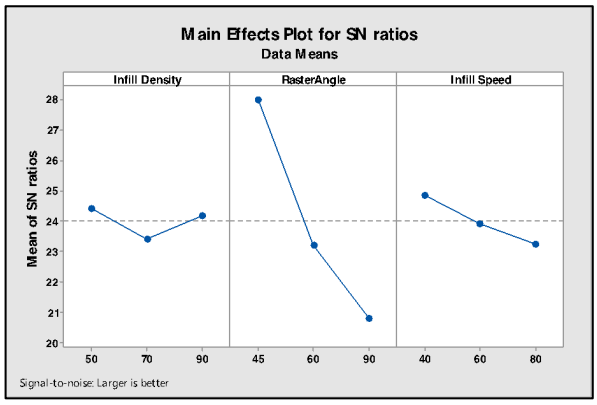

Figure 5.23 Mean effect plots for S/N ratio for PS of 3D printed tensile samples reinforced with wood powder

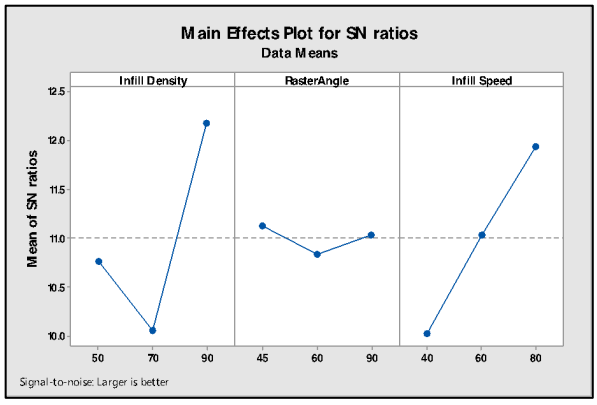

Figure 5.24 Mean effect plots for S/N ratio for %BE of 3D printed tensile samples reinforced with wood powder

5.12 ANALYSIS OF VARIANCE (ANOVA) OF 3D PRINTED TENSILE SAMPLES

Further an analysis of variance (ANOVA) was conducted on the S/N ratio for both PS and %BE of 3D printed specimens (Almond Skin and Wood Powder) to find most dominant parameter affecting PS & %BE and results obtained from the ANOVA represents in Table 5.13 and Table 5.14. ANOVA was performed at a 95% confidence level for the S/N ratios of PS and %BE. Factors with p-values below 0.05 were considered statistically significant. The analysis conducted using Minitab software, identified the most influential parameters and their percentage contributions affecting the PS and %BE of the 3D printed specimens. It has been found from Table 5.13 that predominant factor which is affecting PS (Almond Skin) of the prepared 3D printed specimens was raster angle (64.25%) whereas Table 5.14 shows that predominant factor which is affects %BE of the prepared 3D printed specimens was infill density (52.20%). Further from Table 5.15, raster angle (93.12%) is the predominant factor

which affects PS (Wood Powder) of prepared 3D printed specimens whereas from Table 5.16, it was found that predominant factor which affects %BE of the prepared 3D printed samples was infill density (55.44%).

Table 5.13 ANOVA for PS of 3D printed tensile samples reinforced with almond skin

Source	DOF	Adj SS	Adj MS	F-value	P-value	%age Contribution
Infill Density (%)	2	3.4247	1.7124	27.88	0.035	10.36
Raster Angle	2	21.2350	10.6175	172.89	0.006	64.25
Infill speed (mm/s)	2	8.2685	4.1343	67.32	0.015	25.02
Error	2	0.1228	0.0614	-	-	0.37
Total	8	33.0510	-	-	-	100

Table 5.14 ANOVA for %BE of 3D printed tensile samples reinforced with almond skin

Source	DOF	Adj SS	Adj MS	F-value	P-value	%age Contribution
Infill Density (%)	2	7.5298	3.7649	173.55	0.006	52.20
Raster Angle	2	0.3313	0.1656	7.64	0.116	2.30
Infill speed (mm/s)	2	6.52	3.26	150.28	0.007	45.20
Error	2	0.0434	0.0217	-	-	0.30
Total	8	14.4245	-	-	-	100

Table 5.15 ANOVA for PS of 3D printed tensile samples reinforced with wood powder

Source	DOF	Adj SS	Adj MS	F-Value	P-Value	%age Contribution
Infill Density	2	1.6419	0.8209	4.03	0.199	1.88
Raster Angle	2	81.1353	40.5676	199.16	0.005	93.12

Source	DOF	Adj SS	Adj MS	F-Value	P-Value	%age Contribution
Infill Speed	2	3.9427	1.9714	9.68	0.094	4.53
Error	2	0.4074	0.2037	-	-	0.47
Total	8	87.1272	-	-	-	100

Table 5.16 ANOVA for %BE of 3D printed tensile samples reinforced with wood powder

Source	DOF	Adj SS	Adj MS	F-Value	P-Value	%age Contribution
Infill Density	2	7.0079	3.50397	203.18	0.005	55.44
Raster Angle	2	0.1331	0.06656	3.86	0.206	1.05
Infill Speed	2	5.4651	2.73254	158.44	0.006	43.23
Error	2	0.0345	0.01725	-	-	0.27
Total	8	12.6406	-	-	-	100

5.13 FESEM ANALYSIS OF 3D PRINTED TENSILE SAMPLES

To analyze fracture surface of 3D printed tensile sample, FESEM characterization has been performed having maximum and minimum PS reinforced with almond skin and wood powder as shown in Figure 5.25 and 5.26, respectively. Samples were prepared by cutting 3mm away from the fractured surface. As specimens are non-conductive in nature, gold coating was performed on the fractured surface on both samples. In Figure 5.25 (a), fiber pull out and air gap betweeb layers was observed whereas remaining fractured surface was having lesser voids than sample with minimum PS as shown in Figure 5.25 (b) shows the presence of voids in both specimens contributes to stress concentration and eventually causing failure. Similarly, from 5.26 (a) smaller voids were seen on the fractured surfce whoch indicates the high PS in wood powder reinfroced samples as compared to Figure 5.26 (b). During tensile testing, deformation of adjacent layers led to the formation of crazes at multiple locations and fiber pull out.

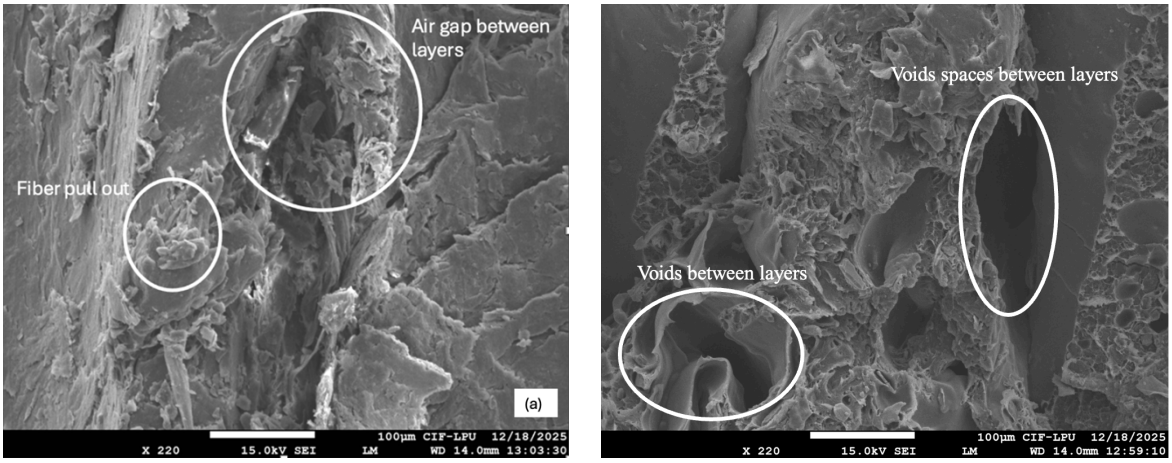

Figure 5.25 FESEM of 3D printed tensile samples reinforced with almond skin having (a) maximum (b) minimum PS

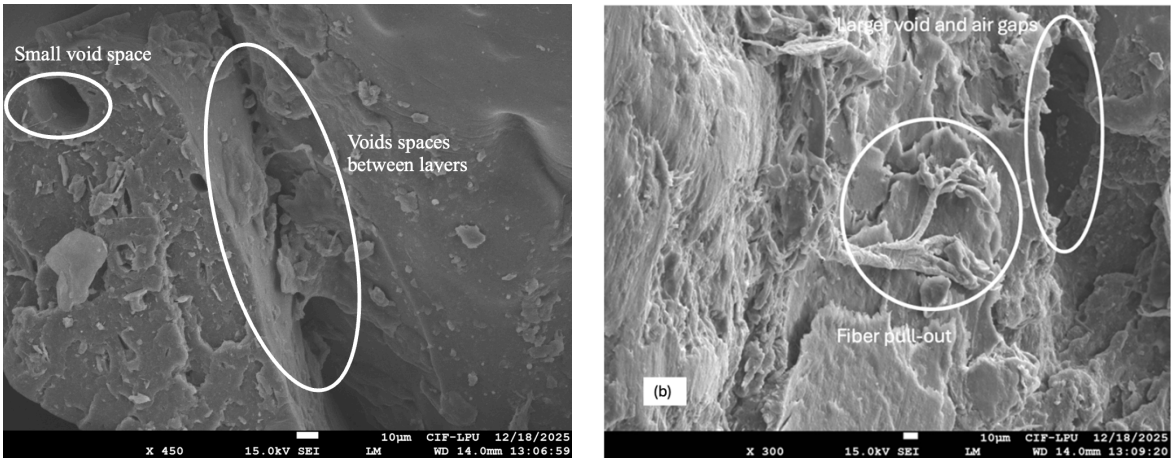

Figure 5.26 FESEM of 3D printed tensile samples reinforced with wood powder having (a) maximum (b) minimum PS

5.14 EDS OF 3D PRINTED TENSILE SAMPLE

EDS was carried out on 3D printed tensile sample having maximum PS to examine its elemental composition along with area mapping to examine elemental distribution on the fractured surface as shown in Figure 5.27. This composition indicates that the specimen is significantly made of organic materials, like from the 2°PLA + almond skin reinforcement, both of which are carbon-rich. Elemental composition of shows 50.87% carbon (C) whereas 49.13% oxygen (O). unwanted elements were not found during the analysis indicating purity of material and proper processing of composite which also supports the increased PS of the sample.

Further from Figure 5.28, it has been observed from EDS that samples reinforced with wood powder carries carbon (C), oxygen (O), sodium (Na), calcium (Ca) and iron (fe). Sample contains 65.27% carbon which is highest amongst all other elements. Further, sample contains

29.86% oxygen and remaining portion was carried by Na, Ca and Fe whoch acts as impurities only as they are present in very small amount i.e. 1.59%, 1.43% and 1.86% respectively. Na which was present in very small amount often occurs in wood but in very low quantity which is having very little or no effect on the mechanical properties of samples. Presence of Ca also confirms cellulosic nature of the material as wood in this case present in trace amounts. It confirms only the presence of natural reinforcement and present in a very small quantity which does not impact or harm the mechanical performance of the sample. The minimal presence of iron may be due to contamination or residual metal particles introduced during material handling.

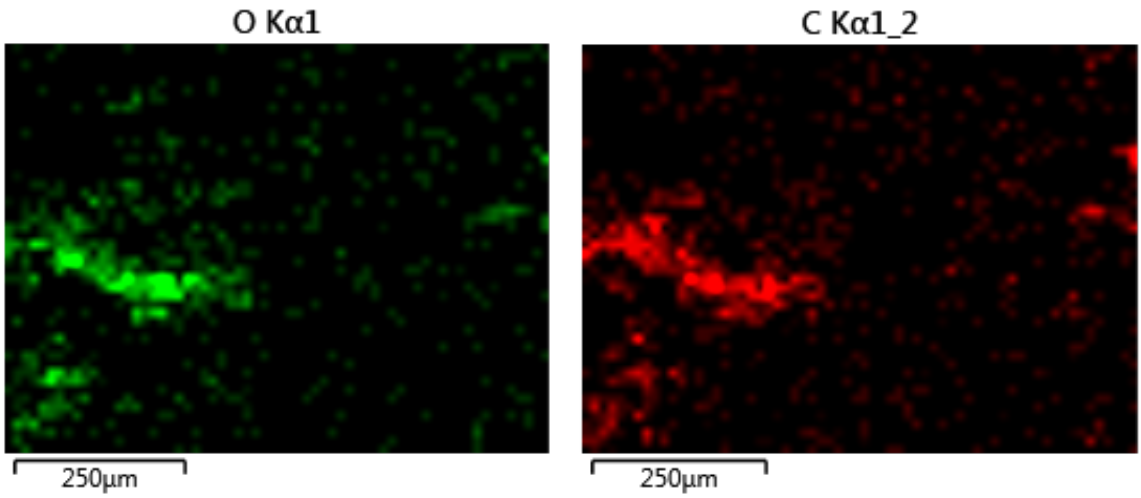

Figure 5.27 EDS of fractured tensile sample having maximum PS reinforced with almond skin

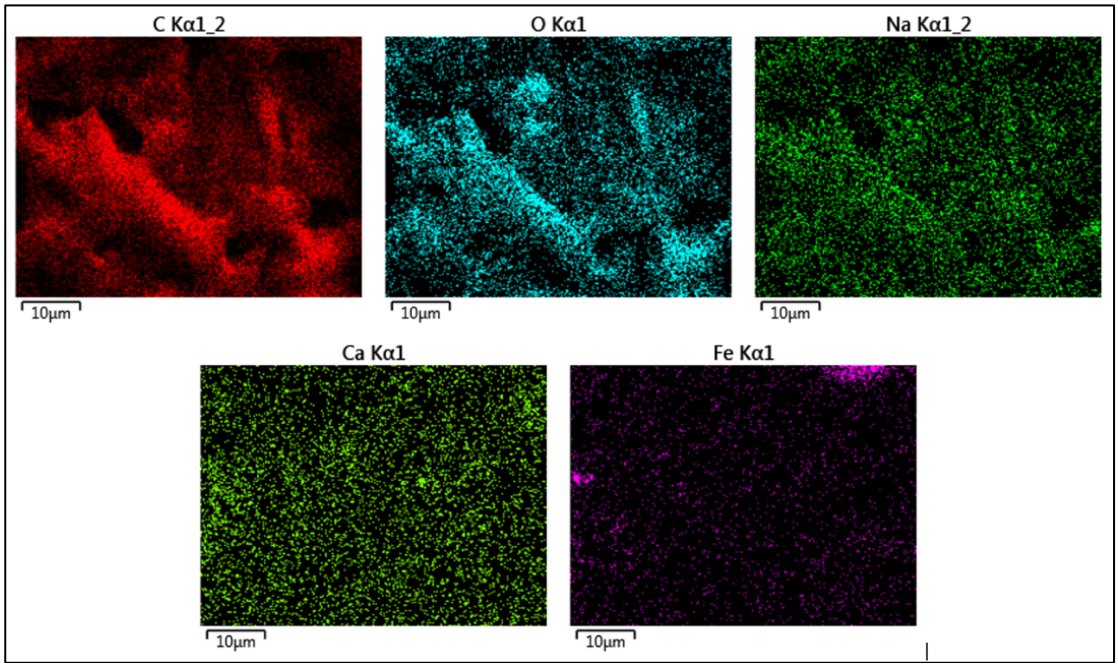

Figure 5.28 EDS of fractured tensile sample having maximum PS reinforced with wood powder

5.15 FLEXURAL TESTING OF 3D PRINTED SAMPLES

Flexural testing of 3D printed specimens was carried using UTM having load capacity of 5KN to determine their mechanical properties such as Peak Strength (PS), Break Strength (BS), Elongation at Peak (%PE), Break Elongation (%BE), elastic modulus (E) and Modulus of Toughness (T).

Flexural testing results for 2° PLA + 6% Almond Skin have been shown in the Table 5.17. From Table 5.18, it has been observed that sample 1 possesses maximum PS and BS which are 34.47 MPa and 34.1 MPa respectively printed at 90% Infill Density, 45° raster angle, 40 mm/s infill speed whereas minimum PS and BS for flexural testing was observed in sample no. 2 which are 17.66 MPa and 16.78 MPa printed at 90% Infill Density, 60° raster angle, 60 mm/s infill speed. Further from Table 5.17, maximum %PE (3.97) and %BE (4.13) was observed again in sample no. 1 printed at 90% Infill Density, 45° raster angle, 40 mm/s infill speed whereas sample no. 5 possesses minimum %PE (2.03) and %BE (2.37) printed at 70% Infill Density, 60° raster angle, 80 mm/s infill speed.

On the other hand, maximum elastic modulus (E) was observed in sample 3 which is 0.7538 GPa printed at 90% Infill Density, 90° raster angle, 80 mm/s infill speed whereas minimum elastic modulus (E) which is 0.4067 GPa was observed in sample no. 1 printed at 90% Infill Density, 45° raster angle, 40 mm/s infill speed.

Further from the Table 5.17, maximum Modulus of Toughness (1.5466 MPa) was observed in sample no. 8 printed at 50% Infill Density, 60° raster angle, 40 mm/s infill speed whereas minimum Modulus of Toughness (0.6642 MPa) was observed in sample no. 2 printed at 90% Infill Density, 60° raster angle, 60 mm/s infill speed. Further from Table 5.18, flexural testing results for 2° PLA + 6% Wood Powder have been shown and from the Table 5.2, it has been observed that sample no. 1 possesses maximum PS and BS which are 31.01 MPa and 29.78 MPa respectively printed at 90% Infill Density, 45° raster angle, 40 mm/s infill speed whereas sample no. 3 possesses minimum PS and BS which are 10.8 MPa and 9.46 MPa respectively printed at 90% Infill Density, 90° raster angle, 80 mm/s infill speed.

Further from Table 5.18, maximum %PE (3.87) and %BE (4.1) was observed again in sample 1 printed at 90% Infill Density, 45° raster angle, 40 mm/s infill speed whereas sample

5 possesses minimum %PE (2.11) and %BE (2.21) printed at 70% Infill Density, 60° raster angle, 80 mm/s infill speed. From Table 5.18, maximum elastic modulus (E) was observed in sample 3 which is 0.8458 GPa printed at 90% Infill Density, 90° raster angle, 80 mm/s infill speed whereas minimum elastic modulus (E) which is 0.3894 GPa was observed in sample no. 1 printed at 90% Infill Density, 45° raster angle, 40 mm/s infill speed. On the other hand, from Table 5.18, maximum Modulus of Toughness (1.1803 MPa) was observed in sample no. 8 printed at 50% Infill Density, 60° raster angle, 40 mm/s infill speed whereas minimum Modulus of Toughness (0.2980 MPa) was observed in sample no. 3 printed at 90% Infill Density, 90° raster angle, 80 mm/s infill speed. Figure 5.29 and Figure 5.30 shows stress vs strain diagram for Almond Skin and Wood powder based on flexural testing results.

Table 5.17 Flexural testing results of 3D printed samples reinforced with almond skin

Sample No.	Infill Density (%)	Raster Angle (°)	Infill Speed (mm/s)	PS (Mpa)	BS (MPa)	%PE	%BE	E (GPa)	T (MPa)
1	90	45	40	35.47	34.1	3.97	4.13	0.4067	1.4578
2	90	60	60	17.66	16.78	3.12	3.44	0.7264	0.6642
3	90	90	80	22.87	21.65	2.57	2.83	0.7538	0.7199
4	70	45	60	29.17	27.39	2.31	2.43	0.4537	1.4311
5	70	60	80	22.98	21.78	2.03	2.37	0.6621	0.8276
6	70	90	40	30.63	29	2.5	2.77	0.5723	1.3316
7	50	45	80	28	26.97	2.67	3.15	0.5561	1.3238
8	50	60	40	21.87	20.35	3.5	3.98	0.4300	1.5466
9	50	90	60	20.01	19.04	2.8	3	0.4598	1.1757

Table 5.18 Flexural testing results of 3D printed samples reinforced with wood powder

Sample No.	Infill Density (%)	Raster Angle (°)	Infill Speed (mm/s)	PS (Mpa)	BS (MPa)	%PE	%BE	E (GPa)	T (MPa)
1	90	45	40	31.01	29.78	3.87	4.1	0.3894	1.0299
2	90	60	60	17.65	16	3.56	3.71	0.6637	0.6307
3	90	90	80	10.8	9.46	2.79	3	0.8458	0.2980
4	70	45	60	21.66	20.37	2.43	2.6	0.5072	1.0185
5	70	60	80	12	10.88	2.03	2.21	0.6308	0.4533
6	70	90	40	11.21	9.70	2.3	2.49	0.5586	0.4446
7	50	45	80	24.2	23	2.98	3.12	0.5287	1.1692
8	50	60	40	16.68	15.23	3.61	3.7	0.4156	1.1803
9	50	90	60	12.21	11.12	2.82	2.91	0.4433	0.7043

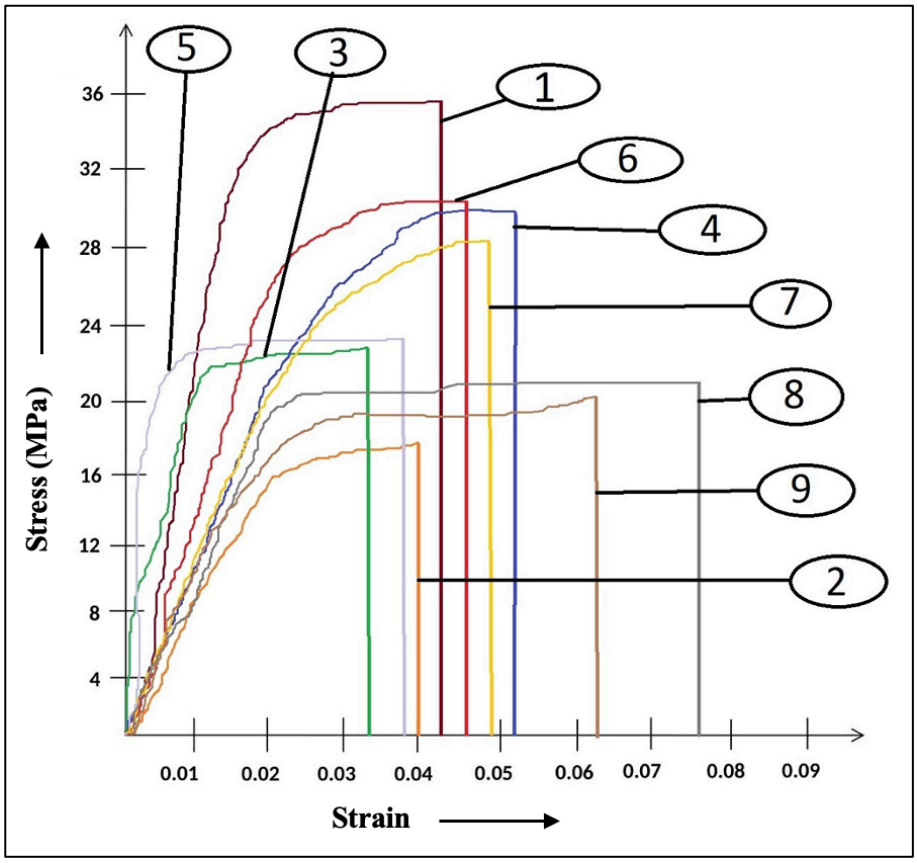

Figure 5.29 Stress-Strain diagram of 3D printed flexural sample reinforced with almond skin

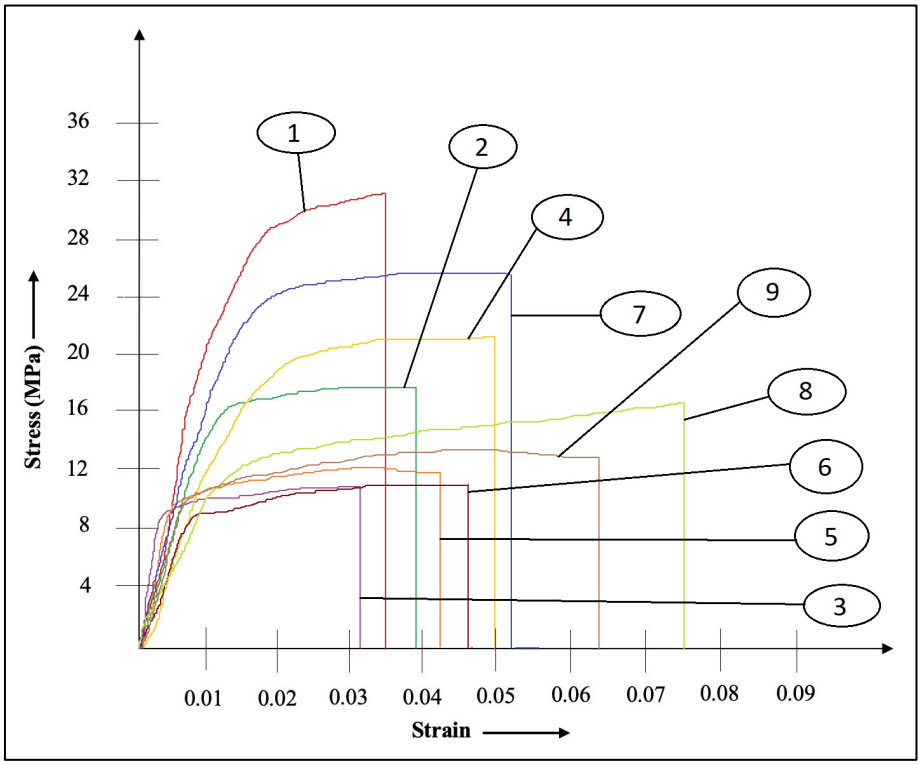

Figure 5.30 Stress Stress-Strain diagram of 3D printed flexural sample reinforced with wood powder

5.16 OPTIMIZATION OF FLEXURAL SAMPLES USING MINITAB

S/N ratio for PS and %BE of 3D printed flexural specimens prepared from 2° PLA + 6% Almond Skin and 2° PLA + 6% Wood Powder filaments have been shown in Table 5.19 and Table 5.20 respectively. Further, based on flexural testing results, mean effect plots have been obtained as shown in Figure 5.31, Figure 5.32, Figure 5.33 and Figure 5.34 using Minitab software for the investigation of effect of FFF parameter on various mechanical properties. From Figure 5.31, it has been observed that for PS, optimized parameters are found to be 70% infill density, 45° raster angle and 40 mm/s infill speed whereas from Figure 5.32, for %BE, optimized parameters are 90% infill density, 60° raster angle and 40 mm/s. Similarly, from Figure 5.32 and Figure 5.33, it has been observed for PS and %BE, optimized parameters are found to be 90% infill density, 45° raster angle and 40 mm/s infill speed.

Table 5.19 S/N ratio for PS and %BE of 3D printed flexural samples reinforced with almond skin

Sample No.	S/N ratio for PS (dB)	S/N ratio for %BE (dB)
1	30.99722	12.319
2	24.93981	10.73117
3	27.18532	9.035729
4	29.29873	7.712125
5	27.227	7.494967
6	29.72294	8.849595
7	28.94316	9.966211
8	26.79698	11.99766
9	26.02494	9.542425

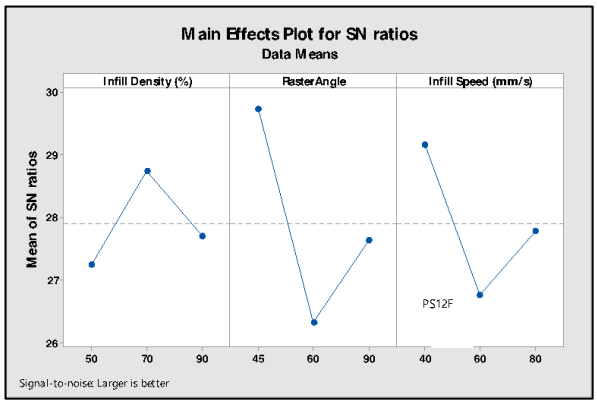

Figure 5.31 Mean effect plots for S/N ratio for PS of 3D printed flexural samples reinforced with almond skin

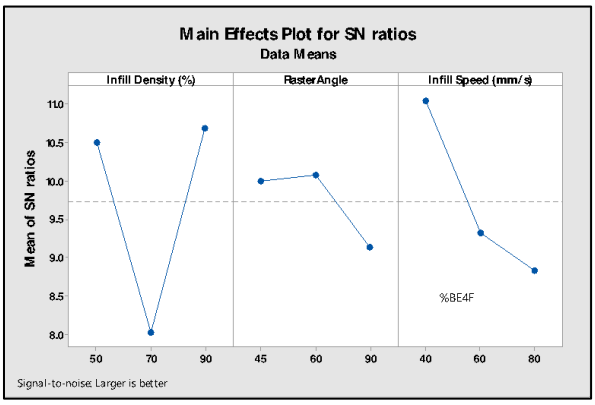

Figure 5.32 Mean effect plots for S/N ratio for %BE of 3D printed flexural sample reinforced with almond skin

Table 5.20 S/N ratio for PS and %BE of 3D printed flexural samples reinforced with wood powder

Sample No.	S/N ratio for PS (dB)	S/N ratio for %BE (dB)
1	29.83004	12.25568
2	24.93489	11.38748
3	20.66848	9.542425
4	26.71317	8.299467
5	21.58362	6.887845
6	20.99211	7.923987
7	27.67631	9.883092
8	24.44392	11.36403
9	21.73431	9.27786

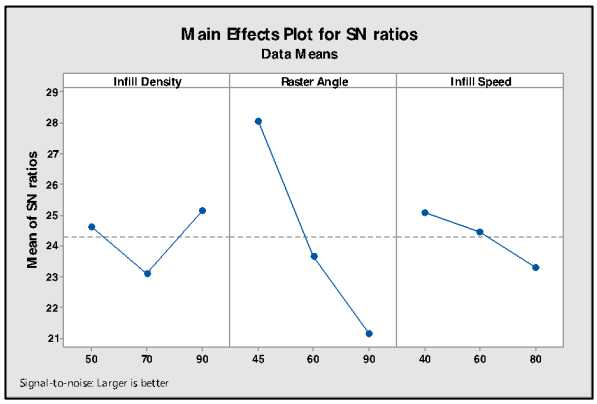

Figure 5.33 Mean effect plots for S/N ratio for PS of 3D printed flexural sample reinforced with wood powder

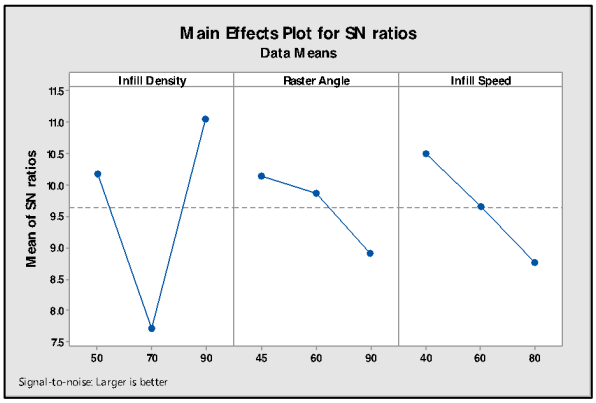

Figure 5.34 Mean effect plots for S/N ratio for %BE of 3D printed flexural sample reinforced with wood powder

5.17 ANALYSIS OF VARIANCE (ANOVA) OF 3D PRINTED FLEXURAL SAMPLES

Further an analysis of variance (ANOVA) was conducted on the S/N ratio for both PS and %BE of 3D printed flexural specimens (for both Almond Skin and Wood Powder) to find most dominant parameter affecting PS & %BE and results obtained from the ANOVA represents in Table 5.21 and Table 5.22. It has been found from Table 5.21 that predominant factor which is affecting PS of the prepared 3D printed specimens was raster angle (58.845%) whereas from Table 5.22, it has been found that predominant factor which is affecting %BE of the prepared 3D printed specimens was infill density (57.461%). Table 5.23 and Table 5.24 shows ANOVA for PS and %BE of 3D printed flexural specimens (Wood Powder) respectively. From Table 5.23, it has been found that predominant factor which affects PS of 3D printed specimens was raster angle (85.82%) whereas from Table 5.24, it has been found that predominant factor which affects %BE of 3D printed specimens was Infill Density (71.58%).

Table 5.21 ANOVA for PS of 3D printed flexural samples reinforced with almond skin

Source	DOF	Adj SS	Adj MS	F-value	P-value	%age Contribution
Infill Density (%)	2	3.5243	1.7621	21.78	0.044	11.586
Raster Angle	2	17.9003	8.9502	110.6	0.009	58.845
Infill speed (mm/s)	2	8.8328	4.4164	54.58	0.018	29.037

Source	DOF	Adj SS	Adj MS	F-value	P-value	%age Contribution
Error	2	0.1618	0.0809	-	-	0.532
Total	8	30.4193	-	-	-	100

Table 5.22 ANOVA for %BE of 3D printed flexural samples reinforced with almond skin

Source	DOF	Adj SS	Adj MS	F-value	P-value	%age Contribution
Infill Density (%)	2	13.3668	6.6834	114.37	0.009	57.461
Raster Angle	2	1.608	0.804	13.76	0.068	6.913
Infill speed (mm/s)	2	8.1705	4.0853	69.91	0.014	35.124
Error	2	0.1169	0.0584	-	-	0.503
Total	8	23.2622	-	-	-	100

Table 5.23 ANOVA for PS of 3D printed flexural samples reinforced with wood powder

Source	DOF	Adj SS	Adj MS	F-Value	P-Value	%age Contribution
Infill Density	2	6.7881	3.3940	11.94	0.077	7.86
Raster Angle	2	74.0758	37.0379	130.30	0.008	85.82
Infill Speed	2	4.8854	2.4427	8.59	0.104	5.66
Error	2	0.5685	0.2842			0.66

Source	DOF	Adj SS	Adj MS	F-Value	P-Value	%age Contribution
Total	8	86.3178				100

Table 5.24 ANOVA for %BE of 3D printed flexural samples reinforced with wood powder

Source	DOF	Adj SS	Adj MS	F-Value	P-Value	%age Contribution
Infill Density	2	18.1703	9.08515	134.77	0.007	71.58
Raster Angle	2	2.5183	1.25917	18.68	0.051	9.92
Infill Speed	2	4.5597	2.27985	33.82	0.029	17.97
Error	2	0.1348	0.06741			0.53
Total	8	25.3832				100

5.18 FESEM ANALYSIS OF 3D PRINTED FLEXURAL SAMPLES

FESEM characterization was carried out for flexural samples reinforcing almond skin and wood powder in 2º PLA possessing maximum PS while flexural testing shown in Figure 5.35 and Figure 5.36, respectively. All FESEM figures shows fiber pull-out while flexural testing but sample with minimum PS was showing larger pull-out area as compared to the sample with maximum PS. Figure 5.35 (b) shows the fiber pull-outs with multiple voids spaces causing reduction in strength as compared to Figure 5.35 (a).

Figure 5.36 (a) depicts fiber pull-outs indicating interfacial bonding which might get happened due to high cooling rate at lower 3D printing temperature. Further, Figure 5.36 (b) shows poor surface appearance with multiple voids at many places on fractured surface which may leads to reduction in mechanical strength of the sample reinforced with wood powder.

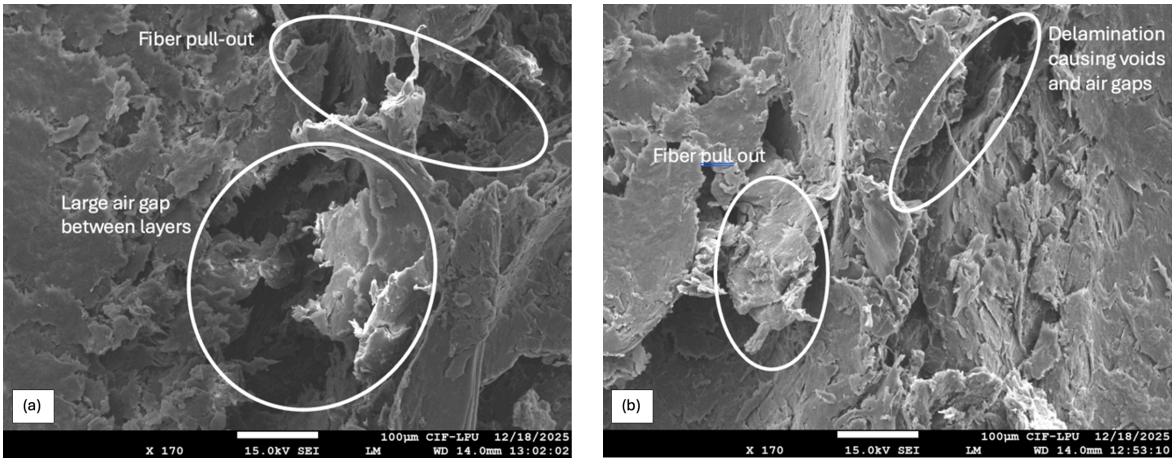

Figure 5.35 FESEM of 3D printed flexural samples reinforced with almond skin having (a) maximum (b) minimum PS

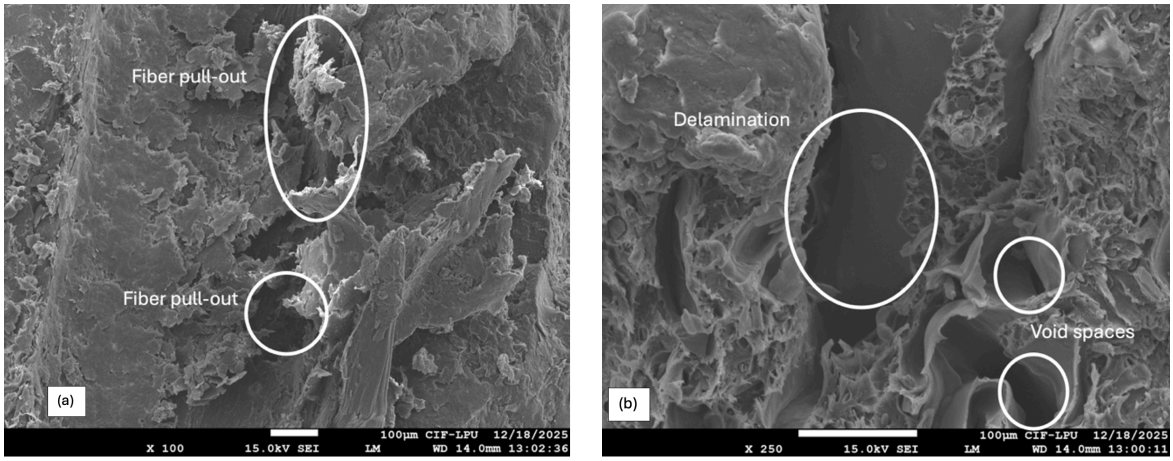

Figure 5.36 FESEM of 3D printed flexural samples reinforced with wood powder having (a) maximum (b) minimum PS

5.19 ENERGY-DISPERSIVE SPECTROSCOPY (EDS) OF FLEXURAL SAMPLE

EDS was carried out on 3D printed flexural sample having maximum PS to identify its elemental composition along with area mapping to examine elemental distribution on the fractured surface as shown in Figure 5.37. Elemental composition of shows 53.51% carbon (C) whereas 46.23% oxygen (O). The minimal presence of iron (Fe) 0.26% may be due to contamination or residual metal particles introduced during material handling.

Further EDS of sample reinforced with wood powder as shown in Figure 5.38 shown 62.67% carbon, 37.12% oxygen and 0.22% nickel (Ni). Traces of nickel in the composite can be attributed to the addition of impurities from processing equipment. It is present in very small amount which has no significant impact on the mechanical properties of the 3D printed composites.

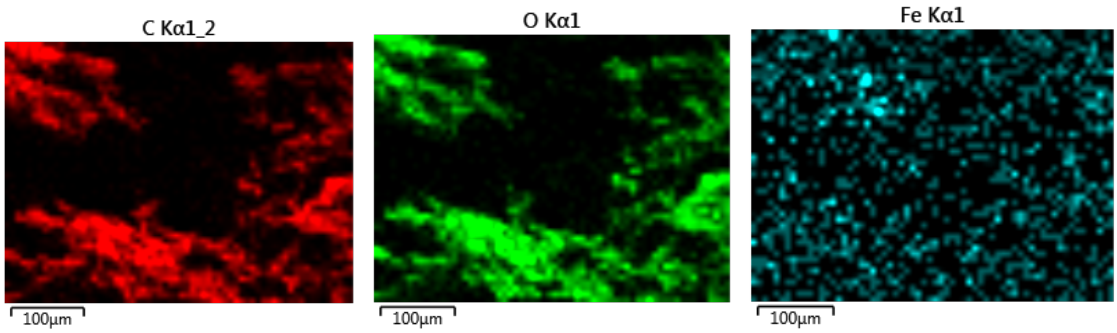

Figure 5.37 EDS of 3D printed flexural sample reinforced with almond skin having maximum PS

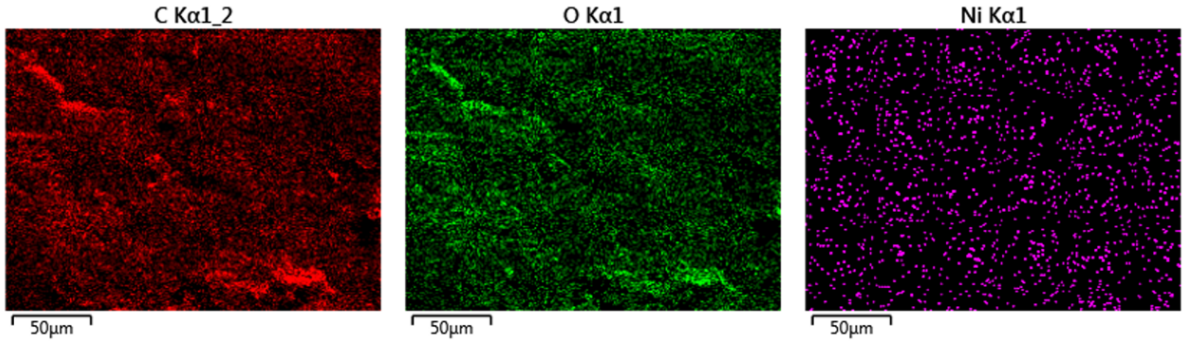

Figure 5.38 EDS of 3D printed flexural sample reinforced with wood powder having maximum PS

5.20 MULTI-RESPONSE OPTIMIZATION OF TENSILE AND FLEXURAL TESTING FOR ALMOND SKIN AND WOOD POWDER

On the basis of mean effect plots for tensile and flexural testing result, a combine optimization for 2º PLA + almond skin and 2º PLA + wood powder has been done via. MiniTab17 when both responses were taken simultaneously [140-141]. Equal importance has been given to both input and output parameters. Defined constraints and recommended parameters levels are shown in Table 5.25 and Table 5.27. The actual response values were calculated using Eq. 8 [142] and obtained results are shown in Table 5.26 and Table 5.28.

$$S/N = -10\ Log\left[\frac{1}{r}\sum_{i=1}^{r}\frac{1}{Y_i^2}\right] \qquad \text{(Eq. 8) [142]}$$

Table 5.25 Input and output parameter constraints for 3D printed samples reinforced with almond skin

Parameter	Goal	3D printed tensile specimen		3D printed flexural specimen	
		Lower range	Upper range	Lower range	Upper range
Infill density (%)	Within region	50	90	50	90
Raster Angle (^{0})	Within region	45	90	45	90
Speed (rpm)	Within region	40	80	40	80
S/N ratio (PS)	Maximize	24.42	30.22	24.93	30.99
S/N ratio (% BE)	Maximize	10.13	14.51	7.49	12.31

Table 5.26 Suggested parametric levels for 3D printed samples reinforced with almond skin

Parameter	3D printed tensile specimen		3D printed flexural specimen	
	Optimized Value	Actual Value	Optimized Value	Actual Value
Infill density (%)	90	90	90	90
Raster Angle (^{0})	45	45	45	45
Speed (rpm)	80	80	40	40
S/N ratio (PS)	28.72	16.64	30.81	17.65
S/N ratio (% BE)	14.14	3.20	12.27	2.36
Desirability	80.60%			

Table 5.27 Input and output parameter constraints for 3D printed samples reinforced with wood powder

Parameter	Goal	3D printed tensile specimen		3D printed flexural specimen	
		Lower range	Upper range	Lower range	Upper range
Infill density (%)	Within region	50	90	50	90
Raster Angle (^{0})	Within region	45	90	45	90
Speed (rpm)	Within region	40	80	40	80
S/N ratio (PS)	Maximize	20.26	28.73	20.66	29.83
S/N ratio (% BE)	Maximize	9.15	13.06	6.88	12.25

Table 5.28 Suggested parametric levels for 3D printed samples reinforced with wood powder

Parameter	3D printed tensile specimen		3D printed flexural specimen	
	Optimized Value	Actual Value	Optimized Value	Actual Value
Infill density (%)	90	90	90	90
Raster Angle (^{0})	45	45	45	45
Speed (rpm)	80	80	40	40
S/N ratio (PS)	27.41	10.30	29.73	10.78
S/N ratio (% BE)	13.24	2.86	12.42	2.20
Desirability	88.17%			

CHAPTER 6

CONCLUSIONS

1. From rheological investigation it has been found that with increase in reinforcement percentage in base matrix, MFI starts decreasing. But on further increase in reinforcement percentage beyond 10%wt., nozzle clogging took place due to increased melt viscosity and brittleness of the composite material which restricts smooth flow through the nozzle.
2. ANOVA results revealed that processing temperature was the most statistically significant parameter for the almond skin-reinforced filaments, contributing 69.20% to peak strength (PS) and 48.82% to elongation at break (%BE). due to interfacial bonding between the matrix and the reinforcement. In contrast, extrusion load emerged as the governing factor for the wood powder-reinforced filaments, accounting for 92.94% to PS and 88.33% to %BE.
3. Further from FESEM and porosity analysis, it has been observed that samples with maximum Peak Strength has lesser voids and porosity percentage which shows better mechanical behavior and superior properties.
4. Thermal analysis shows that composites fabricated by reinforcing almond skin shows superior heat capacity as compared to composites fabricated by reinforcing wood powder.
5. Combined optimized parameters for fused filaments revealed that maximum Peak Strength was observed at 0.1 Nm torque, 7.5 kg load and 195°C temperature for 2° PLA reinforced with almond skin. Similarly, for 2° PLA reinforced with wood powder gives maximum peak strength at 0.3 Nm, 7.5 kg and 175°C.
6. Multilayer printing of tensile and flexural specimens has been successfully done via Fused Filament Fabrication from 2°PLA to obtain desired properties.
7. Infill density came out as predominant factor followed by infill speed and raster angle that affects both mechanical and morphological properties of the prepared specimens. Further 3D printed specimen prepared by reinforcing 2°PLA with almond skin shows superior properties as compared to specimen prepared by reinforcing 2°PLA with wood powder.
8. The optimized 3D printing parameters for both the almond skin and wood powder-reinforced composites were established at a 90% infill density and a 45° raster angle.

The optimized infill speeds were set at 80 mm/s for tensile specimens and 40 mm/s for flexural specimens. Under these manufacturing conditions, the almond skin-reinforced composites exhibited a peak tensile strength of 16.64 MPa and a peak flexural strength of 17.65 MPa. In comparison, the wood powder-reinforced specimens yielded lower values of 10.30 MPa (tensile) and 10.78 MPa (flexural). The higher Peak Strength of flexural specimens indicates their suitability for structural and non structural automobile applications.

9. Multiple Response Optimization using Minitab shows desirability of 80.60% for 2°PLA reinforced with almond skin and 88.17% 2°PLA reinforced with wood powder indicating optimized process parameters satisfactorily meet the combined performance for tensile as well flexural specimens.

SCOPE OF FUTURE RESEARCH WORK

1. The present study focuses on reinforcing 2° PLA with waste almond skin and wood powder to investigate its mechanical, thermal and morphological properties. However, other industrial waste materials such as rice husk, coconut shell, walnut shell and thermosetting polymers remain unexplored as reinforcements for comparative analysis.
2. Current research work focuses on development of composites especially for dashboards used in automobile industries. For future, it can be explored for other automotive components such bumper and door materials etc.

REFERENCES

1. Chawla, Kapil, Rupinder Singh, and Jaspreet Singh. "On recyclability of thermoplastic ABS polymer as fused filament for FDM technique of additive manufacturing." *World Journal of Engineering* 19.3 (2022): 352-360.
2. Singh, Jaspreet, Kapil Chawla, and Rupinder Singh. "Applications of thermoplastic polymers in 3D printing." (2022): 23-32.
3. Singh, Narinder, et al. "Recycling of plastic solid waste: A state of art review and future applications." *Composites Part B: Engineering* 115 (2017): 409-422.
4. Edwards, K. L. "A designers' guide to engineering polymer technology." *Materials & design* 19.1-2 (1998): 57-67.
5. Ranakoti, Lalit, et al. "Critical review on polylactic acid: properties, structure, processing, biocomposites, and nanocomposites." *Materials* 15.12 (2022): 4312. Arora, Amit, and G. W. Padua. "Nanocomposites in food packaging." *Journal of Food science* 75.1 (2010): R43-R49.
6. Arora, Amit, and G. W. Padua. "Nanocomposites in food packaging." *Journal of Food science* 75.1 (2010): R43-R49.
7. Rashid, Adib Bin, et al. "Nanotechnology-enhanced fiber-reinforced polymer composites: Recent advancements on processing techniques and applications." *Heliyon* 10.2 (2024).
8. Christian, P. "Polymer chemistry." *Electrospinning for tissue regeneration*. Woodhead Publishing, 2011. 34-50.
9. Utracki, Leszek A., and Charles A. Wilkie, eds. *Polymer blends handbook*. Vol. 1. Dordrecht: Kluwer academic publishers, 2002.
10. Lithner, Delilah, Åke Larsson, and Göran Dave. "Environmental and health hazard ranking and assessment of plastic polymers based on chemical composition." *Science of the total environment* 409.18 (2011): 3309-3324.
11. Edah, Gabriel O., Joshua O. Atiba, and Ojo SI Fayomi. "Advancements in fibre-reinforced polymers: Properties, applications (A mini review)." *Next Materials* 8 (2025): 100743.
12. Bukvić, Milan, et al. "Production Technologies and Application of Polymer Composites in Engineering: A Review." *Polymers*17.16 (2025): 2187.
13. Yu, Jie, et al. "Thermal degradation of PVC: A review." *Waste management* 48 (2016): 300-314.

14. Dodiuk, Hanna, ed. *Handbook of thermoset plastics*. William Andrew, 2021.
15. Abbood, Imad Shakir, et al. "Properties evaluation of fiber reinforced polymers and their constituent materials used in structures–A review." *Materials Today: Proceedings* 43 (2021): 1003-1008.
16. Rotkovich, A. A., et al. "Development and study of lightweight recycled composite materials based on linear low-density polyethylene and W for radiation application." *Journal of Materials Research and Technology* 30 (2024): 1310-1318.
17. Kliem, Silvia, Marc Kreutzbruck, and Christian Bonten. "Review on the biological degradation of polymers in various environments." *Materials* 13.20 (2020): 4586.
18. Pilapitiya, PGC Nayanathara Thathsarani, and Amila Sandaruwan Ratnayake. "The world of plastic waste: A review." *Cleaner Materials* 11 (2024): 100220.
19. Chamas, Ali, et al. "Degradation rates of plastics in the environment." *ACS Sustainable Chemistry & Engineering* 8.9 (2020): 3494-3511.
20. Ackerman, Frank. "Waste management and climate change." *Local Environment* 5.2 (2000): 223-229.
21. Kibria, Md Golam, et al. "Plastic waste: challenges and opportunities to mitigate pollution and effective management." *International Journal of Environmental Research* 17.1 (2023): 20.
22. Kozderka, Michal, et al. "High impact polypropylene (HIPP) recycling–Mechanical resistance and Lifecycle Assessment (LCA) case study with improved efficiency by preliminary sensitivity analysis." *Journal of cleaner production* 137 (2016): 1004-1017.
23. Jambeck, Jenna, et al. "Challenges and emerging solutions to the land-based plastic waste issue in Africa." *Marine Policy* 96 (2018): 256-263.
24. Silvarrey, LS Diaz, and A. N. Phan. "Kinetic study of municipal plastic waste." *International journal of hydrogen energy* 41.37 (2016): 16352-16364.
25. Geyer, Roland, Jenna R. Jambeck, and Kara Lavender Law. "Production, use, and fate of all plastics ever made." *Science advances* 3.7 (2017): e1700782.
26. Cole, Matthew, et al. "Microplastics as contaminants in the marine environment: a review." *Marine pollution bulletin* 62.12 (2011): 2588-2597.
27. Gao, Yunhu, and André Cabrera Serrenho. "Evaluating the potential to reduce the global demand for polymers." *Resources, Conservation and Recycling* 223 (2025): 108518.
28. Ibrahim, Idowu David, et al. "Need for sustainable packaging: an overview." *Polymers* 14.20 (2022): 4430.

29. Milios, Leonidas, et al. "Plastic recycling in the Nordics: A value chain market analysis." *Waste Management* 76 (2018): 180-189.
30. Gondal, Mohammed A., and Mohammad N. Siddiqui. "Identification of different kinds of plastics using laser-induced breakdown spectroscopy for waste management." *Journal of Environmental Science and Health Part A* 42.13 (2007): 1989-1997.
31. Kalali, Ehsan Naderi, et al. "A critical review of the current progress of plastic waste recycling technology in structural materials." *Current Opinion in Green and Sustainable Chemistry* 40 (2023): 100763.
32. Tsuchimoto, Ichiro, and Yuya Kajikawa. "Recycling of plastic waste: a systematic review using bibliometric analysis." *Sustainability* 14.24 (2022): 16340.
33. Belioka, Maria-Paraskevi, and Dimitrios S. Achilias. "How plastic waste management affects the accumulation of microplastics in waters: A review for transport mechanisms and routes of microplastics in aquatic environments and a timeline for their fate and occurrence (past, present, and future)." *Water Emerging Contaminants & Nanoplastics* 3.3 (2024): N-A.
34. Ragaert, Kim, Laurens Delva, and Kevin Van Geem. "Mechanical and chemical recycling of solid plastic waste." *Waste management* 69 (2017): 24-58.
35. Jiang, Xiaoli, and Buhe Bateer. "A systematic review of plastic recycling: technology, environmental impact and economic evaluation." *Waste Management & Research* (2025): 0734242X241310658.
36. Anwar, Muhammad, Maria E. Konnova, and Sarim Dastgir. "Circular plastic economy for sustainable development: current advances and future perspectives." *RSC Sustainability* (2025): 3, 3724–3840
37. Kalauni, Kishor, et al. "A comprehensive review of recycling and reusing methods for plastic waste focusing Indian scenario." *Waste Management & Research* (2025): 0734242X241308499.
38. Da Silva, Daniel Jose, and Helio Wiebeck. "Current options for characterizing, sorting, and recycling polymeric waste." *Progress in Rubber, Plastics and Recycling Technology* 36.4 (2020): 284-303.
39. Carvalho, Teresa, Fernando Durão, and Célia Ferreira. "Separation of packaging plastics by froth flotation in a continuous pilot plant." *Waste management* 30.11 (2010): 2209-2215.

40. Sanchez-Soto, M., et al. "Blends of HDPE wastes: Study of the properties." *Waste Management* 28.12 (2008): 2565-2573.
41. Singh, Narinder, et al. "Recycling of plastic solid waste: A state of art review and future applications." *Composites Part B: Engineering* 115 (2017): 409-422.
42. Goetz, Alexander FH, et al. "Imaging spectrometry for earth remote sensing." *Science* 228.4704 (1985): 1147-1153.
43. Gondal, Mohammed A., and Mohammad N. Siddiqui. "Identification of different kinds of plastics using laser-induced breakdown spectroscopy for waste management." *Journal of Environmental Science and Health Part A* 42.13 (2007): 1989-1997.
44. Burat, Fırat, Ali Güney, and M. Olgaç Kangal. "Selective separation of virgin and post-consumer polymers (PET and PVC) by flotation method." *Waste Management* 29.6 (2009): 1807-1813.
45. Drelich, J., et al. "Selective froth flotation of PVC from PVC/PET mixtures for the plastics recycling industry." *Polymer Engineering & Science* 38.9 (1998): 1378-1386.
46. Passamonti, Francisco J., and Ulises Sedran. "Recycling of waste plastics into fuels. LDPE conversion in FCC." *Applied Catalysis B: Environmental* 125 (2012): 499-506.
47. Perrone, C. "Operating experience in a washing plant for recycled LDPE film production." *Resources, conservation and recycling* 2.1 (1988): 27-36.
48. Murariu, V., J. Svoboda, and P. Sergeant. "The modelling of the separation process in a ferrohydrostatic separator." *Minerals Engineering* 18.4 (2005): 449-457.
49. Nestore, O., Kajaks, J., Vancovicha, I. *et al.* Physical and mechanical properties of composites based on a linear low-density polyethylene (LLDPE) and natural fiber waste. *Mech Compos Mater* 48, 619–628 (2013).
50. Serranti, Silvia, et al. "An innovative recycling process to obtain pure polyethylene and polypropylene from household waste." *Waste management* 35 (2015): 12-20.
51. Bendimerad, S., et al. "Plastic wastes recovery using free-fall triboelectric separator." *International Journal of Environmental Studies* 66.5 (2009): 529-538.
52. Xiao, Chuanfu, et al. "Electrostatic separation and recovery of mixed plastics." *Society of Plastics Engineers (SPE) Annual Recycling Conference (ARC), Dearborn, Michigan (US)*. 1999.
53. González, Mario Ferreiro, Nooshin Saadatkhah, and Gregory S. Patience. "Experimental methods in chemical engineering: X-ray fluorescence—XRF." *The Canadian Journal of Chemical Engineering* 102.6 (2024): 2004-2018.

54. Al-Salem, S. M., et al. "A review on thermal and catalytic pyrolysis of plastic solid waste (PSW)." *Journal of environmental management* 197 (2017): 177-198.
55. Spinacé, Márcia Aparecida da Silva, and Marco Aurelio De Paoli. "A tecnologia da reciclagem de polímeros." *Química nova* 28 (2005): 65-72.
56. Hamad, Kotiba, Mosab Kaseem, and Fawaz Deri. "Recycling of waste from polymer materials: An overview of the recent works." *Polymer degradation and stability* 98.12 (2013): 2801-2812.
57. Cruz, Sandra A., et al. "Polímeros reciclados para contato com alimentos." *Polímeros* 21 (2011): 340-345.
58. Sadat-Shojai, Mehdi, and Gholam-Reza Bakhshandeh. "Recycling of PVC wastes." *Polymer degradation and stability* 96.4 (2011): 404-415.
59. Al-Salem, S. M., Paola Lettieri, and Jan Baeyens. "Recycling and recovery routes of plastic solid waste (PSW): A review." *Waste management* 29.10 (2009): 2625-2643.
60. Kumar, Sachin, Achyut K. Panda, and Raghubansh Kumar Singh. "A review on tertiary recycling of high-density polyethylene to fuel." *Resources, Conservation and Recycling* 55.11 (2011): 893-910.
61. Harasymchuk, Ivanna, Vladimír Kočí, and Monika Vitvarová. "Chemical recycling: Comprehensive overview of methods and technologies." *International Journal of Sustainable Engineering* 17.1 (2024): 124-148.
62. Chanda, Manas. "Chemical aspects of polymer recycling." *Advanced Industrial and Engineering Polymer Research* 4.3 (2021): 133-150.
63. Al-Salem, S. M., Paola Lettieri, and J. Baeyens. "The valorization of plastic solid waste (PSW) by primary to quaternary routes: From re-use to energy and chemicals." *Progress in Energy and Combustion Science* 36.1 (2010): 103-129.
64. Murariu, V., J. Svoboda, and P. Sergeant. "The modelling of the separation process in a ferrohydrostatic separator." *Minerals Engineering* 18.4 (2005): 449-457.
65. Aznar, María P., et al. "Plastic waste elimination by co-gasification with coal and biomass in fluidized bed with air in pilot plant." *Fuel processing technology* 87.5 (2006): 409-420.
66. Chawla, Kapil, Rupinder Singh, and Jaspreet Singh. "Segregation and recycling of plastic solid waste: a review." *Advances in Materials Science and Engineering: Select Proceedings of ICFMMP 2019* (2020): 205-221.

67. Alabi, Oluwaseyi O., et al. "Advanced technologies for plastic waste recycling: examine recent developments in plastic waste recycling technologies." *RSC advances* 15.48 (2025): 40541-40557.
68. Ignatyev, Igor A., Wim Thielemans, and Bob Vander Beke. "Recycling of polymers: a review." *ChemSusChem* 7.6 (2014): 1579-1593.
69. Rezaei, Fateme, et al. "SO x/NO x removal from flue gas streams by solid adsorbents: a review of current challenges and future directions." *Energy & fuels* 29.9 (2015): 5467-5486.
70. Sun, Yongxia, Ewa Zwolińska, and Andrzej G. Chmielewski. "Abatement technologies for high concentrations of NOx and SO2 removal from exhaust gases: A review." *Critical Reviews in Environmental Science and Technology* 46.2 (2016): 119-142.
71. Karmakar, Ganga P. "Regeneration and recovery of plastics." *Encyclopedia of materials: plastics and polymers* (2022): 634.
72. Rahimi, AliReza, and Jeannette M. García. "Chemical recycling of waste plastics for new materials production." *Nature Reviews Chemistry* 1.6 (2017): 0046.
73. Mobarak, Md Hosne, et al. "Recent advances of additive manufacturing in implant fabrication–a review." *Applied Surface Science Advances* 18 (2023): 100462.
74. Jadhav, Aniket, and Vijay S. Jadhav. "A review on 3D printing: An additive manufacturing technology." *Materials Today: Proceedings* 62 (2022): 2094-2099.
75. Rasiya, Gulnaaz, Abhinav Shukla, and Karan Saran. "Additive manufacturing-a review." *Materials Today: Proceedings* 47 (2021): 6896-6901.
76. Islam, Md Aminul, et al. "Additive manufacturing in polymer research: Advances, synthesis, and applications." *Polymer Testing* 132 (2024): 108364.
77. Saleh Alghamdi, Saad, et al. "Additive manufacturing of polymer materials: Progress, promise and challenges." *Polymers* 13.5 (2021): 753.
78. Djonyabe Habiba, Rachel, Cândida Malça, and Ricardo Branco. "Exploring the potential of recycled polymers for 3D printing applications: a review." *Materials* 17.12 (2024): 2915.
79. Krznar, Matic, and Slavko Dolinsek. *Selective laser sintering of composite materials technologies*. na, 2010.
80. Dastjerdi, Ali Ahmadi, Mohammad R. Movahhedy, and Javad Akbari. "Optimization of process parameters for reducing warpage in selected laser sintering of polymer parts." *Additive manufacturing* 18 (2017): 285-294.

81. Lupone, Federico, et al. "Process phenomena and material properties in selective laser sintering of polymers: a review." Materials 15.1 (2021): 183.
82. Halloran, John W., et al. "Photopolymerization of powder suspensions for shaping ceramics." *Journal of the European Ceramic Society* 31.14 (2011): 2613-2619.
83. Pham, D. T., and C. Ji. "Design for stereolithography." *Proceedings of the Institution of Mechanical Engineers, Part C: Journal of Mechanical Engineering Science* 214.5 (2000): 635-640.
84. Kim, Hochan, Jae-Won Choi, and Ryan Wicker. "Scheduling and process planning for multiple material stereolithography." *Rapid Prototyping Journal* 16.4 (2010): 232-240.
85. Szilvśi-Nagy, Márta, and G. Y. Matyasi. "Analysis of STL files." *Mathematical and computer modelling* 38.7-9 (2003): 945-960.
86. Fu, Zongwen, and Carolin Körner. "Actual state-of-the-art of electron beam powder bed fusion." *European Journal of Materials* 2.1 (2022): 54-116.
87. Negi, Seema, et al. "Review on electron beam based additive manufacturing." *Rapid Prototyping Journal* 26.3 (2020): 485-498.
88. Wohlers, Terry. "Making products by using additive manufacturing." *Manufacturing Engineering* 146.4 (2011).
89. Singh, Sunpreet, et al. "Current status and future directions of fused filament fabrication." *Journal of Manufacturing Processes* 55 (2020): 288-306.
90. Herzberger, Jana, et al. "Polymer design for 3D printing elastomers: recent advances in structure, properties, and printing." *Progress in Polymer Science* 97 (2019): 101144.
91. Kantaros, Antreas, et al. "Advanced composite materials utilized in FDM/FFF 3D printing manufacturing processes: the case of filled filaments." *Materials* 16.18 (2023): 6210.
92. Mwema, Fredrick Madaraka, and Esther Titilayo Akinlabi. "Basics of fused deposition modelling (FDM)." *Fused deposition modeling: strategies for quality enhancement*. Cham: Springer International Publishing, 2020. 1-15.
93. Abbas, Asyraf, et al. "Performance of bioresorbable peptide incorporated polymers produced for fused deposition modelling (FDM)." *Next Materials* 5 (2024): 100223.
94. Billah, Kazi Md Masum, et al. "Thermomechanical characterization of short carbon fiber and short glass fiber-reinforced ABS used in large format additive manufacturing." *Additive Manufacturing* 35 (2020): 101299.

95. Bhandari, Sunil, Roberto A. Lopez-Anido, and Douglas J. Gardner. "Enhancing the interlayer tensile strength of 3D printed short carbon fiber reinforced PETG and PLA composites via annealing." *Additive Manufacturing* 30 (2019): 100922.
96. Cao, Mengyu, et al. "Investigation of carbon fiber on the tensile property of FDM-produced PLA specimen." *Polymers*14.23 (2022): 5230.
97. Ismail, Khairul Izwan, et al. "Tensile properties of in situ 3D printed glass fiber-reinforced PLA." *Polymers* 15.16 (2023): 3436.
98. Kalimuthu, Mayandi, et al. "Production and characterization of biodegradable polylactic acid composites 3D filament from agro waste." *Interactions* 245.1 (2024): 225.
99. Kumar, K. Shiva, and A. Chennakesava Reddy. "Mechanical properties of 3D-printed Onyx-fibreglass composites: Role of roof layers on tensile strength and hardness–Using anova technique." *Next Materials* 8 (2025): 100650.
100. R. Kumar, K. Chawla, and J. Singh, "Fabrication and Characterization of Almond Skin Powder Reinforced PLA Based Composite Filaments for Fused Filament Fabrication," Journal of Polymer and Composites 13, no. 2 (2025): 530–539.
101. Kumar, Sumodh, et al. "Mechanical characterization of 3D printed MWCNTs/HDPE nanocomposites." *Polymer Testing*114 (2022): 107703.
102. Kariz, Mirko, et al. "Effect of wood content in FDM filament on properties of 3D printed parts." *Materials Today Communications* 14 (2018): 135-140.
103. Kartal, Fuat, and Arslan Kaptan. "Sustainable reinforcement of PLA composites with waste beech sawdust for enhanced 3D-Printing performance." *Journal of Materials Engineering and Performance* 34.14 (2025): 15248-15259.
104. Kozień, Dawid, Krzysztof Malata, Zuzanna Krysińska, Krystian Misieńko, Jurij Delihowski, Wojciech Banaś, Zuzanna Seweryn et al. "Fabrication and Characterization of PLA-Based Ceramic Composite Filaments for FDM 3D Printing." *Crystals* 16, no. 1 (2026): 46.
105. Lau, H. Y., et al. "Effect of kenaf fiber loading on the tensile properties of 3D printing PLA filament." *Materials Today: Proceedings* (2023).
106. de León, A. Sanz, A. Domínguez-Calvo, and S. I. Molina. "Materials with enhanced adhesive properties based on acrylonitrile-butadiene-styrene (ABS)/thermoplastic polyurethane (TPU) blends for fused filament fabrication (FFF)." *Materials & Design* 182 (2019): 108044.
107. Lourenço, Bruno, Rita Serôdio, Ana Clara Marques, Raquel Galante, Ricardo Claudio, and Célio G. Figueiredo-Pina. "PLA/Kahili Ginger Fiber Biocomposites Processed by

Fused Filament Fabrication: Physical and Mechanical Characterization." *Polymer Composites* (2026).

108. Makannavar, Rahul, R. Keshavamurthy, and Mallikarjun Biradar. "Mechanical properties of graphite filled ABS parts developed by fused deposition modelling." *IOP Conference Series: Materials Science and Engineering*. Vol. 577. No. 1. IOP Publishing, 2019.
109. Masood, S. H., and W. Q. Song. "Thermal characteristics of a new metal/polymer material for FDM rapid prototyping process." *Assembly Automation* 25.4 (2005): 309-315.
110. Memiş, Melisa, and Dilşad Akgümüş Gök. "Development of Fe-reinforced PLA-based composite filament for 3D printing: Process parameters, mechanical and microstructural characterization." *Ain Shams Engineering Journal* 16.2 (2025): 103279.
111. Maqsood, Nabeel, and Marius Rimašauskas. "Characterization of carbon fiber reinforced PLA composites manufactured by fused deposition modeling." *Composites Part C: Open Access* 4 (2021): 100112.
112. Husain, Minhaz, Gurwinder Singh, Ranvijay Kumar, and Rupinder Singh. "On Parametric Optimization of Fused Filament Fabrication for Processing Secondary Recycled PLA Composite." *National Academy Science Letters* (2026): 1-9.
113. Petousis, Markos, et al. "On the substantial mechanical reinforcement of Polylactic Acid with Titanium Nitride ceramic nanofillers in material extrusion 3D printing." *Ceramics International* 49.10 (2023): 16397-16411.
114. Rodriguez-Pacheco, Luis C., et al. "Novel 3D printing filaments: PLA and zinc carbonate basic composites for laser-assisted thermal decomposition." *Journal of Materials Research and Technology* 31 (2024): 2266-2278.
115. Ryder, Matthew A., et al. "Fabrication and properties of novel polymer-metal composites using fused deposition modeling." *Composites Science and Technology* 158 (2018): 43-50.
116. Santos, Natália V., and Daniel CT Cardoso. "3D printing of vegetable yarn-reinforced polymer components." *Journal of Cleaner Production* 415 (2023): 137870.
117. Saleh, Mustafa, et al. "Development of PLA/recycled-desized carbon fiber composites for 3D printing: Thermal, mechanical, and morphological analyses." *Journal of Materials Research and Technology* 29 (2024): 2768-2780.

118. Schmitz, D. P., et al. "Effect of printing parameters on the electromagnetic shielding efficiency of ABS/carbonaceous-filler composites manufactured via filament fused fabrication." *Journal of Manufacturing Processes* 65 (2021): 12-19.
119. Singh, Rupinder, et al. "On mechanical, thermal and morphological investigations of almond skin powder-reinforced polylactic acid feedstock filament." *Journal of Thermoplastic Composite Materials* 35.2 (2022): 230-248.
120. Sharma, Ravinder, Rupinder Singh, and Ajay Batish. "Study on barium titanate and graphene reinforced PVDF matrix for 4D applications." *Journal of Thermoplastic Composite Materials* 34.9 (2021): 1234-1253.
121. Shunmugam, Muthu Natarajan, et al. "Enhancing Mechanical Properties of PLA Filaments through Orange Peel Powder Reinforcement: Optimization of 3D Printing Parameters." *Applied Science and Engineering Progress* 17.4 (2024): 7536-7536.
122. Stoof, David, Kim Pickering, and Yuanji Zhang. "Fused deposition modelling of natural fibre/polylactic acid composites." *Journal of Composites Science* 1.1 (2017): 8.
123. Suvanjumrat, Chakrit, Kanchanabhorn Chansoda, and Watcharapong Chookaew. "Additive manufacturing advancement through large-scale screw-extrusion 3D printing for precision parawood powder/PLA furniture production." *Cleaner Engineering and Technology* 20 (2024): 100753.
124. Tambrallimath, Vijay, et al. "Thermal behavior of PC-ABS based graphene filled polymer nanocomposite synthesized by FDM process." *Composites Communications* 15 (2019): 129-134.
125. Thirugnanasamabandam, Arunkumar, et al. "Wood flour/ceramic reinforced polylactic acid based 3D–printed functionally grade structural material for integrated engineering applications: a numerical and experimental characteristic investigation." *International Journal of Lightweight Materials and Manufacture* 8.1 (2025): 74-86.
126. Trivedi, Alok Kumar, and M. K. Gupta. "3D printed PLA based bionanocomposites with improved mechanical and dynamic mechanical properties: effect of varying CNC reinforcements." *Cellulose* (2025): 1-17.
127. Wang, Andong, et al. "Carbon fiber-reinforced PLA composite for fused deposition modeling 3D printing." *Polymers* 16.15 (2024): 2135.
128. Yang, Leipeng, et al. "Effects of carbon nanotube on the thermal, mechanical, and electrical properties of PLA/CNT printed parts in the FDM process." *Synthetic Metals* 253 (2019): 122-130.

129. Zhang, Zhongsen, Bingyan Cao, and Ning Jiang. "The mechanical properties and degradation behavior of 3D-printed cellulose nanofiber/polylactic acid composites." *Materials*16.18 (2023): 6197.

130. Zhao, Guixiang, et al. "Tensile properties of 3D-printed CNT-SGF reinforced PLA composites." *Composites Science and Technology* 230 (2022): 109333.

131. Teresa Rodríguez-Hernández, M., J. L. Angulo-Sánchez, and A. Pérez-Chantaco. "Determination of the molecular characteristics of commercial polyethylenes with different architectures and the relation with the melt flow index." *Journal of applied polymer science* 104.3 (2007): 1572-1578.

132. Kumar, Ravi, Kapil Chawla, and Jaspreet Singh. "Mechanical Assisted Blending of Secondary Recycled PLA with Almond Skin for Fused Filament Fabrication." *International Conference on Design and Manufacturing Technologies*. Singapore: Springer Nature Singapore, (2024): pp. 73-82

133. Shenoy, A. V., and D. R. Saini. "Melt flow index: More than just a quality control rheological parameter. Part I." *Advances in Polymer Technology* 6.1 (1986): 1-58.

134. Davim, J. Paulo. "Design of optimisation of cutting parameters for turning metal matrix composites based on the orthogonal arrays." *Journal of materials processing technology* 132.1-3 (2003): 340-344.

135. Wagner, J. R., E. M. Mount, and H. F. Giles. "11-Twin Screw Extruder Equipment." *Extrusion (Second Edition)* (2014): 125-148.

136. Chawla, Kapil, Jaspreet Singh, and Rupinder Singh. "Mechanical investigations on secondary recycled ABS-based composite multi-layered tensile and flexural specimens prepared by fused filament fabrication." *Progress in Additive Manufacturing* 8.6 (2023): 1195-1208.

137. Besterfield, H.D., Micna, C.B., Besterfield, G.H. and Sacre, M.B. (2010), Total Quality Management, 3rd edition, Prentice Hall.

138. Bremner, T., A. Rudin, and D. G. Cook. "Melt flow index values and molecular weight distributions of commercial thermoplastics." *Journal of Applied Polymer Science* 41.7-8 (1990): 1617-1627.

139. Chawla, Kapil, Jaspreet Singh, and Rupinder Singh. "On recyclability of thermosetting polymer and wood dust as reinforcement in secondary recycled ABS for nonstructural engineering applications." *Journal of Thermoplastic Composite Materials* 35.7 (2022): 913-937.

140. Singh, Jaspreet, Rupinder Singh, and Harwinder Singh. "Experimental investigations for dimensional accuracy and surface finish of polyurethane prototypes fabricated by indirect rapid tooling: a case study." *Progress in Additive Manufacturing* 2.1 (2017): 85-97.

141. Singh, Jaspreet, Rupinder Singh, and Harwinder Singh. "Investigations for improving the surface finish of FDM based ABS replicas by chemical vapor smoothing process: a case study." *Assembly Automation* 37.1 (2017): 13-21.

142. Singh, Rupinder, et al. "Waste management by recycling of polymers with reinforcement of metal powder." *Composites Part B: Engineering* 105 (2016): 23-29.